T.C.

AKSARAY UNIVERSITY

GRADUATE SCHOOL OF NATURAL AND APPLIED SCIENCE

DEPARTMENT OF ELECTRICAL ELECTRONIC AND COMPUTER ENGINEERING

MODELLING AND SIMULATION OF A PROPULSION ELECTRIC VEHICLE SYSTEM

MASTER OF SCIENCE THESIS

Mohammed AYAD RADHI ALKHAFAJI

SUPERVISOR

Assoc. Prof. Dr. Yunus UZUN

AKSARAY, 2019

AKSARAY UNIVERSITY

GRADUATE SCHOOL OF NATURAL AND APPLIED SCIENCES

ACCEPTANCE CERTIFICATE

Aksaray University, Institute Of Science and Technology Approval **MOHAMMED AYAD RADHI ALKHAFAJI**, M.Sc. with thesis student No. **162338502**, successfully presented the M.Sc. thesis titled "**MODELLING AND SIMULATION OF A PROPULSION ELECTRIC VEHICLE SYSTEM**", prepared after satisfying all the requirements identified in the concerned bylaws, before the jury whose signatures are affixed below.

Thesis Advisor: Assoc. Prof. Dr. Yunus Uzun
Aksaray University
I approve that this thesis is a Master Thesis in scope and quality ....

Asst. Prof. Dr. Filiz SARI
Aksaray University
I approve that this thesis is a Master Thesis in scope and quality ....

Asst. Prof. Dr. Serdar ÇİÇEK
Nevşehir Hacı Bektaş Veli University
I approve that this thesis is a Master Thesis in scope and quality ....

Date of Defence: 21/02/2019

I agree that this thesis, which is accepted by the jury, has fulfilled the requirements for being a Master Thesis.

....

Assoc. Prof. Dr. M.Ali HINIS

DECLARATION

I declare that I write this work as a master thesis without any help and a way that would be contrary to academic rules and scientific ethics, morals, and traditions.

I declare that I will endure all moral and legal consequences that will arise if this situation is found to be contrary to my statement, regardless of a certain time period by the Institute.

Mohammed Ayad Radhi Alkhafaji

ACKNOWLEDGEMENT

Foremost, I am very thankful to the Almighty Allah for giving me the strength and the ability to accomplish this work. I would like to express my sincere gratitude to Assoc. Prof .Dr. Yunus Uzun for being the supervisor of my work. He offered me all the essential information necessary to make my thesis solid and useful. Additionally, I would also like to thank my wife “Teba Hussein”, who continued supporting me to across this part of life. Similarly, I seize the opportunity to extend my thanks to all my friend as well as all my other colleagues for kindly helping and supporting. Finally, a special thanks to my family, brothers, sisters and their families for their continuous encouragement.

Mohammed Ayad Radhi Alkhafaji

AKSARAY, 2019

TABLE OF CONTENTS

Page

ACKNOWLEDGEMENT ... i
TABLE OF CONTENTS ... ii
ABSTRACT ... iv
ÖZET ... v
LIST OF FIGURES ... vi
LIST OF TABLES ... viii
LIST OF ABBREVIATIONS ... ix
1. INTRODUCTION ... 1
1.1 Background About Electric Vehicles Components ... 1
1.2 Electric Vehicles Classification ... 2
1.2.1 The classical EV system ... 3
1.2.2The propulsion EV system ... 3
1.2.3 The traction EV system ... 4
1.2.4 The four-wheel two motors EV system ... 5
1.2.5The four-wheel EV system ... 6
1.3 Reported Studies About Electric Vehicles ... 7
1.4 The Purpose of This Thesis ... 11
1.5 Thesis Outlines ... 12
2. SIMULATION AND ANALYSIS OF SYNRM ... 13
2.1 SynRM Operation Theory And Features ... 13
2.2 Mathematical Model of SynRM ... 16
2.3 Mathematical Model of Stationary Field Transformation ... 18
2.4 Voltage Source Inverter Mathematical Theory ... 20
2.5 SynRM Block System Simulation ... 22
2.6 The Results of SynRM Model Simulation ... 26
2.7 Conclusion ... 30
3. THEORY OF SYNRM CONTROL SYSTEM ... 31
3.1 The Concept of SynRM Speed Control ... 31
3.1.1 Traditional-PID controller ... 32
3.1.2 Cascade-PID controller ... 34
3.1.3 Lead-Lag-controller ... 35
3.1.4 Simulation and results of cascade-PI and lead-lag-controller ... 35
3.1.5 Simulation and results of cascade-PI, PID and lead-lag-controller ... 40
3.2 The PSO Algorithm ... 45
3.2.1 Simulink and results for the cascaded-controller with PSO ... 49
3.3 Conclusions ... 54
4. THE PROPULSION ELECTRIC VEHICLE CONSTRUCTION ... 55
4.1 The Components of Propulsion Electric Vehicle System ... 55
4.1.1 The electronic device (EDC) ... 56
4.1.2 The propulsion electric vehicle drive system ... 59
4.1.3 The source of energy in an electric vehicle ... 59
4.2 The Simulation of EDC Model ... 60
4.2.1 The simulation and result of the EDC system ... 60
4.3 Simulation Result of The PEV System ... 62
4.4 The Resistive Forces of EV ... 64
4.4.1 Simulink model of the resistive-torque in EV ... 65
4.5 The Driving Cycle of the Electric Vehicle ... 66
4.6 The Simulation Result of Driving Cycles System ... 67
4.6.1 The first driving cycle ... 67

4.6.2 The second driving cycle 71
4.6.3 The third driving cycle 74
4.7 Conclusion 78
5. CONCLUSIONS AND FUTURE WORKS 79
5.1 Conclusions 79
5.1.1 The aim of using the SynRM in the PEV 79
5.1.2 The SVPWM technology 80
5.1.3 The PSO strategy 81
5.1.4The purpose of using EDC 81
5.1.5The cascaded-PI and PID controllers 81
5.1.6 The driving cycle 82
5.2 Future Works 83
REFERENCES 84
THESIS APPENDIX 87
Appendix A. Switching condition and vectors of the output. 87
Appendix B. Characteristics of the EV's battery. 87
Appendix C. Electric vehicle parameters. 87
Appendix D. Tuning of PID controller using Particle Swarm Optimization 88
CURRICULUM VITAE 93

M.Sc. THESIS

MODELLING AND SIMULATION OF A PROPULSION ELECTRIC VEHICLE SYSTEM

MOHAMMED AYAD RADHI ALKHAFAJI

Aksaray University
Graduate School of Natural and Applied Sciences
Department of Electrical Electronic and Computer Engineering

Supervisor: Assoc. Prof. Dr. Yunus Uzun

ABSTRACT

Electric Vehicles (EVs) are a scientific revolution in the development of cars and clean energy concerning the use of electricity as a source of energy instead of fuel. Raise in global warming, polluting the environment and loss of petroleum products make the EVs the perfect choice to overcome these problems. The main purposes of the electric vehicles are powerful structure, less of maintenance and less of power. Each one of these characteristics originated from the drive system because the drive system signifies the backbone of the EVs. In this particular thesis, there is two synchronous reluctance motor (SynRM) which have been used to operate the vehicle. In this system, the space vector pulse width modulation inverter for voltage source (VS-SVPWMI) has been employed to convert the DC battery voltage to three-phase AC voltage that feeds the electric motor. The optimized cascaded PID controller is used to regulate the SRM speed. Particle Swarm Optimization (PSO) algorithm has been applied to reach the value of the optimal parameter for the controller. Electronic differential controller (EDC) and electric vehicle system model were simulated. The EDC regulates the electric vehicle performance balance under the various procedure and road conditions. The proposed electric vehicle gives a stable and suitable performance along the different road conditions for each driving cycle. Matlab/Simulink program was used to control the propulsion drive electric vehicle system in this study.

Keywords: SynRM, SVPWM, Inverters, d-q Transformation, Electric vehicle, EDC, PSO algorithm, Driving cycle, Matlab/Simulink.

February, 2019; 93 pages

YÜKSEK LİSANS TEZİ

İTMELİ BİR ELEKTRİKLİ ARAÇ SİSTEMİNİN MODELLEMESİ VE SİMÜLASYONU

MOHAMMED AYAD RADHI ALKHAFAJI

Aksaray Üniversitesi
Fen Bilimleri Enstitüsü
Elektrik Elektronik ve Bilgisayar Mühendisliği Bölümü

Tez Danışmanı: Doç. Dr. Yunus Uzun

ÖZET

Elektrikli Araçlar, enerji kaynağı olarak benzin yerine elektriğinin kullanılması bakımından arabaların gelişiminde bilimsel bir devrimdir. Global ısınma artışı, çevre kirliliği ve petrol üretimindeki azalma elektrikli araçları bu problemlerin üstesinden gelmek için mükemmel bir seçenek haline getirmiştir. Elektrikli araçların temel amaçları sağlam yapı, daha az bakım ve daha düşük enerji tüketimidir. Sürücü sistem, lektrikli araçların omurgasını oluşturduğu için bu özelliklerin her biri sürücü sisteminden kaynaklanmaktadır. Bu tez çalışmasında, aracı çalıştırmak amacıyla kullanılan iki adet eş zamanlı relüktans motor (SynRM) bulunmaktadır. Bu sistemde, DA batarya gerilimini üç fazlı AC gerilime dönüştürerek elektrik motorunu beslemek amacıyla gerilim kaynağı için uzay vektör darbe genişlik modülasyonlu dönüştürücü (VS-SVPWMI) kullanılmıştır. ARM hızını ayarlamak için, optimize edilmiş kademeli PID denetleyici kullanılmıştır. Denetleyici için en uygun parametre değerine ulaşmak amacıyla Parçacık Sürü Optimizasyonu (PSO) uygulanmıştır. Elektronik diferansiyel denetleyici (EDD) ve elektrikli araç sistemi modeli benzetimi yapılmıştır. EDD, çeşitli işlem ve yol şartlarında, elektrikli aracın performans dengesini düzenlemektedir. Önerilen elektrikli araç her bir sürüş biçimi için farklı yol şartlarında kararlı ve uygun bir performans sağlamaktadır. Bu çalışmada, itme sürüşlü elektrikli aracı kontrol etmek için Matlab/Simulink programı kullanılmıştır.

Anahtar Kelimeler: SynRM, SVPWM, Dönüştürücüler, d-q Dönüştürme, Elektrikli araç, EDD, PSO algoritması, Sürüş döngüsü, Matlab/Simulink.

Şubat 2019; 93 sayfa

LIST OF FIGURES

Page

Figure 1.1. The charging-station of EV and in sweden. 2
Figure 1.2. The classical electric vehicle platform system. 3
Figure 1.3. The propulsion EV platform system..4
Figure 1.4. Traction EV platform system. 4
Figure 1.5. Four-wheel-two motors drive EV platform system. 5
Figure 1.6. The four-wheel drive EV system...6
Figure 2.1. The mechanical design contents of IM and SynRM……………..……………...14
Figure 2.2. Losses comparison between SynRM and IM motors. 15
Figure 2.3. IE4 SynRM from ABB company. 15
Figure 2.4. SynRM d-q axis equivalent circuit. 16
Figure 2.5. The direct and quadratic voltage transformation. 18
Figure 2.6. Three-phase voltage-source inverter circuit connected to power supply. 20
Figure 2.7. The six sectors of the SVPWM. 21
Figure 2.8. SynRM model block design. 23
Figure 2.9. The SynRM drive system block. 23
Figure 2.10. The block simulation of two axis of SynRM...24
Figure 2.11. The d-q transformation matrix block..24
Figure 2.12. The direct-axis current block...25
Figure 2.13. The quadrature-axis current block...25
Figure 2.14. The SynRM speed at 25 Hz of frequency with no load condition. 27
Figure 2.15. The SynRM torque at 25 Hz of frequency with no load condition. 27
Figure 2.16. The q-axis current at 25 Hz of frequency with no load condition. 27
Figure 2.17. The d-axis current at 25 Hz of frequency with no load condition. 28
Figure 2.18. The SynRM speed at and 50 Hz of frequency with no load condition. 28
Figure 2.19. The SynRM torque at no load condition and 50 Hz of frequency. 28
Figure 2.20. The SynRM speed at with 20 Nm of load at 1.4 second. 29
Figure 2.21. The SynRM torque at with 20 Nm of load applied at 1.4 second. 29
Figure 3.1. Speed control simulation of the SynRM by using SVP…………………………32
Figure 3.2. Traditional-PID-controller...33
Figure 3.3. General design for cascade control system...35
Figure 3.4. The cascaded control design for SynRM...36
Figure 3.5. Simulink model for cascade-PI and lead- lag controller. 37
Figure 3.6. SynRM speed control at 1500 rpm with no load condition. 38
Figure 3.7. The SynRM torque control at1500 rpm with no load condition...........................39
Figure 3.8. The SynRM speed control at steps of speed. 39
Figure 3.9. The SynRM torque control at steps of speed...39
Figure 3.10. The SynRM speed control with 1500 rpm and 50 Nm of load applied at 3.5 second. 40
Figure 3.11. The SynRM torque control at 1500 rpm with 50 Nm of load applied at 3.5 second. 40
Figure 3.12. Simulink model for PI, PID and lead-lag controllers. 41
Figure 3.13. The SynRM speed control at 1500 rpm with no load condition.........................42
Figure 3.14. The SynRM torque control at 1500 rpm and no load condition. 43
Figure 3.15. The SynRM speed control with steps of speed..43
Figure 3.16. The SynRM torque control with steps of speed. 43
Figure 3.17. The SynRM speed control with 1500 rpm and 50 Nm step of load applied at 3.5 second. 44

Figure 3.18. The SynRM torque control with 1500 rpm and 50 Nm step of load applied at 3.5 second.. 44
Figure 3.19. General flow chart for PSO algorithm...46
Figure 3.20. Simulink model for PSO fitness function...49
Figure 3.21. PID simulink system by apply the PSO alograthim. 50
Figure 3.22. The SynRM speed control with 1500 rpm with no load condition. 52
Figure 3.23. The SynRM torque control with 1500 rpm with no load condition. 53
Figure 3.24. The SynRM speed control with steps of speed..53
Figure 3.25. The SynRM torque control with steps of speed. 53
Figure 3.26. The SynRM speed control with 1500 rpm and 50 Nm steps of load applied at 3.5 second. 54
Figure 3.27. The SynRM torque control with 1500 rpm and 50 Nm steps of load applied at 3.5 second. 54
Figure 4.1. The main components of the propulsion EV system platform………………….56
Figure 4.2. An EV platform driven in a curve road……………………………………….. 56
Figure 4.3. The input and output of the EDC on the curve road………………………… 57
Figure 4.4. The propulsion EV chain construction drive by one motor……………………. 59
Figure 4.5. The simulation of EDC system…………………………………………………60
Figure 4.6. The EV moving with 80 km/h speed rate at the straight road…………………... 61
Figure 4.7. The EV turn right with 80 km/h speed rate at the curve road with +11 degree steering angle………………………………………………………….... 61
Figure 4.8. The EV turn left with 80 km/h speed-rate at the curve-road with +11 degree steering angle…………………………………………………………….61
Figure 4.9. Modelling and simulink of PEV model………………………………………... 63
Figure 4.10. The effective forces of the EV in an inclined road…………………………....64
Figure 4.11. Modelling and simulation of the resistive-force………………………………65
Figure 4.12. The first driving cycle of the EV includes three stages………………………. 68
Figure 4.13. The linear speed of the EV…………………………………………………. 69
Figure 4.14. The linear speed at the left wheel of the EV…………………………………. 69
Figure 4.15. The linear speed at the right wheel of the EV………………………………... 69
Figure 4.16. The torque at the left wheel of the EV……………………………………….. 70
Figure 4.17. The torque at the right wheel of the EV……………………………………… 70
Figure 4.18. The second driving cycle of the EV include three different stage…….............72
Figure 4.19. The linear speed of the EV at three stages……………………………………. 72
Figure 4.20. The linear speed at the right wheel the EV…………………………………… 73
Figure 4.21. The torque at the right wheel of the EV……………………………………… 73
Figure 4.22. The torque of the left wheel of the EV……………………………………….. 73
Figure 4.23. The third drive cycle with four stages……………………………………….. 75
Figure 4.24. The linear speed of the EV at 80 km/h of speed rate………………………… 75
Figure 4.25. The linear speed of the left wheel…………………………………………… 76
Figure 4.26. The linear speed of the right wheel………………………………………… 76
Figure 4.27. The torque of the left wheel………………………………………………… 77
Figure 4.28. The torque of the right wheel………………………………………………... 77
Figure 4.29. The complete drive cycle simulition system………………………………….. 78
Figure 4.30. Single simulator system for testing the steering-wheel……………………… 78

LIST OF TABLES

Page

Table 2.1. The component parameters of the SynRM. 25
Table 2.2. The characteristics output of the SynRM. 30
Table 3.1. The characteristics and parameters of the tradition controller …………………......34
Table 3.2. The parameters and values of the cascade controller. 37
Table 3.3. Manually tuned of the cascade controller. 40
Table 3.4. The characteristics of PSO algorithm. 51
Table 3.5. PSO strategy tuned in cascade controller parameters. 51
Table 4.1. The load information for the first driving cycle…...……………………………..70
Table 4.2. The load information for the second driving cycle. 74
Table 4.3. The loads information for the third cycle. 77
Table 5.1. A compression with result between SynRM and SRM features that has applied at the EV system ...………….………………………….…………...………………..80

LIST OF ABBREVIATIONS

AC	Alternating current
ASD	Adjustable Speed Drive
ASR	Acceleration Slip Regulation
BLDC	Brushless Direct Current
CAN	Controller Area Network
DC	Direct current
EDC	Electronic Differential Controller
EMF	Electro Motive Force
EV	Electric Vehicle
FLC	Fuzzy Logic Controller
HEV	Hydride Electric Vehicle
HFSMC	Hybrid Fuzzy Sliding Mode Control
IAE	Integrated Absolute Error
ICM	Internal Combustion Engine
IM	Induction Motor
ISE	Integrated of Square Error
ITSE	Integrated of Time weight Square Error
MCMMS	Multi Converter Multi Machine System
PEV	Pure Electric Vehicle
PID	Proportional Integral Derivative
PMSM	Permanent Magnet Synchronous Motor
PSO	Particle Swarm Optimization
PWM	Pulse Width Modulation
RPM	Revolutions Per Minute
SA	Simulated Annealing
SISO	Single Input Single Output
SMC	Sliding Mode Control
SPA	Split Parallel Architecture
SOC	State of Charge
SRM	Switch Reluctance Motor
SVM	Space Vector Modulation
SVPWM	Space Vector Pulse Width Modulation
SynRM	Synchronous Reluctance Motor
VSI	Voltage Source Invertor
VS-SVPWM	Voltage Source Space Vector Pulse Width Modulation
4WDEVS	Four Wheel Drive Electric Vehicle System
4WDTMEVS	Four Wheel Drive Two Motor Electric Vehicle System
$\mathbf{A_f}$	Frontal Surface Area
B	Viscous friction coefficient
$\mathbf{C_1}$	Self-recognition PSO coefficient.
$\mathbf{C_2}$	Social PSO coefficient.
$\mathbf{C_d}$	aerodynamic drag coefficient
D(i)	The Wanted Output
$\mathbf{d_\omega}$	Width of Electric Vehicle

$\mathbf{e(t)}$	Error Signal
$\mathbf{f_r}$	Rolling Resistance Force Constant
$\mathbf{f_s}$	Switching Frequency
$\mathbf{g}$	Gravity Acceleration
$\mathbf{I_d}$	Stator Direct Axis Current
$\mathbf{I_q}$	Stator Quadrature Axis Current
$\mathbf{J}$	Moment of inertia
$\mathbf{k_d}$	Derivative gain of PID controller
$\mathbf{k_i}$	Integral gain of PID controller
$\mathbf{k_p}$	Proportional gain of PID controller
$\mathbf{L_d}$	Direct Axis Reluctance
$\mathbf{L_q}$	Quadrature Axis Reluctance
Lw	Vehicle length
$\mathbf{m}$	Vehicle Total Mass
$\mathbf{n_{ref}}$	Reference Speed
P	Number of poles
R	Radius of the Road
$\mathbf{R_s}$	Stator resistance
$\mathbf{T_e}$	Electromagnetic torque
$\mathbf{T_L}$	Load torque
$\mathbf{T_s}$	Sampling Period
$\mathbf{T_z}$	Switching Period
$\mathbf{u(t)}$	control output
Va,Vc,Vb	Motor three phase voltages
$\mathbf{V_d}$	Direct Axis Voltage
$\mathbf{V_L}$	Left Wheel Linear Speed
$\mathbf{V_q}$	Quadrature Axis Voltage
$\mathbf{\bar{V}_{ref}}$	Inverter Reference Voltage
$\mathbf{V_R}$	Right Wheel Linear Speed
$\mathbf{v_s}$	Source voltage
$\boldsymbol{\omega_r}$	Motor Angular Speed
$\boldsymbol{\omega_m}$	Angular speed of the motor
$\boldsymbol{\omega_v}$	Vehicle Linear Speed
x	Random position of PSO
y(i)	The output model
$\boldsymbol{\alpha}$	Inverter Sector Angle
$\boldsymbol{\beta}$	Slope Angle of The Road
$\boldsymbol{\delta}$	Steering Angle of the Road
$\boldsymbol{\rho_{air}}$	Air Density

1. INTRODUCTION

1.1 Background About Electric Vehicles Components

Recently, most of the vehicles factories have moved to the manufacture and development of electric vehicles (EVs) also known as Pure Electric Vehicle (PEV). The main reasons for this development were; reducing accidents, oil economy, clean environment, global warming and the decrease of the available natural resources. Therefore, a new generation of vehicles achieves these goals.

Besides, the EV invention is an older innovation, it had been initially suggested in the 19th century, but into notification that the last few years it required a significant role and became famous as Internal Combustion Engine (ECI) (Roukas, 2013). The central obstacles to this types of car from evolving are a high cost of component exceptionally, high voltage batteries, limited rate of speed and a rareness of infrastructures of charging stations (Karamuk et al., 2013).

In addition, the EVs have been used as taxis and as personal cars to travel around in the city because the existence of trains and planes to move for the extended distant areas. Now in most European, Eastern of Asia Nations and North America has used the EVs as taxis due to its low cost compared to ECI. Besides, the EVs are so prevalent in Sweden. The solar charging station is omnipresent around the city due to its low price as compared to ECI that results in the new production of vehicles have two main benefits are maintaining the clean surroundings and reducing the price. An EV in charging station in Sweden is shown in Figure 1.1.

Moreover, the synchronous reluctance motor (SynRM) has become an essential part of many electrical and mechanical industries in a few recent years. The SynRM has several characteristics and features which made it different from other types of electric motor that previously used in many sectors in the same field and especially for the EV.

Figure 1.1. The charging station of EV and in sweden (URL-2).

1.2 Electric Vehicles Classification

Usually, the electric vehicles divided into two types, which are hydride electric vehicles (HEV) and Pure Electric Vehicles (PEV). The small breeds that divided from both of these kinds depending on different aspects associated with the driving system, vehicle constrictions, costumer’s arrangement and along with other issues depend on the design specification (Karamuk et al., 2013; Roukas, 2013).

Moreover, the structure of the electric vehicle varies from one type to another. Where the structure of the vehicle can be designed from single, double, trouble and quadrature electric motors depending on the vehicle type. The classification of the EV depends on the location of the electric motor and the design mechanism. The pure electric vehicles could be organized into five type and each model will be described as below (Salem, 2013; Gasbaoui, 2012) :

1.2.1 The classical EV system

The classic electric vehicle is considered as the first and simplest type of the EV order, which it has a center single motor in the vehicle construction that pushes the rear wheels of the EV. In addition, both of the electric motors and the vehicle platform are considered as a subsystem of the EV construction. According to the characteristics and the manufacturing of the EV, the drive system depends on the reliability of the electric motor and battery to provide the car with sufficient power. Therefore, the drive system represented by the electric motor should provide high torque and large load capability. The DC motor has utilized due to the simplicity of control as well as the sum of variation in speed and torque. Figure 1.2 reveals the classic EV system.

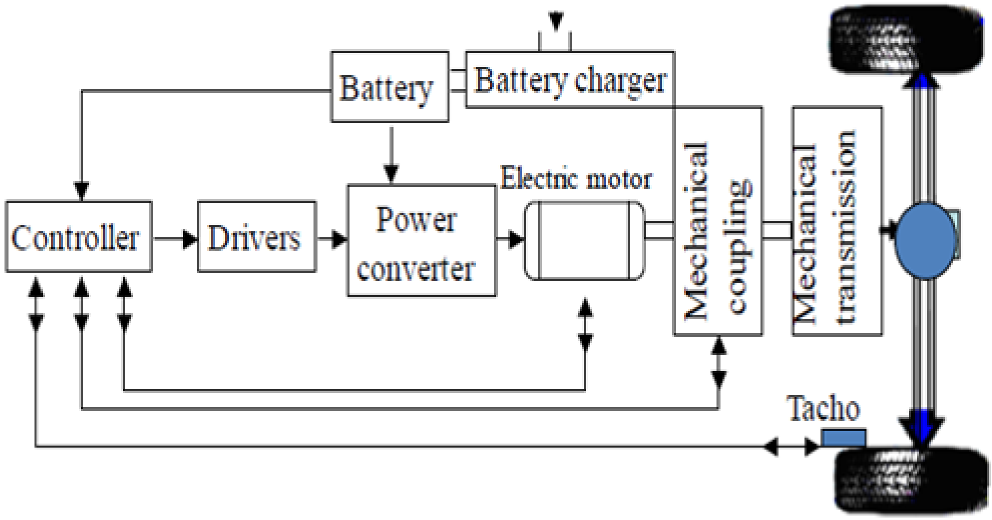

Figure 1.2. The classical electric vehicle platform system (Salem, 2013).

1.2.2 The propulsion EV system

The propulsion electric vehicles are considered as the second type of the pure electric vehicles, which include a dual electric motor that guarantee the drive of both rear driving wheels and each motor work separately. The inner construction system for this type of EV has controlled by an EDC system that ensures the robustness of the motor vehicle. In addition, the propulsion electric vehicle system process has referred to as a multi-converter/multi-machine system (MCMMS). Moreover, the pure electric vehicle is much simplified and similar to the traditional mechanical vehicle in the work way, because of slipping issues from the curvature or slope “inclined” angle roads. This model of the EV has utilized in this thesis. The propulsion EV platform system is shown in Figure 1.3.

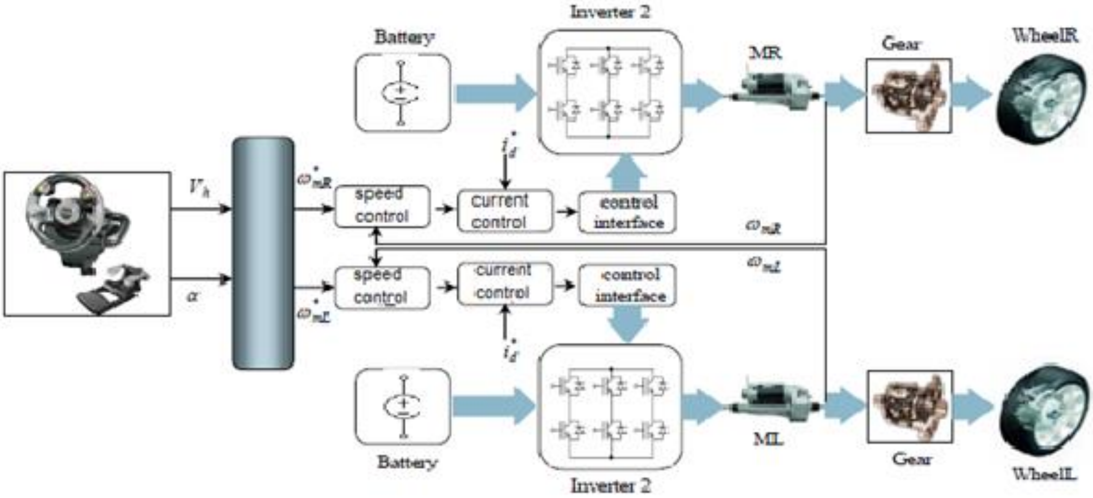

Figure 1.3. The propulsion EV platform system (Hartani et al., 2009).

1.2.3 The traction EV system

The traction electric vehicle system considered as the third type of the pure electric vehicles order, which it has dual motors in its construction like the propulsion electric vehicle system, but those motors drive both of the frontal wheels of the EV. Besides, the principle of performing nearly the same in MCMMS of the propulsion electric vehicle. Traction EV platform system is shown in Figure 1.4.

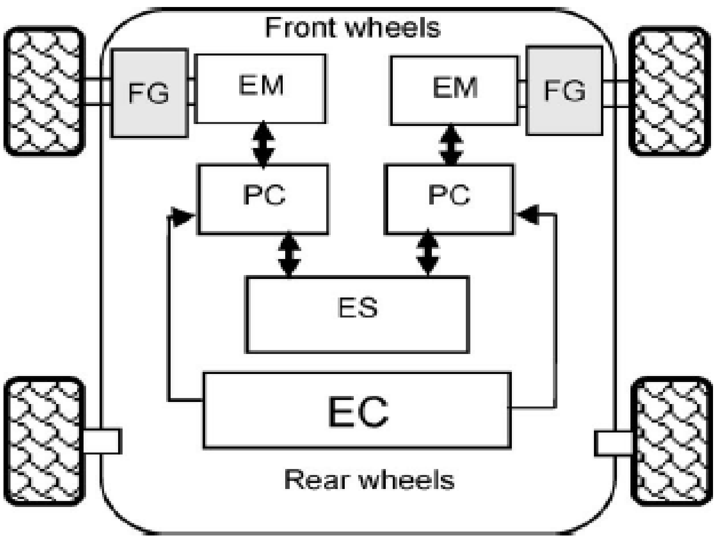

Figure 1.4. Traction EV platform system (Tabbache et al., 2011).

1.2.4 The four-wheel two motors EV system

The Four-Wheel Two Motors Drive EV System (4WD TMEVS) is considered as the forth type of the pure electric vehicle order, also this type is relatively similar to the regular SUV. The principle design includes two electric motors which each motor drives and control both of two wheels. In addition, the first electric motor status in the front of the vehicle platform to push the front wheels. Besides, the next motor drive status in the rear of the vehicle platform to push the rear wheels. Moreover, the acceleration slip regulation (ASR) is another kind of control techniques, which has employed to control both of motors to guarantee a secure and effective movement of this vehicle type in various road conditions. Figure 1.5 reveals a Four Wheel Two Motors Drive EV system.

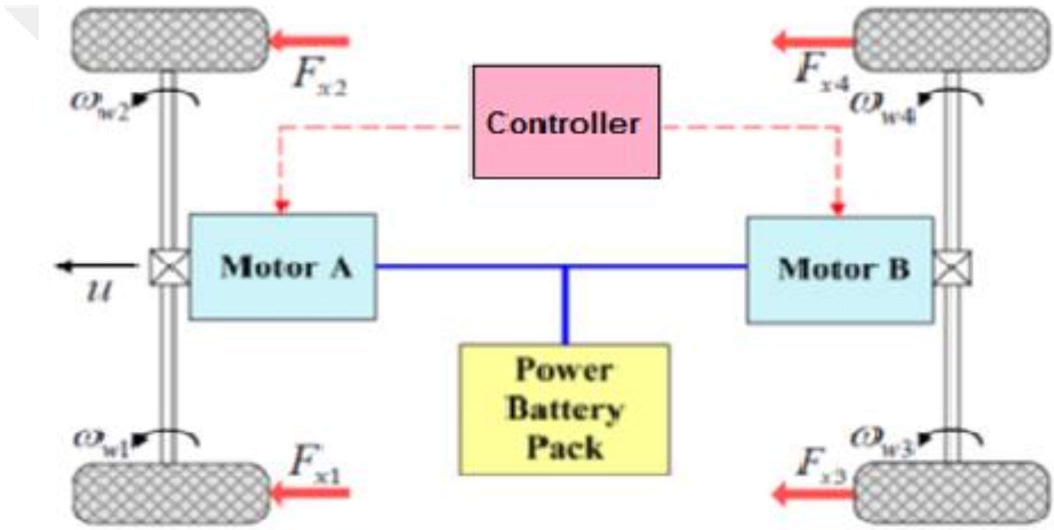

Figure 1.5. Four wheel-two motors drive EV platform system (He et al., 2014).

1.2.5 The four-wheel EV system

The Four Wheel Drive EV System (4WD EVS) is considered as the fifth type of the pure electric vehicle order, which includes four electrical motors in principle design of the vehicle and each motor drives one wheel separately. This vehicle is characterized by a high rate of control and high capacity of transformation with many various roads such as sloping, slippery and elevated roads. Besides, the driving speed rate is calculated separately for each motor depending on a various road condition. To reduce the difference between the actual steering-torque and the reference steering-torque of the vehicle, both of the vehicle speed and the steering-wheel position are controlling this problem. Figure 1.6 reveals a four-wheel drive EV system. As explained in Figure 1.5, the sort of this well-known EVs that categorized according to the job of the drive system the many known electric drive systems that have been utilized in EV is induction motors (IM), brushless DC motors (BLDC), permanent magnet synchronous motors (PMSM), change reluctance motor (SRM) and DC motors.

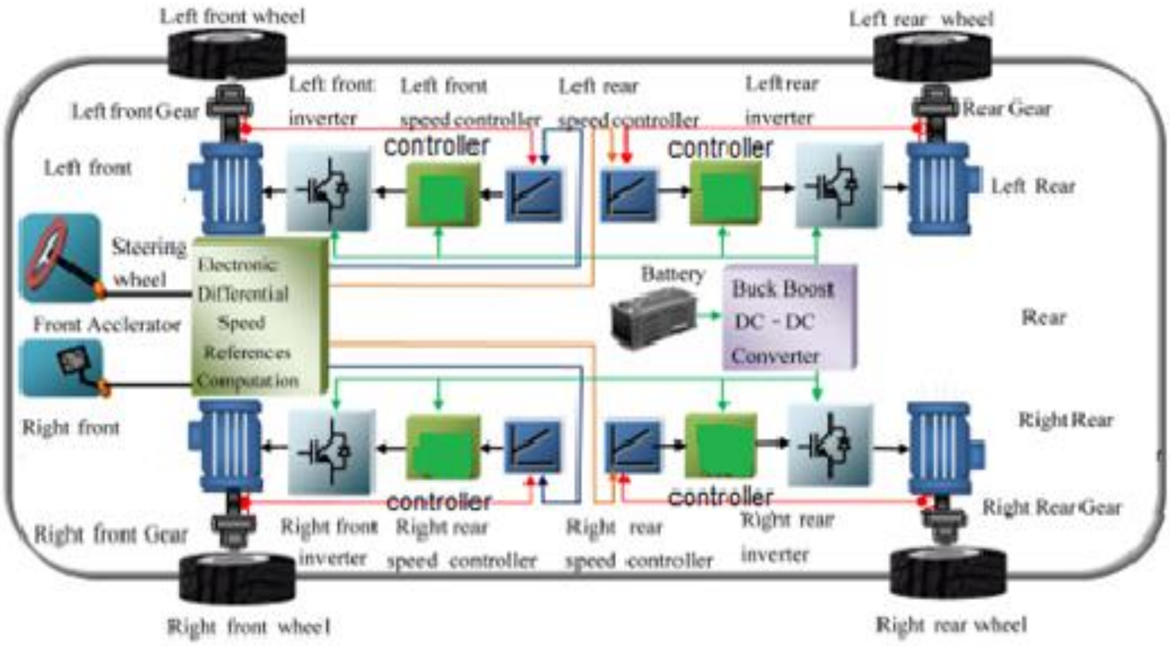

Figure 1.6. The four-wheel drive EV system (Gasbaoui, 2012).

1.3 Reported Studies About Electric Vehicles

Since decades, the computer and the electronic devices have been considerably evolved and improved. Besides, the smart and optimum control utilized to fit with the new technology needs and has become quite popular. The channels are getting to be familiar over decades that controls the PEVs. The hydride EVs became renowned as the tradition vehicles. Hence, the survey of EVs are representing as follows:

Malan and Kamper (2001) suggested an HEV, which has a little reluctance synchronous machine drive has introduced. The device is controlled for maximum torque per ampere or minimal kVA that makes sure that the machine has been worked relatively near the optimum efficacy for all load conditions. Besides, the simulation and the quantified results demonstrate that using the little reluctance synchronous machine drive creating a peak torque of 150 Nm, the weight of the vehicle is1480 kg, also it accelerates from zero to 60 km/h in 19 seconds. The assortment of the HEV on a single battery charge is quantified as 90 km/h in 60 km/h.

Chan (2002) suggested development topics for both EVs and HEVs, which urge the entry of engineering and plastic art into the construction and design of vehicles to meet customer demands. Moreover, the HEV has a disadvantage in the complexity to find the optimal parameters to the multiple energy sources. As compassion between the EVs and the HEVs preferred that EVs have a little problem than HEVs.

Van den Bossche (2003) beginning with the genesis of their specific car standards in the 20^{th} century introduces the growth of standardization concerning electrically driven vehicles with the past and future. Besides, it has suggested an encountered consequence of the study on both sides.

Hassan et al., (2005) suggested a contrast involving the Particle Swarm Optimization (PSO) and Genetic Algorithm (GA). To inspect the claim that PSO has accurately the same efficacy "locating the true global optimum solution" since the GA but with considerably better computational efficiency "fewer function tests" by applying statistical evaluation and appropriate hypothesis testing. The GA and PSO's performance comparison is executed with two different systems that determine and optimization the problems to control the E

Azzeh (2007) presented the design, execution and evaluation results of the Controller Area Network (CAN) control system for MR2. Besides, the 312Vdc battery voltage has been switched into an intermediate voltage of 48Vdc. Moreover, this configuration is considered more effective than the 12Vdc distribution system, because lighter and smaller cables may be utilized to carry the exact same quantity of power. The power distribution that operates with 48Vdc offers a perfect and stable output power for the EV.

Boyd and Nelson (2006) specify the performance strategy to get a Split Parallel Architecture (SPA). The HEV is accomplished by calculating power part losses. The results of the calculations specify fuel consumption can decrease while maintaining auto emissions. Besides, for an HEV operating the motor of the vehicle in its areas of efficiency does not guarantee that the vehicle operation.

Sivanandam (2007) indicated a PSO Algorithm and Simulated Annealing algorithm (SAA). Besides, the PSO and SAA performs allocation of jobs in a distributed computing platform. Particle Swarm Optimization with reducing inertia is executed which yields an outcome that was much better than inaction. The results attest the technique that is proposed is efficient and successful in discovering solutions.

Haddoun et al. (2008) proposed a neural network control arrangement (NNCA) for EV system also that control machine promise to induce a car equilibrium with no utilization of the reduction equipment, so it became possible to have torque and speed in every wheel with two IM signifies the EV's drive method. In addition, a neural network algorithm was used to compute the car rate. EDC has been utilized to calculate the benchmark speed. After simulation and assessing of the EV system, it has demonstrated it a functional and efficient operation. The network control system provides a functionality to the EV platform.

Nasri et al., (2009) proposed a Hybrid Fuzzy Sliding Mode Control (HFSMC) to control driving wheels motors of the EV and it was replaced by the fuzzy logic control system (FLC), which this type of control gives a stability performance to control the driving wheels of the EV. Besides, the system fulfilled an efficient and stable control response with no overshoot. The rising time is mastered with good disturbances rejections as compared with the classical control law. Besides, there was two IMs had been used as a drive system. The reduction gears have been used to ensure the transition of motor torque to the driving wheels.

Nasri et al., (2010) used a new control technology to control an EV platform. Besides, he compares it with other technologies and reveals the best control strategy from the outcomes result that has been gathering them from the versions tests of the control systems. The first technique is the regulator that rely on PI controllers, which control the drive system's rate. The FLC has been employed and tested for two of IM drive, which makes the EV system sensitive for version road conditions because advancement is given. The several load states have been applied to the EV to test the activity of the system and the speed rate response.

Tuncay et al., (2011) designed a new brand and introduced a new program system of the EV and designed the axle drive system for the HEV. Besides, he used two electric motors in the design to drive the rear wheels of the EV. The EDC was placed instead of the mechanical differential, which deepened on the wheel steering angle detection as well as the acceleration pedal rate. Moreover, several street conditions are analyzed and test results that were potent are obtained the optimum designs for electric drive, the ICE and Battery Power. Driving cycles are investigated to test the EV system.

Gasbaoui (2012) suggest a new version of EVs, which include four IMs and every single motor connected to one of those four wheels of the EV. Besides, this system known as Four Wheels Drive Electric Vehicle (4WDEV). Besides, the suggested control system for this particular EV process is direct torque control based upon the space vector modulation (SVM). The lithium-ion battery has been utilized as a DC source of the motor vehicle. The EDC system calculates the benchmark rate of electricity and torque to every motor in line with the street specification. The major novel of the work will be to make sure that the first battery state of charge equivalent seventy percent. Moreover, the model has been tested in various rate and topology states, which results this system could be successfully executed to 4WDEV.

Ravi and Palani (2013) suggested a new control strategy for controlling the EV that was the ED control system. The PIC microcontroller (PIC-16F877A) has been used for controlling the system which is made up of two BLDC motors. Besides, it guarantees the driver of both rear driving wheels. Besides, each wheel has been controlled so that every wheel turn at rate requirements that were different. The MATLAB/Simulink program is utilized to simulate the EMF zeroes rear crossing detection process BLDC motor. The performance satisfactory has given by the results with the digital control scheme that ensures the equilibrium of the EV in the road conditions.

Hongwen et al., (2014) proposed a new version of an ASR program system for the 4WDEV that drive the front wheels of the EV. The ASR control approach contains three handle control modes, which are; the control modes average distribution of inter-axle torque, the optimal distribution of inter axle torque and independent control of the optimal slip rate respectively. Besides, the drive's system includes two of PMSMs for building the EV system. Therefore, the dual electric motors are sharing work simultaneously to drive the EV, which is divided as one motor drive the rear wheels and another drive the front wheels of the EV with respect the equation of slip rate that specific describing the minimal of the tire slide procedure in an auto speed situation.

1.4 The Purpose of This Thesis

This study thesis aims to simulate and design the essential elements of the propulsion electric vehicle infrastructure and enhance those features by using different strategies to choose the optimal result after the simulation. Therefore, this work also includes design and simulation of synchronous reluctance motor (SynRM) that have used to drive the EV and suggests two axes version with utilizing the cascade conventional PID controllers to control the speed rate of SynRM. While the PSO strategy has used to get optimal the parameters and apply them in the other controllers. Hence, this thesis concentrates on controlling the vehicle's speed and test the response activity of the EV by applied many different loads in several road conditions.

1.5 Thesis Outlines

This thesis study has included five sections, which explained by the following points:

1. Section 1: Represents an introduction to the work and reported studies about electric vehicles.

2. Section 2: Represents a complete design of the SynRM model. The design and modeling of the SynRM have implemented by Matlab/Simulink program. Besides, the results reveal of SynRM model's validity to succeed under an operation condition with complete the design of SynRM and simulate the six sectors of the motor by utilized the Space Vector Pulse Width Modulation voltage source inverter (SVPWM).

3. Section 3: Represent the speed and torque control of the SynRM model by using the PSO strategy and cascade-PI, PID and lead-lag controller. In besides, the PSO algorithm has applied to discover the value of the optimal parameter. The simulation results demonstrated that the PSO strategy confers a significant advancement in the SynRM speed rate response better than the rest of the controllers. Hence, a comparison made between the PSO algorithm and the traditional cascade controllers with different motor speed, torque and loads to get a better strategy to control the SynRM model.

4. Section 4: Represent a complete simulation and design for propulsion electric vehicle. The EDC controller system has proposed that is considered as a successful alternative of the gearbox in the ICE vehicles. Besides, the driving cycle topology has applied to the PEV system and it includes three different drive-cycles. Therefore, each drive cycle has many stages with different road-condition to test the functionality and stability of the EV under several road conditions and different road-angles.

5. Section 5: Represents the discuss conclusions and suggestions for future works.

2. SIMULATION AND ANALYSIS OF SYNRM

2.1 SynRM Operation Theory And Features

The SynRM is one of several synchronous machines. The structure of the SynRM rotor has manufactured without winding or magnet material. As a comparison between SynRM with other types of reluctance motors like IM, BLDC motor and switch reluctance motor SRM, the result shows that SynRM is precision in manufacturing, simple structure. Besides, it has a distinctive property like low torque average, more substantial torque pulsation and low power factor. In fact, the SynRM may give a high stable performance in contrast with other AC drives compared with IM. The SynRM is a three-phase motor operated by three-phase of space vector inverter.

Generally, the SynRM is a kind of synchronous machines that have no winding or permanent magnet on the rotor and salient poles, also it has a fragmented rotor of the numerous barriers. The reason for made the reluctance motor rotor form laminated axially steel it has to dominate low torque response and unsuitable power factor, although older versions of reluctance motor have lacked this technology of manufacturing. The stator-winding layout of SynRM is quite similar to the IM.

Besides, once the magnetic field flow in the stator winding and according to the rotor structure it is a low and high hesitation area, also they signify practically the magnetic poles (Fellani and Abaid, 2013; Malan and Kamper, 2001; Consoll, et al.,1999). The rotor design in SynRM has rotated to reach the low reluctance areas and drifting away of the high reluctance areas in the same time of rotate, the reason of this work strategy to achieve the magnetic field synchronous speed. The stator formula to both of SynRM and IM are the same signal into the rotating frame.

Therefore, the SynRM considered as an appealing and famous choice for numerous industrial and automotive applications due to all of those significant and unusual characteristics (Khubalkar et al., 2017; Emadi, 2005; Reddy et al., 2012). The earliest versions of SynRMs have used a caged rotor directly; the most crucial reason that pristine SynRMs do not have beginning torque attributes.

Moreover, the modern SynRM is using the newest kinds of inverters and field orientation control technology (FOC) along with the pulse width modulation (PWM) which supply a convenient technique for control the motor without any rotor (Soltani and Zarchi, 2004). The speed variable parameters have used in SynRM motor system design to correct the motor speed drive due to several elements like energy conservation, control situation, velocity and enhancement of the transient response characteristics. A motor speed controller aims to take a signal representing, the reference speed and to drive the motor at that reference speed (Fellani and Abaid, 2013).

In addition, the control system consists of a SynRM, a voltage source space vector inverter, a controller and speed settings controllers that been feedback from the system. The primary reason for using feedback in these systems is to be able to obtain a reference-point regardless of any variation or other concern in the characteristics the system back to the reference point. Figure 2.1 shows the SynRM rotor flux barrier and IM motor rotor cage.

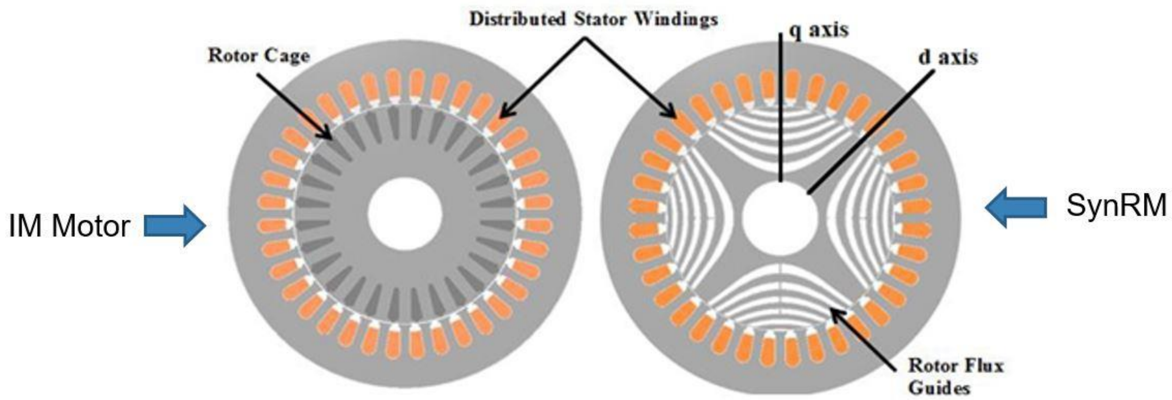

Figure 2.1. The mechanical design contents of IM and SynRM (Donaghy, 2016).

Moreover, the most attractive charestrictics of SynRM against IMs ,BLDC motors and SRMs that has preveslly using in the electric vehcle desine are:

A. The power output of SynRM is about 80% of the IM output torque, while the SynRM has half of the power Losses when compare it with the IM.
B. With the same dissipated power the SynRM has, i.e. with the same temperature of the stator winding, it have a higher torque produced than IM.
C. The SynRM benefit on BLDC motor its robustness and inexpensive rotor structure.
D. The SynRM benefit when compare it with the SRM it has a very much lower torque ripple (Sathyan, 2013; Fellani and Abaid, 2013).

Figure 2.2 shows a power losses comparison between the IM and SynRM. Moreover, Figure 2.3 shows the SynRM that has taken from the datasheet of ABB motors.

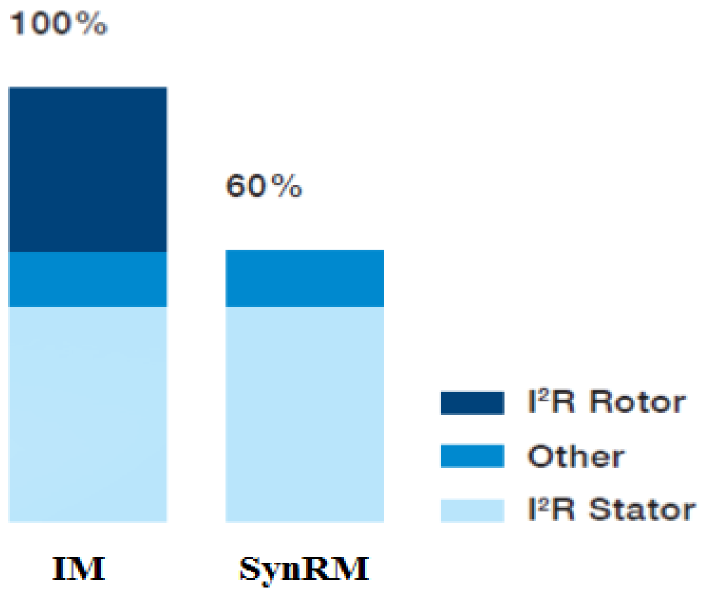

Figure 2.2. Losses comparison between SynRM and IM motors (Sathyan, 2013).

Figure 2.3. IE4 SynRM from ABB company (URL-1).

2.2 Mathematical Model of SynRM

As mentioned earlier, The SynRM version is quite similar to the induction motor IM. The difference is by neglecting the rotor losses from the IM equations. The three-phase version of SynRM is perfect for assessing motor under performance conditions and control activity. The evaluation is used in the vector control procedure which is the version has utilized. Therefore, the two axes of the SynRM model have employed for its control synthesis. This SynRM version is a powerful instrument for simulation of all AC machines such. In addition, there are two axes readily available: the direct-axis (d) and the quadrature-axis (q), which clarifies the maximum and minimum hesitation regions. The electricity should not alter during transformation. The SynRM's model has described by the following equations (Sathyan, 2013; Fellani and Abaid, 2013):

$$V_d = \mathrm{R}_s \mathrm{I_d} + \frac{\mathrm{d}\lambda_d}{dt} - \omega_\mathrm{r}\lambda_\mathrm{q} \tag{2.1}$$

$$V_q = \mathrm{R}_s \mathrm{I_q} + \frac{\mathrm{d}\lambda_q}{dt} + \omega_\mathrm{r}\lambda_\mathrm{d} \tag{2.2}$$

$$\lambda_\mathrm{d} = \mathrm{L_d I_d} \tag{2.3}$$

$$\lambda_\mathrm{q} = \mathrm{L_q I_q} \tag{2.4}$$

Where:

- L_d and L_q : The direct and quadratic axis twisting self-inductance measured at Henri unit (H).
- R_s : signify the stator winding resistance in an ohm (Ω).
- ω_r: The rotor angular speed in radian per minute (rad/sec).
- λ_d and λ_q: The flux rate of direct and quadratic axis.

Besides, the SynRM motor can be revealed from its d-q stationary axis equal circuits as in Figure 2.2.

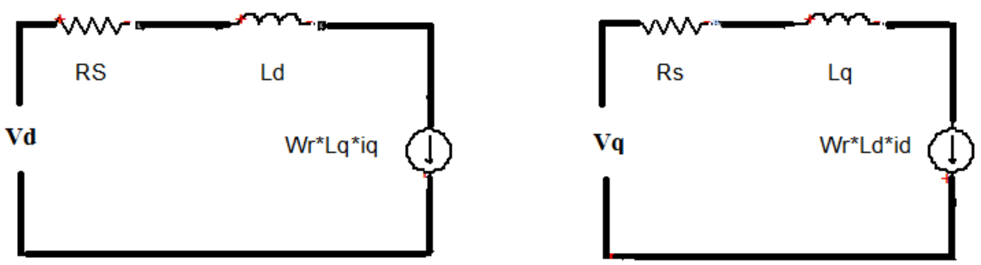

Figure 2.4. SynRM d-q axis equivalent circuit (Fellani, a et al., 2013).

Both of each of equations 2.3 and 2.4 the over could acquire shift speed as will detect in equations 2.5 and 2.6 as follows:

$$\frac{d\lambda_d}{dt} = V_d - R_s I_d + \omega_r \lambda_q \tag{2.5}$$

$$\frac{d\lambda_q}{dt} = V_q - R_s I_q - \omega_r \lambda_d \tag{2.6}$$

From equation 2.5 the change-speed rate of the direct axis current could be gained in equation 2.6.

$$\frac{dI_d}{dt} = \frac{1}{L_d}(V_d - R_s I_d + \omega_r L_q\, I_q) \tag{2.7}$$

Besides, with equation 2.6 the change-speed rate of the quadratic axis current could be gained in equation 2.8.

$$\frac{dI_q}{dt} = \frac{1}{L_q}(V_q - R_s I_q + \omega_r L_d\, I_d) \tag{2.8}$$

In addition, obtain the torque equation for SynRM can as trace in equation 2.9.

$$T = \frac{3}{4}\,\frac{P}{2}\,\left(L_d - L_q\right) I_d I_q \tag{2.9}$$

Where T signifies the electromagnetic torque of this SynRM at Newton per meter (N/m).The speed rate can be acquired by the following equation.

$$\frac{d\omega_r}{dt} = \frac{P}{J}(T_e - T_L) \tag{2.10}$$

Where:

- P : The amount of poles is pairs of this motor and load.
- J : The moment of inertia coefficient of the motor in kilogram square meter ($K_g M^2$).
- T_L : The load torque to the engine inside newton per meter (N/m).

The Laplace transformation to the torque equation is given below in equation 2.11.

$$T = \frac{3}{2}\, P\left(L_d - L_q\right) i_d i_q - (B\omega_r + J\frac{d\omega r}{dt}) \tag{2.11}$$

Where:

- B is the viscous friction coefficient of the motor (Fellani and Abaid, 2013).

2.3 Mathematical Model of Stationary Field Transformation

The transformation from the mechanical model has done by using the d-q transformation, which is used for the vector control method of the synchronous motor machine. The base of the idea which is the windings of the stator are distributed a d-q axis is an effective tool for simulation of all AC machines including the SynRM (Tran, 2012). When Three-phase balanced and adjusted windings are asymmetries to the two-phase equilibrium windings deliver rotating magnetic field speed Φ and value are equal. The Three-phase windings are identical with the two-phase windings. The d-q transformation is well-balanced three-phase V_d, V_b and V_c into balanced two-phase V_d and V_q as shown in Figure 2.3. The conversion matrix is explained in equation 2.12. The simulation is shown in Figure 2.9.

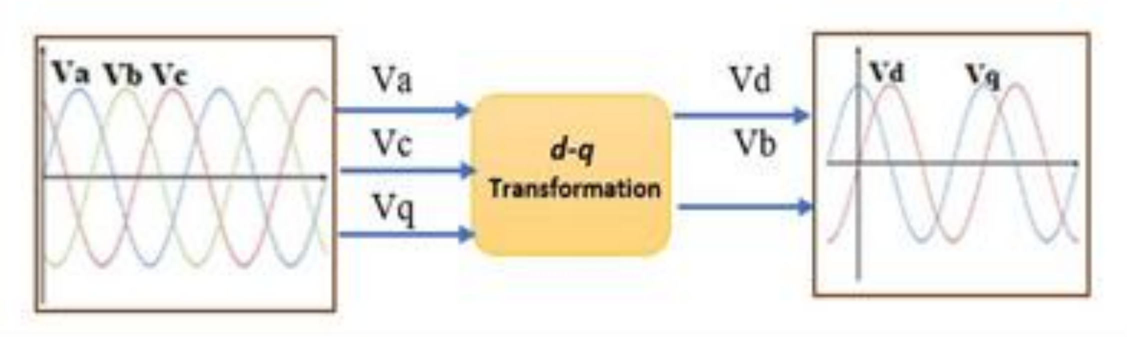

Figure 2.5. The direct and quadratic voltage transformation.

The transformation matrix T has used to convert voltage or current vector fromV_d, V_b and V_c reference frame into V_d and V_q reference frame (Consoli et al., 1999; Daud and Alsayid, 2013).

$$\begin{bmatrix} V_d \\ V_q \\ V_o \end{bmatrix} = \mathbf{T} \begin{bmatrix} V_a \\ V_b \\ V_c \end{bmatrix} \tag{2.12}$$

Where:

- T : The transformation matrix.
- V_d, V_q : The two axes voltages.

The transformation matrix uses either in the synchronous framework as shown in equations 2.12 and 2.13 (Daud and Alsayid, 2013; Tahi et al., 2011).

$$\mathbf{T} = \sqrt{\frac{2}{3}} \cdot \begin{bmatrix} \cos\frac{\pi}{\tau_p}x & \cos(\frac{\pi}{\tau_p}x - \frac{2}{3}\pi) & \cos(\frac{\pi}{\tau_p}x + \frac{2}{3}\pi) \\ -\sin\frac{\pi}{\tau_p}x & -\sin(\frac{\pi}{\tau_p}x - \frac{2}{3}\pi) & -\sin(\frac{\pi}{\tau_p}x + \frac{2}{3}\pi) \\ \frac{1}{\sqrt{2}} & \frac{1}{\sqrt{2}} & \frac{1}{\sqrt{2}} \end{bmatrix} \quad (2.13)$$

$$\mathbf{T^{-1}} = \sqrt{\frac{2}{3}} \cdot \begin{bmatrix} \cos\frac{\pi}{\tau_p}x & -\sin\frac{\pi}{\tau_p}x & \frac{1}{\sqrt{2}} \\ \cos(\frac{\pi}{\tau_p}x - \frac{2}{3}\pi) & -\sin(\frac{\pi}{\tau_p}x - \frac{2}{3}\pi) & \frac{1}{\sqrt{2}} \\ \cos(\frac{\pi}{\tau_p}x + \frac{2}{3}\pi) & -\sin(\frac{\pi}{\tau_p}x + \frac{2}{3}\pi) & \frac{1}{\sqrt{2}} \end{bmatrix} \quad (2.14)$$

Where:

- τ_p: The time.
- x : The phase angle.

Moreover, the stationary frame as shown in equations 2.14 and 2.15 (Tahi et al., 2011).

$$\mathbf{T} = \sqrt{\frac{2}{3}} \begin{bmatrix} 1 & \frac{-1}{2} & \frac{-1}{2} \\ 0 & \frac{\sqrt{3}}{2} & \frac{-\sqrt{3}}{2} \\ \frac{1}{\sqrt{2}} & \frac{1}{\sqrt{2}} & \frac{1}{\sqrt{2}} \end{bmatrix} \quad (2.15)$$

$$\mathbf{T^{-1}} = \sqrt{\frac{2}{3}} \begin{bmatrix} 1 & 0 & \frac{1}{\sqrt{2}} \\ \frac{-1}{2} & \frac{\sqrt{3}}{2} & \frac{1}{\sqrt{2}} \\ \frac{-1}{2} & \frac{-\sqrt{3}}{2} & \frac{1}{\sqrt{2}} \end{bmatrix} \quad (2.16)$$

Where T^{-1} represents the inverse transformation matrix

2.4 Voltage Source Inverter Mathematical Theory

As a definition of an inverter, it is a power electronic circuit that converts the DC voltage source into AC voltage source, depending on the inverter work type the voltage transformation could be into a single phase, two phases or three phases. An inverter motors that are ingesting and utilized in frequency factor and voltage for variable rate application. The Pulse Width Modulation (PWM) method that is much popular to SVPWM technique that has utilized due to the DC bus voltage. Additionally, as compared to the SPWM it provides more significant performance and awareness can be achieved and which imply an output voltage can get. The amounts represented the output of inverter as distance phase, or distance vectors are this SVPWM notion. A premise is the amounts of the three-phase are; the quantity, the steady-state and transient states. Besides, may be suitable for distance vector representation this is among the benefits of this SVPWM technique once the steady state condition is the sole requirement for phasor representation. The Space Vector Modulation (SVM) technique has evolved as a vector strategy to Pulse Width Modulation (PWM) for three-phase inverters. Therefore, Figure 2.4 shows the converter circuit includes six MOSFET transistors and electricity supply represent the fundamental Three-Phase Voltage-Source. The SVPWM inverter is a scheme for creating a wave, which generates a voltage to the total harmonic distortion, is reduced. This strategy restricts distance vectors to be implemented in line with the area.

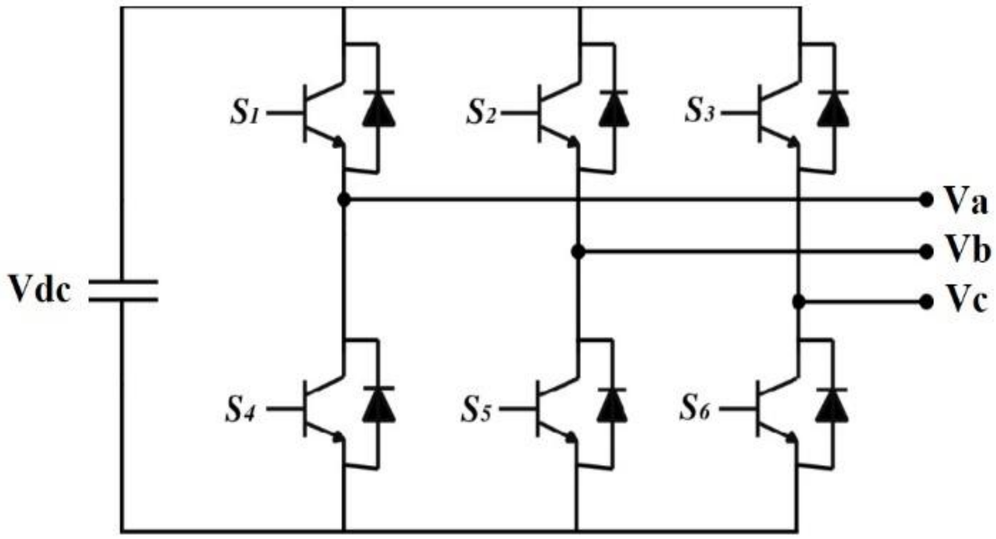

Figure 2.6. Three phase voltage source inverter circuit (Zheng, 2018).

The calculation of switching instants has done by using SVM plot based upon the representation of shifting vectors in the plane of the frame. Figure 2.5 shows the six sectors of the distance vector and the distance-vector of stage voltages (Emadi, 2005; Fratta and Vagati, 1992). Among the PWM Approaches that are significant and famous is SVPWM method for VSI for the controlling of AC Machines, for example, IMs, PMSM and SynRM.

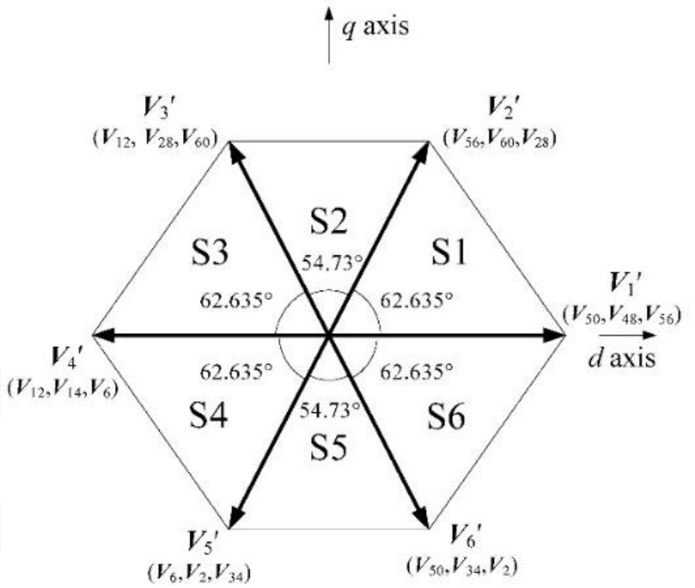

Figure 2.7. The six sectors of the SVPWM (Zheng, 2018).

The SVPWM-technique demonstrates that the distance vector modulation method creates from DC bus voltage possess distortion with the voltage generated and higher efficacy. The reference voltage and its angle of this distance vector inverter are contingent on the d-q transformation as shown in Figure 2.3.

$$\| \mathrm{V_{ref}} \| = \sqrt{\mathrm{V_d^2} + \mathrm{V_q^2}} \quad (2.17)$$

$$\alpha = \tan^{-1}\left(\frac{\mathrm{V_d}}{\mathrm{V_q}}\right) = \omega_s t = 2\pi f_s t \quad (2.18)$$

$$V_{ref}T_s = \left(\mathrm{V_1 T_a} + \mathrm{V_2 T_b} + \mathrm{V_{0,7} T_o}\right) \quad (2.19)$$

$$T_z = (T_a + T_b + T_o\ ) \quad (2.20)$$

$$V_{ref} = V_{ref}e^{j\alpha} \quad (2.21)$$

$$\mathrm{V_1} = \frac{2}{3}\ V_d\ , \mathrm{V_{0,7}} = 0\ , \mathrm{V_2} = \frac{2}{3}\ V_d e^{j\frac{\pi}{3}} \quad (2.22)$$

The source-space vector has been assumed to be constant during one switching cycle to get high switching frequency. The zero vectors refer to the start of switching which is the switching period T_Z or full null per vectors per T_S. Besides, each of nulls has duration width of (T_o/2), so the space vector equations can be descried as the following below:

$$\textbf{Re:}\ V_{ref}\cos\alpha\, T_z = \frac{2}{3}\, V_{dc}T_a + \frac{1}{3} V_{dc}T_b \tag{2.23}$$

$$\textbf{IM:}\ V_{ref}\sin\alpha\, T_z = \frac{1}{\sqrt{3}}\, V_{dc}T_b \tag{2.24}$$

$$T_a = \frac{\sqrt{3}\, T_z V_{ref}}{V_{dc}} \sin(\frac{\pi}{3} - \alpha) = T_z * m_a * \sin(\frac{\pi}{3} - \alpha) \tag{2.25}$$

$$T_b = \frac{\sqrt{3}\, T_z V_{ref}}{V_{dc}} \sin(\alpha) = T_z * m_a * \sin(\alpha) \tag{2.26}$$

$$T_o = (T_z - T_a - T_b) \tag{2.27}$$

Where:

- m_a: The modulation index of SVPWM inverter.
- V_{dc}: The DC voltage in (v).

$$m_a = \frac{\sqrt{3}\, V_{ref}}{V_{dc}} \quad (0 \leq \alpha \leq 60) \tag{2.28}$$

$$T_a = \frac{\sqrt{3}\, T_z V_{ref}}{V_{dc}} (\sin(\frac{\pi}{3} - \alpha + \frac{n-1}{3}\pi)) = \frac{\sqrt{3}\, T_z V_{ref}}{V_{dc}} * (\sin(\frac{n\pi}{3} - \alpha)) \tag{2.29}$$

$$T_b = \frac{\sqrt{3}\, T_z V_{ref}}{V_{dc}} (\sin(\alpha - \frac{n-1}{3}\pi)) \tag{2.30}$$

2.5 SynRM Block System Simulation

The direct and quadratic axis voltages have framed to represent the SynRM model design. The voltages equations of SynRM which mounted in equations 2.1 and 2.2 are implemented in Matlab/Simulink environment block as in Figure 2.6. The linear and quadratic axis voltages have represented the input of SynRM block system. The result of simulation that serves by both of speed and torque. The complete Simulink model of the SynRM drive system is shown in Figure 2.7, it consists of three main blocks. Figure 2.6 shows the SynRM block design. The d-q transformation matrix block is shown in Figure 2.9. Moreover, Simulink block of two axes SynRM is shown in Figure 2.8 and the block current of the two axes direct and quadrature are shown in the Figure 2.10 and Figure 2.11. The parameters that have used in SynRM desigs is shown in Table 2.1.

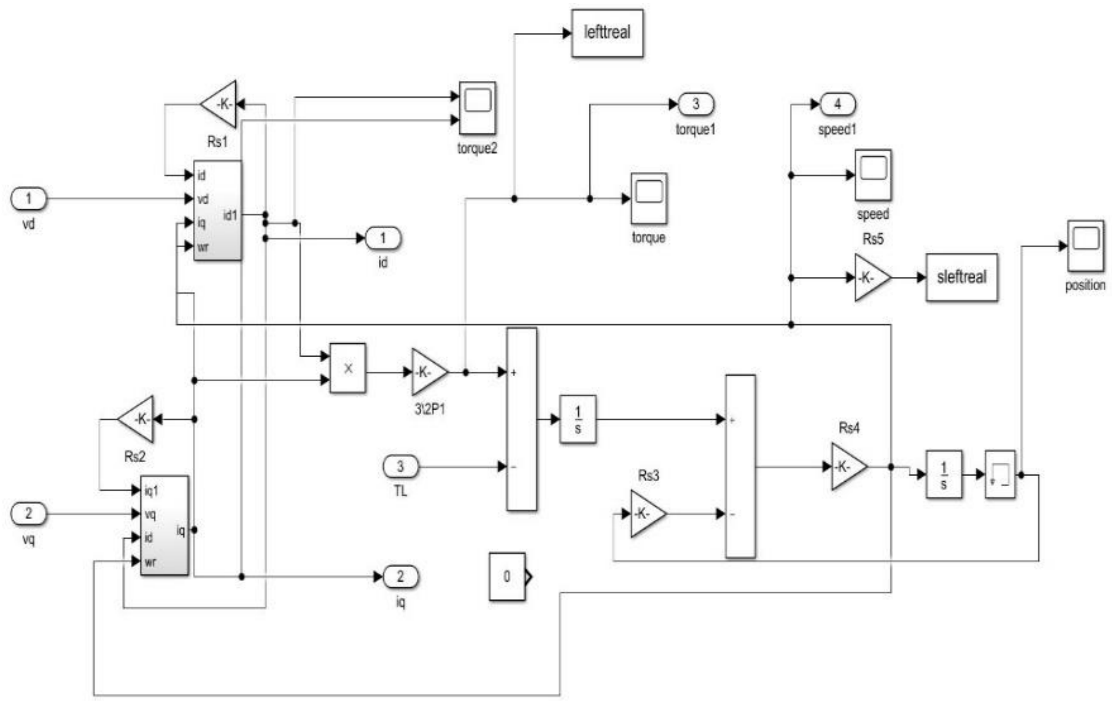

Figure 2.8. SynRM model block design.

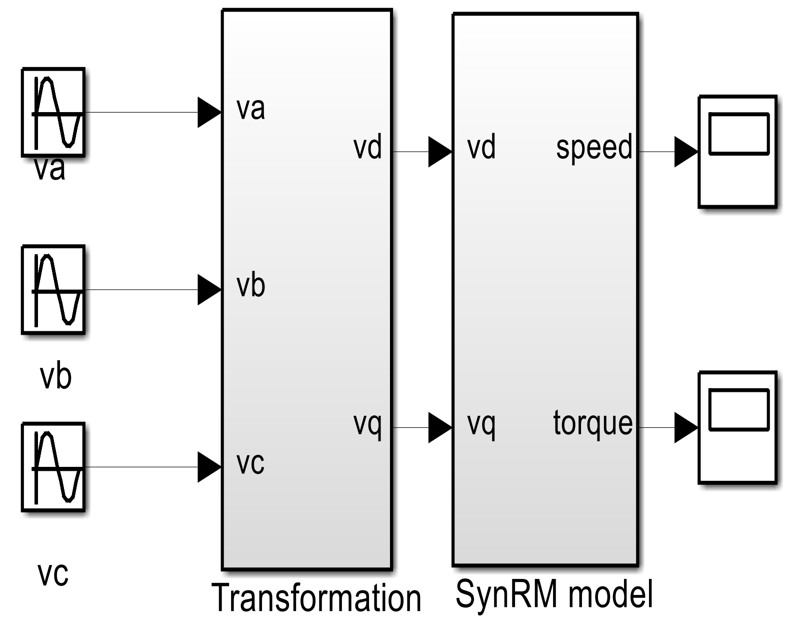

Figure 2.9. The SynRM drive system block.

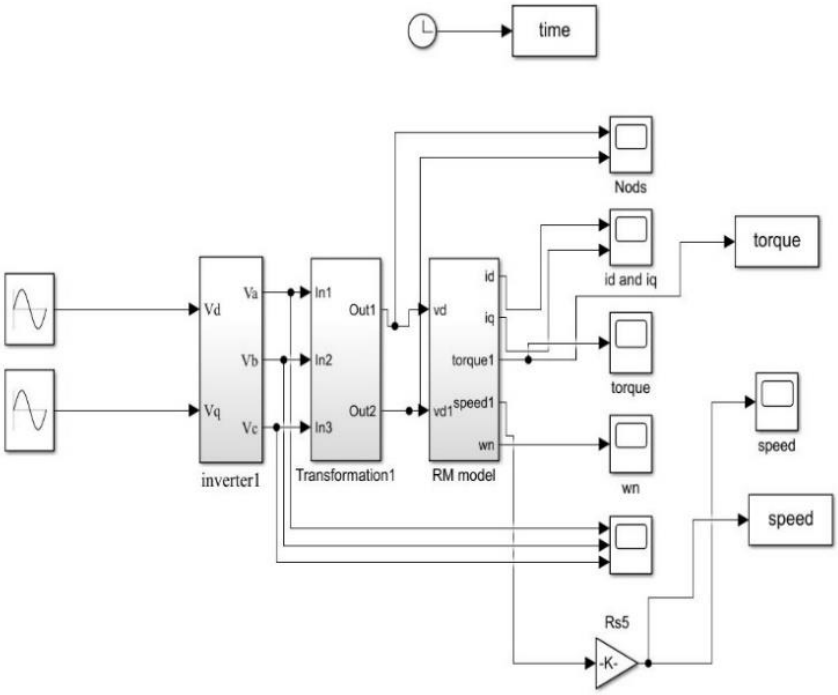

Figure 2.10. The block simulation of two axis of SynRM.

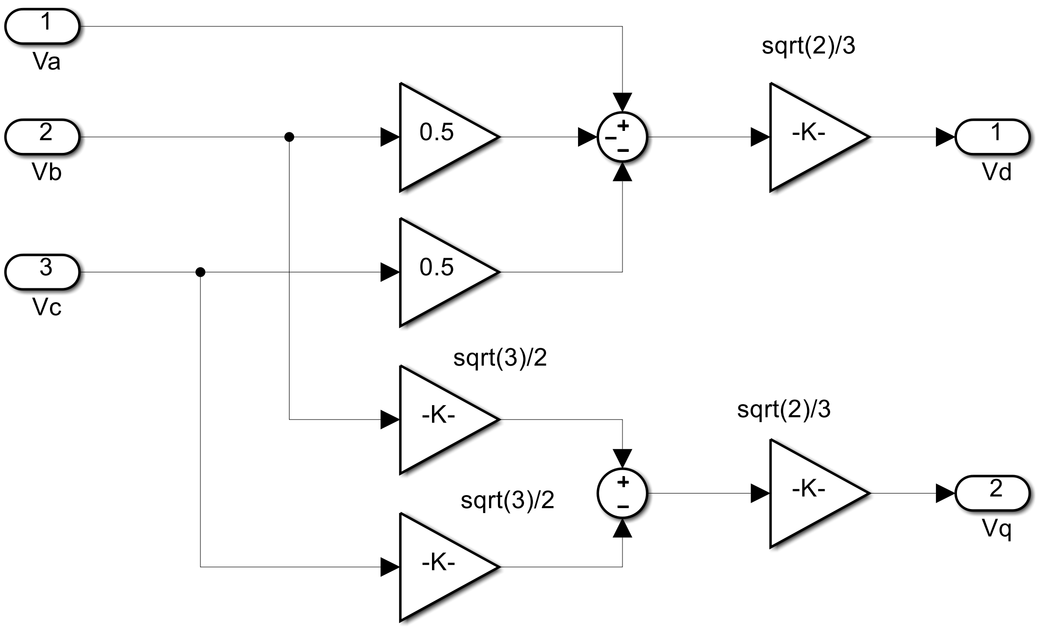

Figure 2.11. The d-q transformation matrix block.

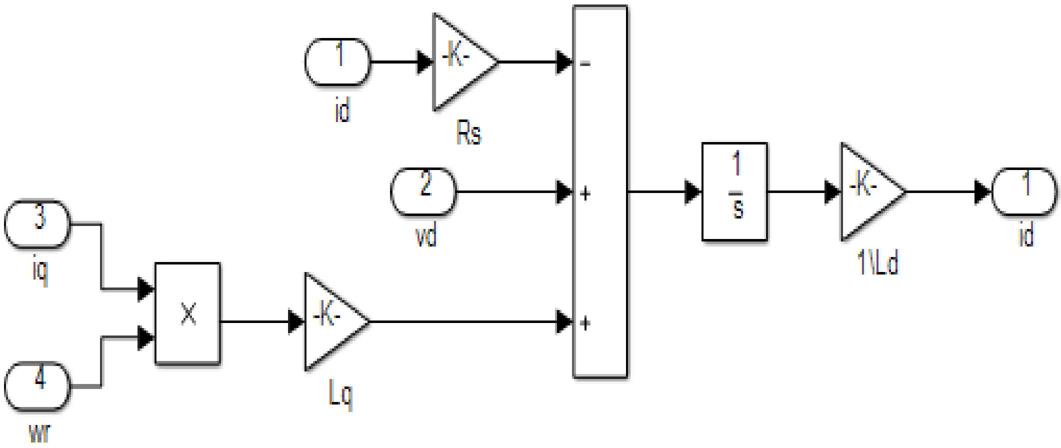

Figure 2.12. The direct-axis current block.

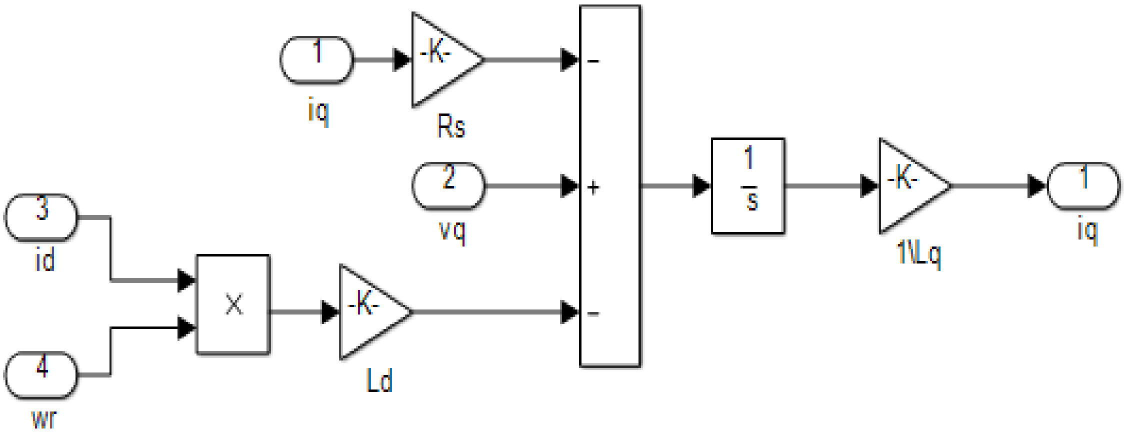

Figure 2.13. The quadrature-axis current block.

Table 2.1. The component parameters of the SynRM.

Parameter	**Values**	**Units**
Ld	6.0645	mH
Lq	0.910	mH
Rs	0.0265	Ohm
J	0.245	kgm^2
B	0.0000009	N.m.s
P	2	poles

2.6 The Results of SynRM Model Simulation

The simulation results are explained in this section. The features for your SynRM, which exited through providing two-phase voltages V_d and V_q as shown in Figure 2.8. The simulation result that depending on the systems design are determines as the points below:

A. Figure 2.14 shows the speed of SynRM about 1500 rpm started with (0 to 1500) rpm from (0 to 1) second at 25 Hz of the frequency with no load condition.
B. Figure 2.15 The SynRM torque at 25 Hz of the frequency with no load condition started from 0 to 1500 at the second zero of running. Then, decrease to 1000 at the second 0.2 of running then stabilizes at 50 from during each operating period of the SynRM.
C. Figure 2.16 represents the q-axis current at 25 Hz of the frequency with no load condition start at 300 at the zero second the first time of running then decrease to be stable at 188 in the 0.8 second due to running time.
D. Figure 2.17 represents the d-axis current at 25 Hz of the frequency with no load condition start at 300 at the zero seconds the first time of running then decrease to be stable at 188 in the 0.8 second due to running time.
E. Figure 2.18 represents the motor speed with 50 Hz frequency at no load condition. The motor speed has continued increase from (0 to 3000) rpm at the first moment from the run time to the 0.8 seconds of run time, then the motor speed stay stable during each operating period.
F. Figure 2.19 represents the motor torque with 50 Hz frequency at no load condition that reaches the 640 at the first moment of running time, then continue decreasing to be stable at approximately 15 in the 0.8 second of the operation time.
G. Figure 2.20 represents the motor speed with no control action and frequency of 25 Hz operation frequency start from 0 seconds and continued increasing to reach 1500 rpm in the 0.8 seconds of the operating time. Then after applied 20 Nm load at 1.4 seconds, the motor speed has decreased from 1500 rpm to 1400 rpm at 1.52 second of operating time to be stable at the same speed during each operating period.
H. Figure 2.21 represents the motor torque with no control action and frequency of 25 Hz operation frequency, the torque starts from 500 at the zero seconds after that continue decreasing to reach 20 at 0.8 seconds after that be stable on zero. Then after applied 20 Nm load at 1.4 seconds, the motor torque has increase from zero to 50 to be stable at this value during each operating period.

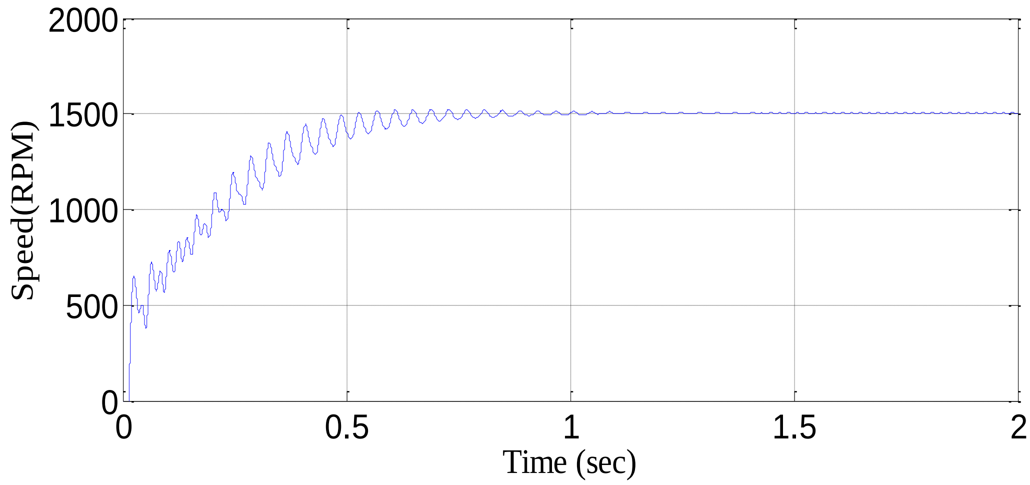

Figure 2.14. The SynRM speed at 25 Hz of frequency with no load condition.

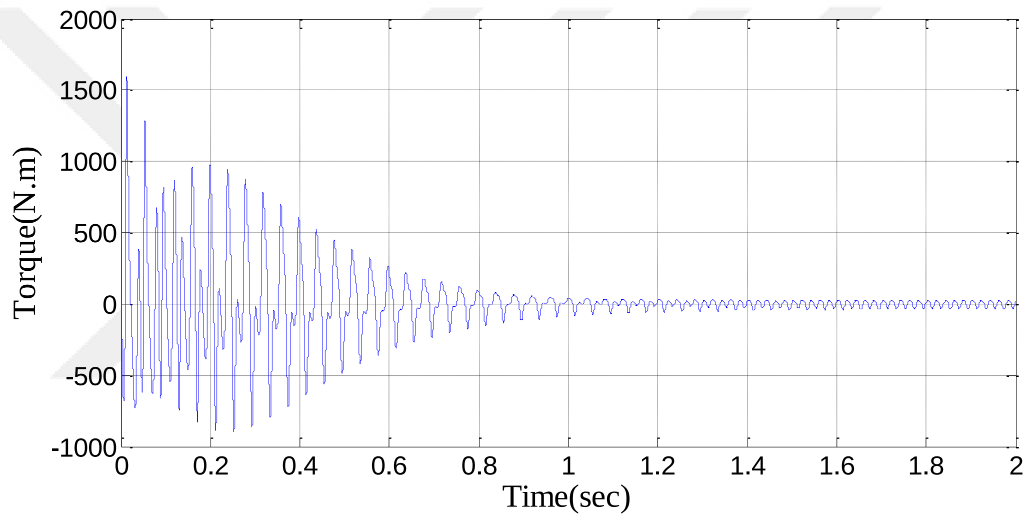

Figure 2.15. The SynRM torque at 25 Hz of frequency with no load condition.

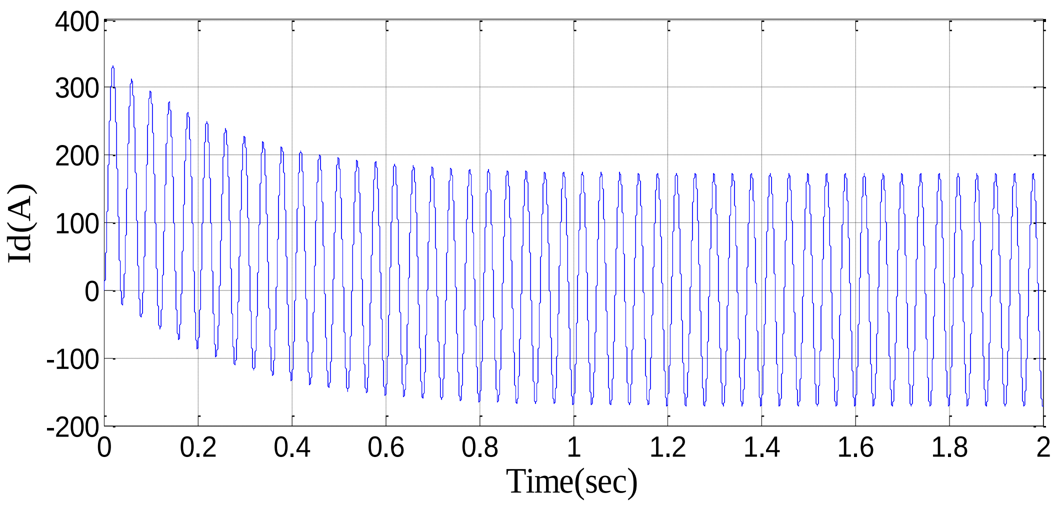

Figure 2.16. The q-axis current at 25 Hz of frequency with no load condition.

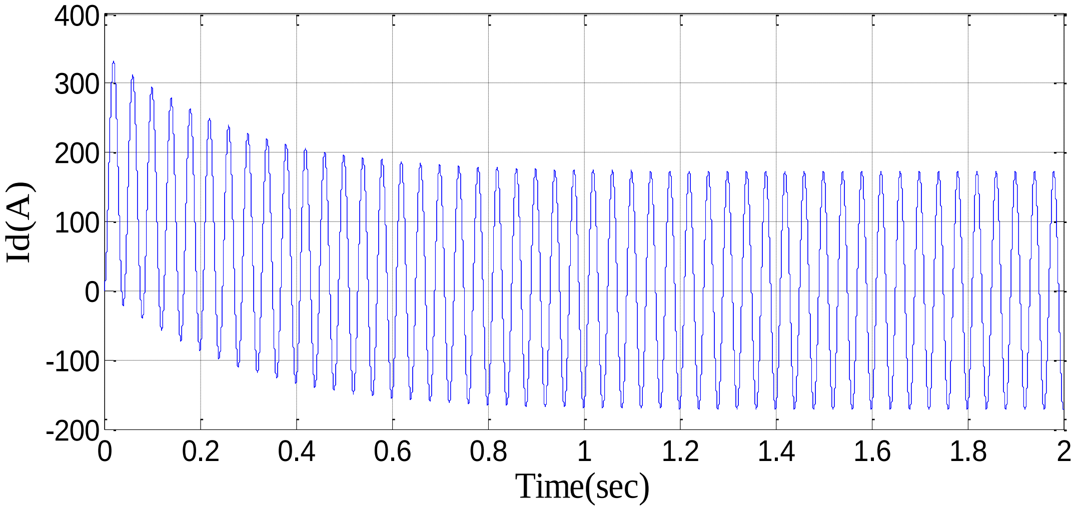

Figure 2.17. The d-axis current at 25 Hz of frequency with no load condition.

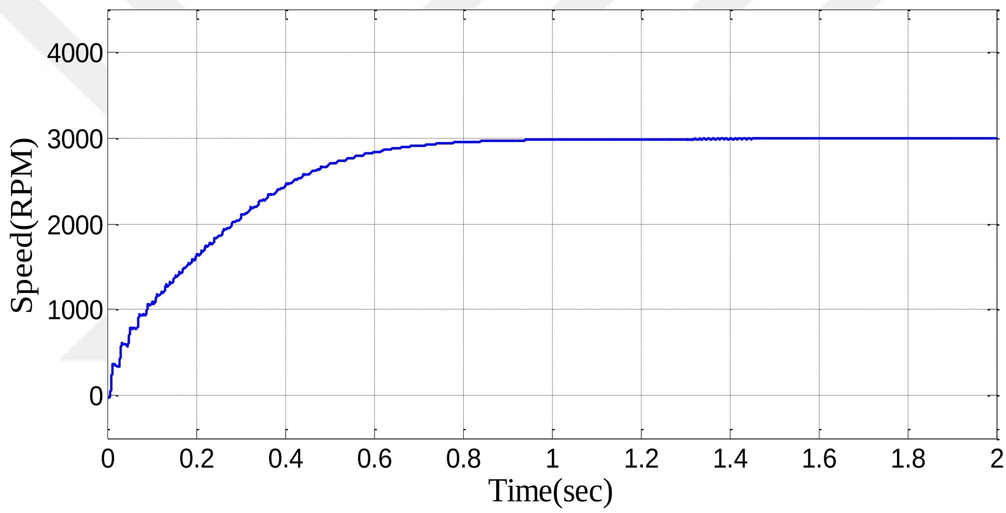

Figure 2.18. The SynRM speed at and 50 Hz of frequency with no load condition.

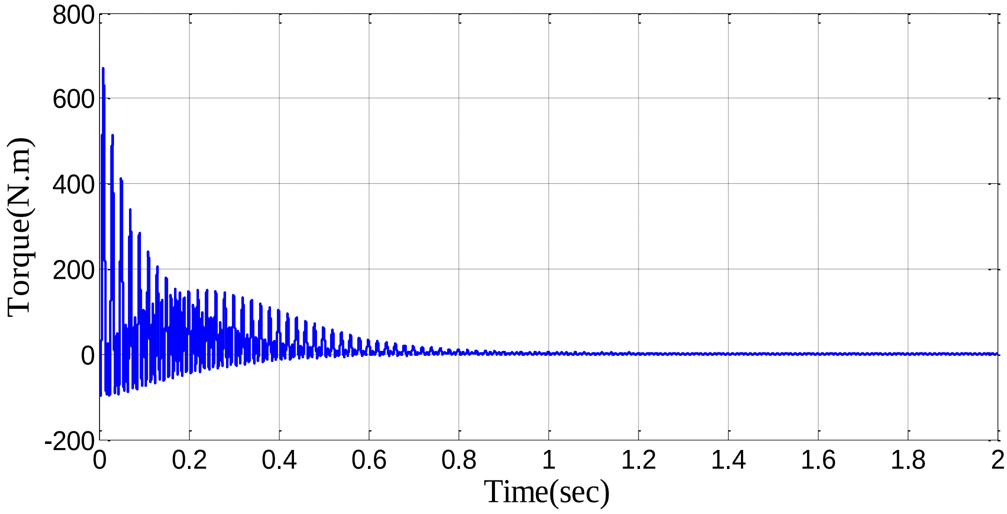

Figure 2.19. The SynRM torque at 50 Hz of frequency with no load condition.

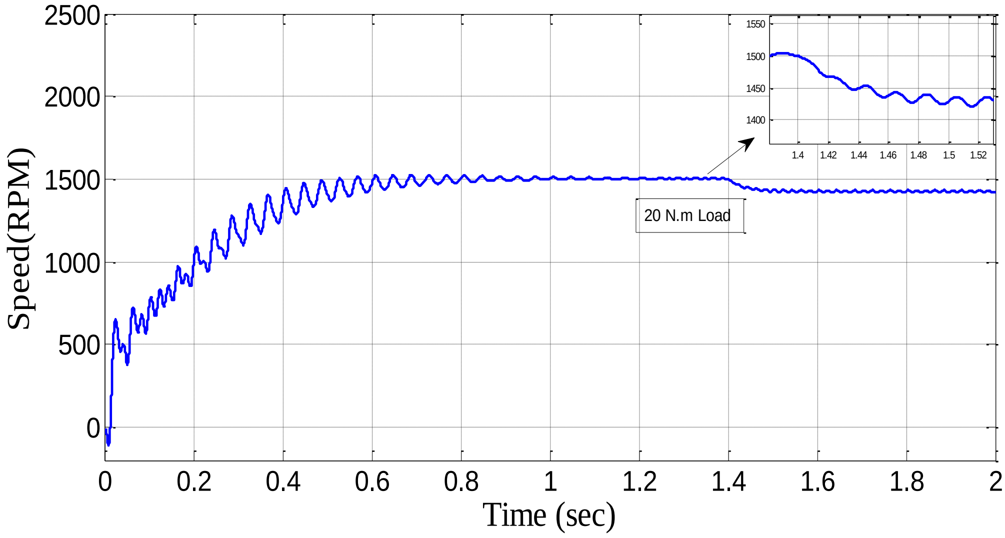

Figure 2.20. The SynRM speed at with 20 Nm of load at 1.4 second.

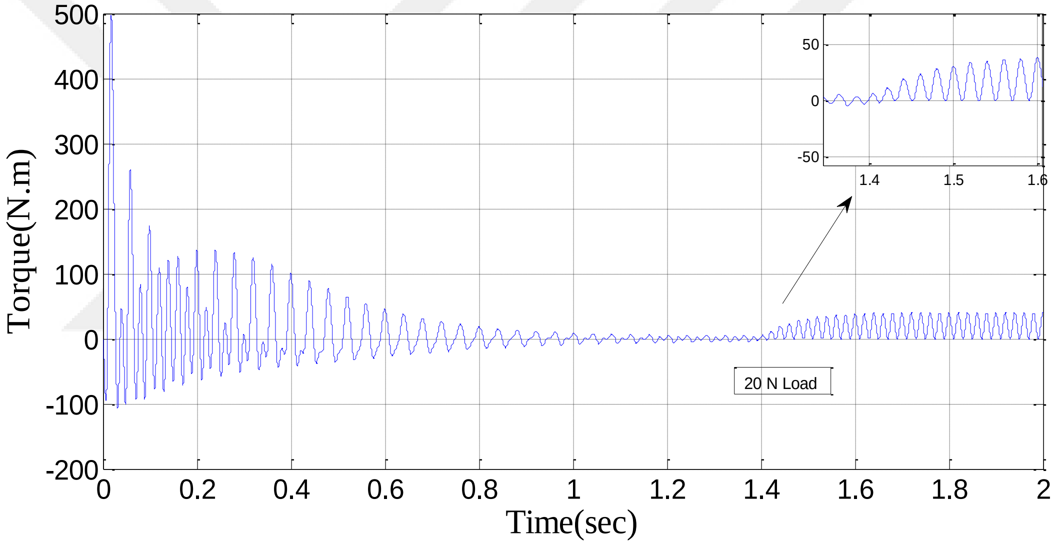

Figure 2.21. The SynRM torque at with 20 Nm of load applied at 1.4 second.

2.7 Conclusion

The central reason in the dynamic model of d-q axes is to convert the three-phase voltage into parallel two-phase and fed to the SynRM. By controlling the performance frequency, the engine speed will be controlled. The results reveal that since the SynRM has two ways this motor's rate is 3000 rpm. Due to the absence of control activity, the SynRM speed decline when implementing the load when connecting the motor into the static transformation that is d-q axis, which the motor functionality does not change because the conversion matrix provides the power. The results demonstrated that the SynRM version legitimate under different operation conditions. Hence, the output result of the SynRM model design and simulate as shown in Table 2.2.

Table 2.2. The characteristics output of the SynRM.

The output power	46	kw
The rate of speed	3000	rpm
Operation frequency	100	Hz
Efficiency at full load	94.8%	---
Current	103	A
Torque	144	Nm
Torque Ratio	1.6	---

3. THEORY OF SynRM CONTROL SYSTEM

3.1 The Concept of SynRM Speed Control

The SynRM have marvelous attributes make this motor ideal choice for various industrial applications like; elevators, fans and electric vehicles, etc. The rate control is a significant variable and takes a vital role in these applications and programs. The sensor speed controller is typically required due to space and cost saving to achieve high performance of SynRM speed control.

Generally, there are two sensor control approaches; vector control and torque control. Therefore, the vector control method is the most popular approach sensor control (Haddoun et al., 2008). Besides, the parameters of SynRM are constants that the direct axis current within this control strategy has been selected to be continuous and attempted to keep the current value as small as possible. The outer loop has used to control motor speed. The inner circle to control the quadrature axis current.

Moreover, there are three control-loops in the control system that control both of the motor speed and the torque. The adjustable speed drives "ASD" of AC machines have been majorly improved in recent years and regarded as a means to convert electrical energy to mechanical function in a wide assortment of industrial applications (Soltani and Zarchi, 2004). The inverter that fed motors is utilized broadly in ASD systems that are high performance.

Finally, when the synchronous machine is provided by a current controlled VS-SVPWM inverter, then the stator currents have been determined by the desired speed or coveted electromagnetic torque as well as the synchronous motor originated by the inverter and the instantaneous currents of the stator accompany their benchmark values (Tahi et al., 2011). The implementation Simulink model of SynRM speed control that fed by SVPWM voltage source inverter is shown in Figure 3.1 with the controller circuit. Besides, each controller will be explained in this chapter.

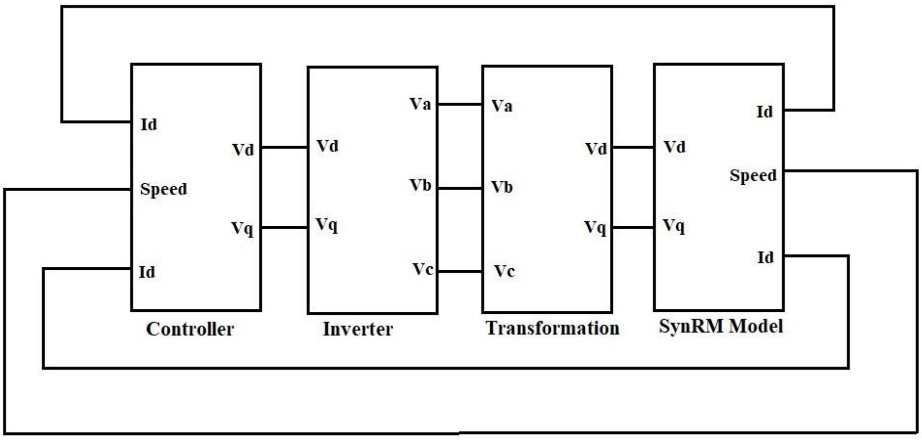

Figure 3.1. Speed control simulation of the SynRM by using SVPWM.

3.1.1 Traditional-PID controller

Generally, between millions of control loops in an essential process of industry sector, PID controllers use between 90-97 percent of the situations. Besides, between 20-30 percent has recognized that sole controllers in the process sector are tuned manually (Garpinger, 2015). In addition, the conventional “Traditional" PID controllers have considered as predominantly used controls in the control-process sector, due to it has a simple structure and easy platform parameters. The reason of using the feedback system; a quiet and stable substitution in control systems would be able to acquire a set point without matter disturbances, noise or some variation in characteristics (Ansari et al., 2011; Tahi et al., 2011). A PID tradition controller defines an “error” value since the variation between an obtained procedure variable and the set point. The controller attempts to create the error signal as little as possible by tampering the input signal into the control procedure. The PID control algorithm includes three different continuous parameters, also it has principally referred to as equivalent or derivative value. Hence, the mathematical fundamentals of the PID controller is represented in the next equation (Ansari et al., 2011).

$$u(t) = k_p e(t) + k_i \int e(t)dt + k_d \frac{d}{dt} e(t) \tag{3.1}$$

The Laplace transform function of the PID controller is written as specified by:

$$G_{PID}(s) = k_p + \frac{k_i}{S} + S.k_d \tag{3.2}$$

Where:

- K_P: Proportional gain.
- K_i: Internal gain.
- K_d: Derivative gain.
- e(t): Error value.

Figure 3.2 shows the block structure of the PID controller. Table 3.1 provides comprehensive ramifications of every control parameters Kp, Ki and Kd on a conventional closed-loop system. In particular control processing, it might require just one or two parameters to provide an appropriate control system. The PI-controllers are vastly common since the derivative action is extremely sensitive to the noise influence. Whereas while, if there is absolutely no integral term, it might prevent the system from reaching its target value due to its control activity (Tahi et al., 2011).

Moreover, the single loop of PID controller does not give a proper functionality. Then, the arising need for full controller loops to represent the solution for the control issue. The cascaded controller signifies the solution to the inappropriate priority problem.

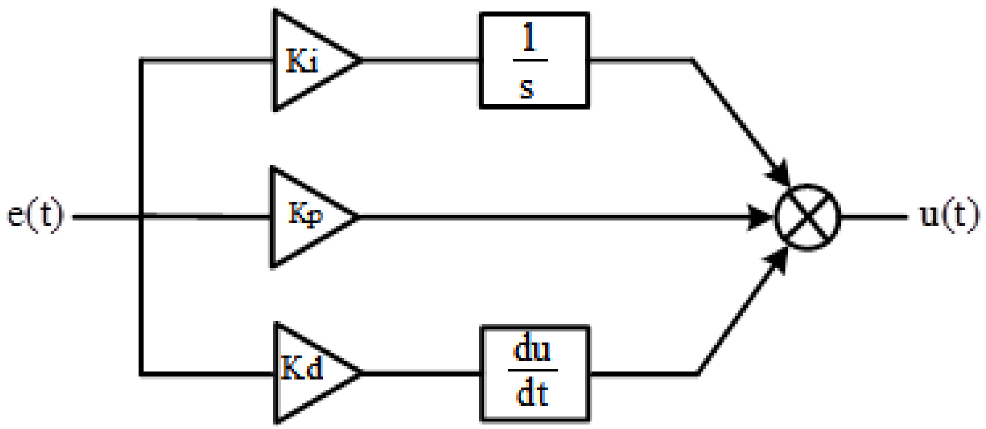

Figure 3.2. Traditional PID controller (Tahi et al., 2011).

.

Table 3.1. The characteristics and parameters of the tradition controller.

Responses / Parameters	Peak Time	Skip Time	Time of Settlement	Stable and wrong status
K_P	Decrease	Increase	Simple change	Decrease
K_I	Decrease	Increase	Increase	Neglect
K_d	Simple change	Decrease	Decrease	Simple change

3.1.2 Cascade-PID controller

One or several control loops in the main loop occur at the cascade control system. Typically, there is a single control, but on occasion, there might exist two or more inner control loops inside the main loop. The secondary control loop is known as the "initial loop" or "First loop" inside the principal loop, also the control in this loop is known as the "secondary control" or "slave control".

Moreover, the main loop is known as the "outer loop" or "external loop" and the control inside this loop is known as the "primary controller", "principal controller" or "master controller". The slave controller set point, which is the control signal that has calculated via the principal controller (Hartani et al., 2009). The cascade controller has used to secure much the better performance when compared it with single loop controls. Besides, the cascade control may provide a linear relationship between the factors over the typical single-loop controller and the actuator has used in several applications process. With consideration, the secondary loop case it might consider a new actuator, which gives much better linearity and proportionality status like the control rate valve (Hartani et al., 2009). The control amelioration the cascade control has qualified by raising information regarding the process. This type of control procedure process shows in Figure 3.3.

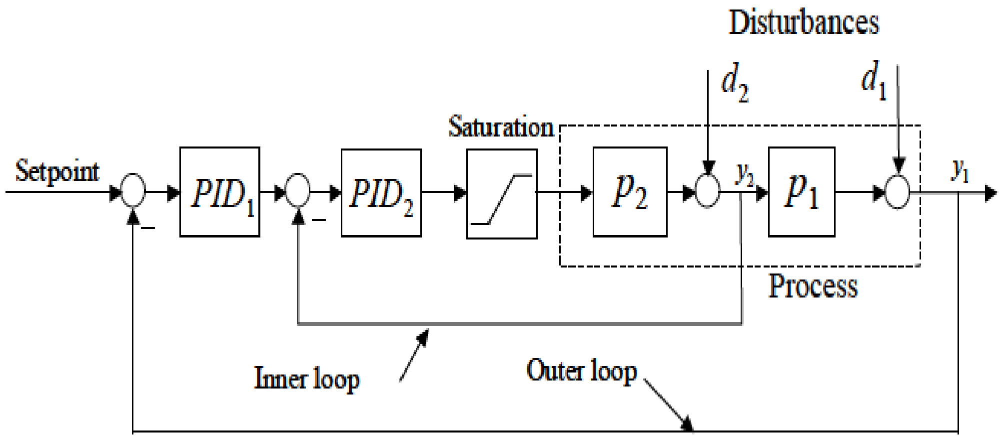

Figure 3.3. General design for cascade control system (Huang et al., 2003).

3.1.3 Lead-Lag controller

The control system layout has made a response with the lead-lag compensator to improve the steady-state operation.

In addition, the PID cascade compensation improves the tremendous progress during the past three decades technical management control systems straightforward procedures from the frequency domain, the lead-lag compensator has used after the PID and PI controller, therefore as another phase compensators are utilized to provide a joins performance between both the controllers.

Moreover, the lead-lag has utilized to conquer the single-director or single-Lag limitation and its produces the system has stabilized operation since it is regarded as a cascaded involving. The next sequence compensator represented from the lead-lag compensator mathematical explanation in the frequency domain is given by the equation 3.3 (Tahi et al., 2011).

$$G_C(s) = \mathrm{K}\,\frac{s^2+s+1}{s^2+s} \tag{3.3}$$

3.1.4 Simulation and results of cascade-PI and lead-lag controller

There is a single cascade controller include multi-control loops have utilized in industrial processes. Because it gives the benefit in its simplicity of implementation and set the parameter of this controlled type manually. Besides, the disadvantages of this control type are an exiguity of interaction flexibility adjustment as a compare with overall multivariable control, which has a few robust tools for its design.in this case, to complete the control process for this types of control there is a control engineering team that tunes the Single-input Single-output (SISO) for the PID controller manually.

Moreover, there is a single simple technique to tune a multi-loop PID control, which is by tuning control loops step by step with rejecting the interaction of loops entirely. Besides, that has carried out by setting the (i) loop of the PID control for the install transfer function. With the case of re-tuning the complete loops together, the system will have steady functionality and gives a suitable load disturbance response. The suggested of the lead-lag compensator has been used to restrain the quadrature-axis (q) that present in the SynRM.

Simultaneously, Figure 3.4 represents the SynRM cascaded control system and Figure 3.5 explains the simulation for the cascaded PI controller model with the lead-lag compensator. Table 3.2 reveals the cascaded controller parameters value of the cascaded controller system that has utilized by a strategy known as "trial and error". The Figures that start from 3.6 to 3.11 reveals the SynRM speed rate and torque due to different working condition.

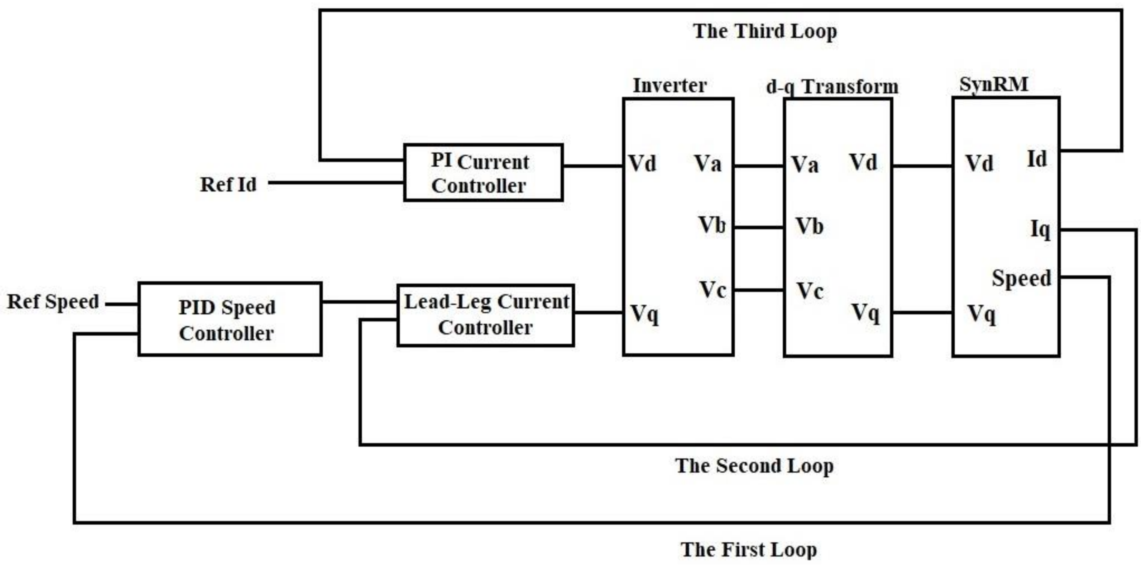

Figure 3.4. The cascaded control design for SynRM.

Table 3.2. The parameters and values of the cascade controller.

The type of Controller	**Speed Controller**		**Quadratic axis Current Controller**		
The Parameters	K_P	K_I	K_3	K_P	K_I
The Result value	60.245	17.672	22	2130	9.8

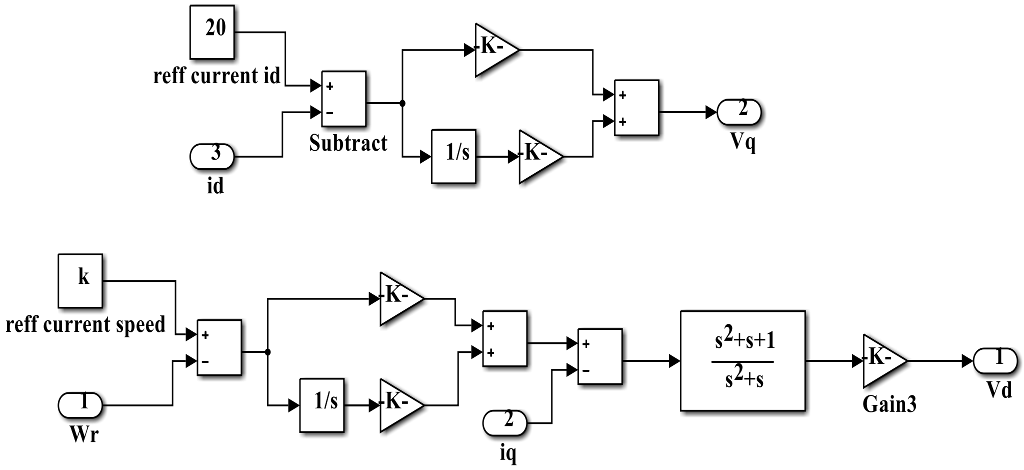

Figure 3.5. Simulink model for cascade-PI and lead- lag controller.

The activity of using the cascade-PI and lead-lag-controller to control the SynRM speed and torque could be descript by the next Figures. Therefore, the result of simulation could be determined as the description below:

A. Figure 3.6 shows the speed control of SynRM about 1500 rpm started with (0 to 1500) rpm from (0 to 0.1) seconds at 25 Hz of the frequency with no load condition. Then, the motor speed continues stable as the curve between 1501 and 1504 that started from 0.1 seconds and continue during each operating period of the SynRM.
B. Figure 3.7 represent the control of SynRM torque that started at 2000 in the first moment of operating time, then decreased to be stable at about 350 in the 0.1 second of operation time. Then, continue stable at this value during each operating period of the SynRM.
C. Figure 3.8 represent the running stapes of the SynRM speed at 25 Hz of the frequency with no load condition that started from (0 to 500) rpm in the first moment of the operating time. The second step has started in the 0.7 second of time to change the motor speed in to 1000 rpm. Hence, the third step has started in the 1.5 second of the

motor speed to change the motor speed in to 1500 rpm.

D. Figure 3.9 represent the torque of SynRM at the change steps of SynRM speed. The first step show the torque has reach to 400 at the first moment of the operating time and after that it has decreased to reach and be stable on 30 in the 0.8 second. The second step has started from 0.8 second to 1.5 second of time to change the torque from 30 in to 500 after that the torque decease to 188 at the seam step. Finally, the third step has started from 1.5 second of time and continue during each operating period, the torque start with 810 and after that decease to 188 in the seam step to be stable during each operating period.

E. Figure 3.10 represents the motor speed with no control action and frequency of 25 Hz operation frequency start from zero second and continued increasing to reach 1500 rpm in the 0.8 seconds of the operating time. Then after applied 50 Nm load at 3.5 seconds, the motor speed has decreased from 1500 rpm to 1350 rpm at 3.5 seconds after that continue rising at 3.7 seconds of time to reach the 1500 rpm gain in the second 10 of operating time to be stable at the same speed during each operating period.

F. Figure 3.11 represents the motor torque with no control action and frequency of 25 Hz operation frequency start from zero second and continued increasing to reach 1500 in the zero seconds of the operating time after that decrease to be stable at 200 in the second 0.8. Then, when applied 50 Nm load at 3.5 seconds, the motor speed has increased from 200 to 350 at 3.5 seconds after that continue rising at 3.7 seconds of time to reach the 360in the second four of the operating time to be stable at the same speed during each operating period.

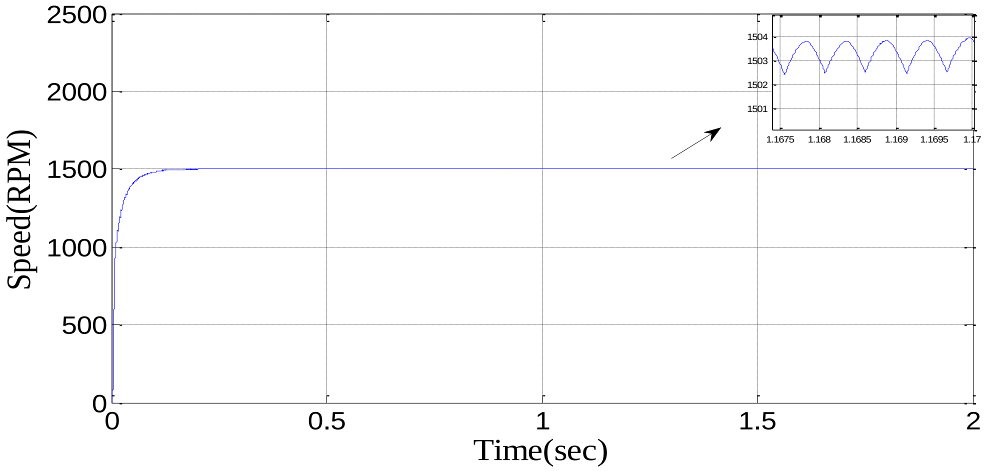

Figure 3.6. SynRM speed control at 1500 rpm with no load condition.

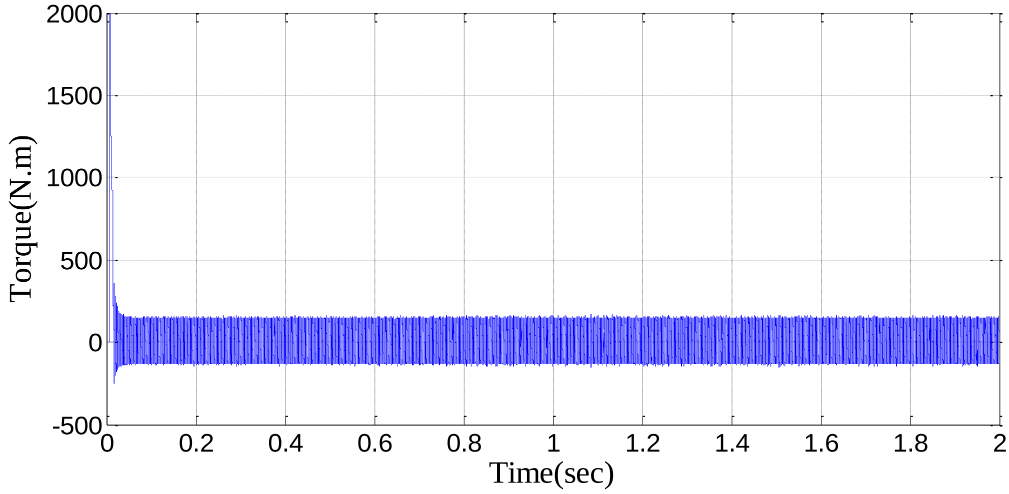

Figure 3.7. The SynRM torque control at1500 rpm with no load condition.

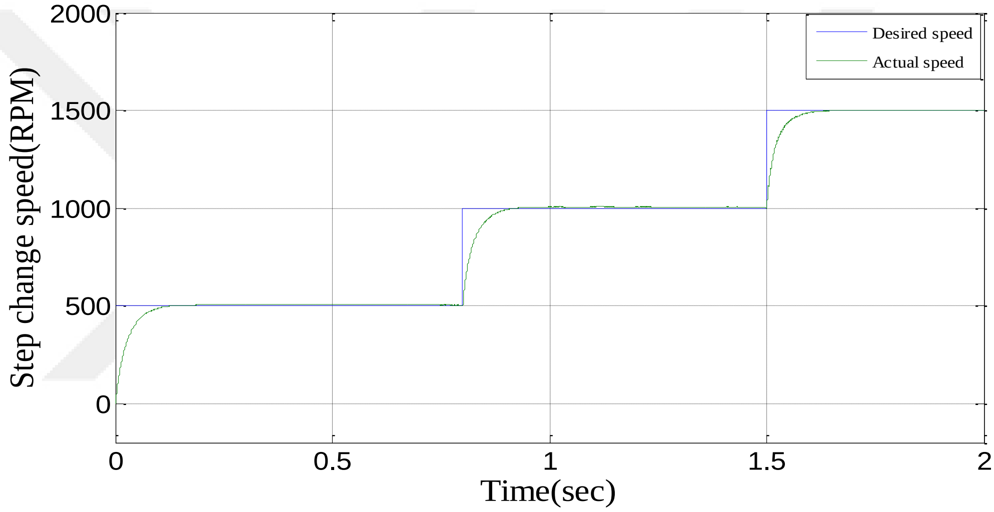

Figure 3.8. The SynRM speed control at steps of speed.

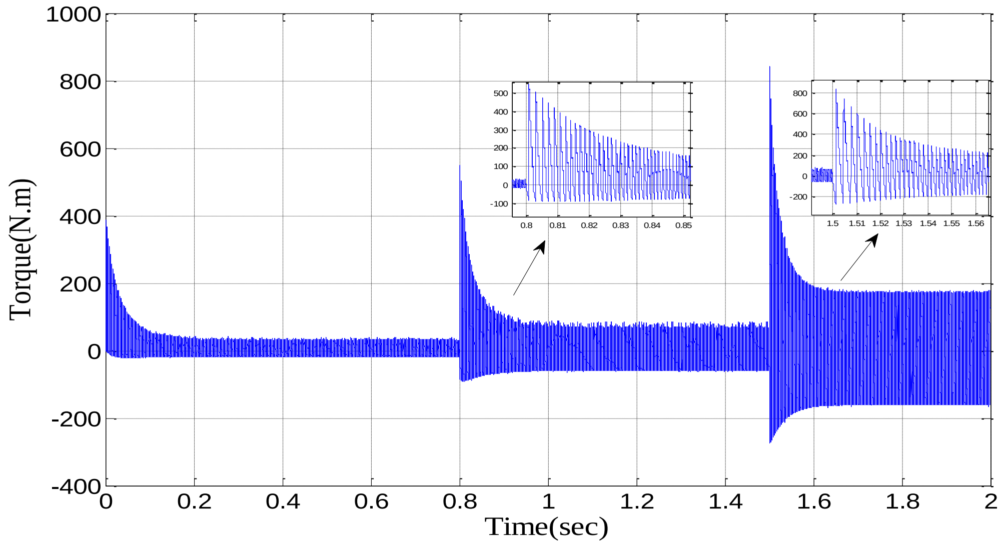

Figure 3.9. The SynRM torque control at steps of speed.

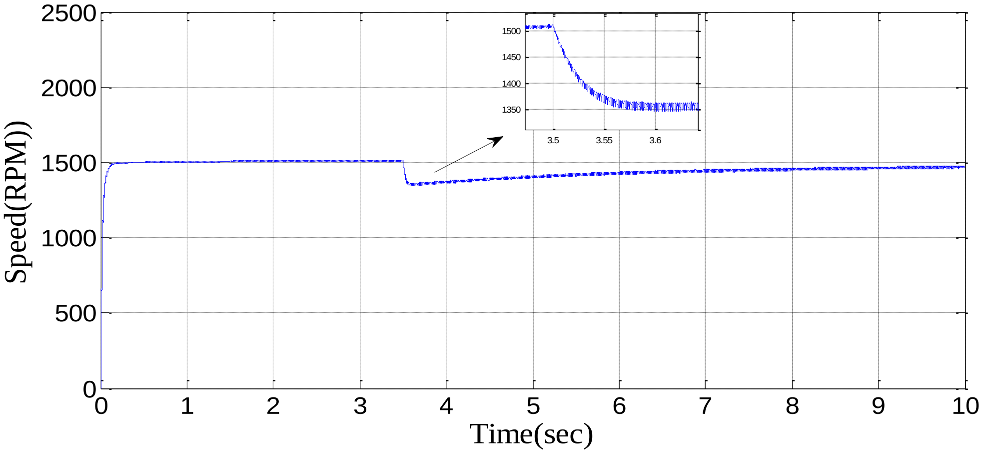

Figure 3.10. The SynRM speed control with 1500 rpm and 50 Nm of load applied at 3.5 second.

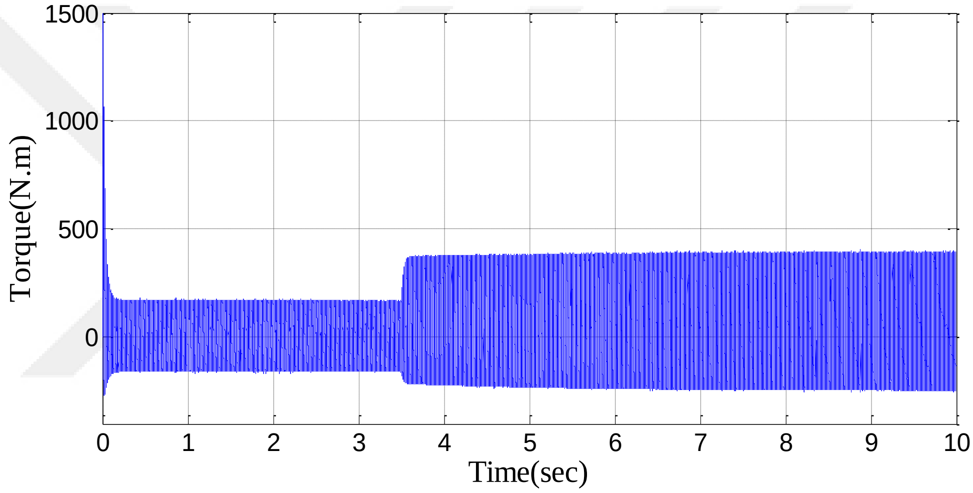

Figure 3.11. The SynRM torque control at 1500 rpm with 50 Nm of load applied at 3.5 second.

3.1.5 Simulation and results of cascade-PI, PID and lead-lag controller

The PI controller at the speed rate control has substituted via PID controller, which the metering activity gives improve the motor speed and torque activity. As shown in the Table 3.2, the cascaded PI and PID control parameters that have utilized via trial-error strategy. Besides, Figure 3.12 shows the Matlab/Simulink program has employed to simulate the PI and PID-cascaded controller. The Figures that start with 3.13 to 3.18 reveals the SynRM speed rate and the torque due to several working conditions. Hence, suggests the motor originated from the control in Figure 3.12.

Table 3.3. Manually tuned of the cascade controller.

The Type of Controller	Speed Controller			Quadratic Axis Current Controller		
The Parameter	K_P	K_I	K_d	K_3	K_P	K_I
The value	40	10	1	22	1200	10

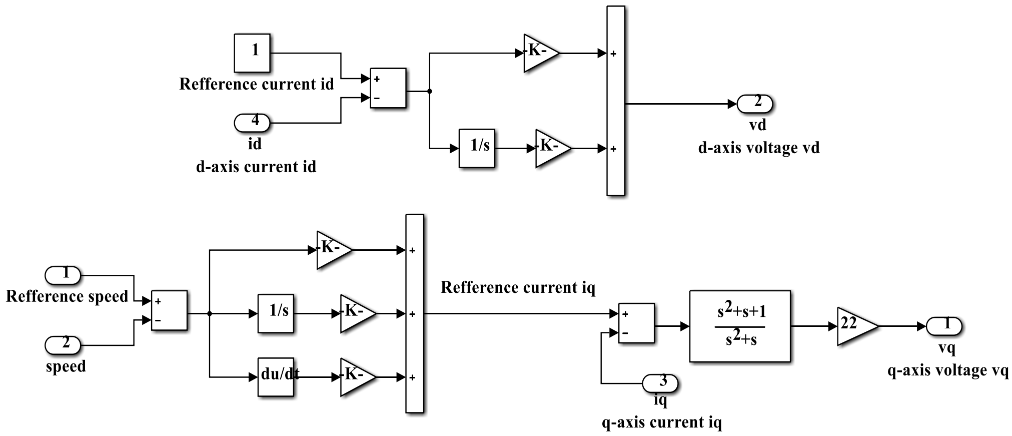

Figure 3.12. Simulink model for PI, PID and lead-lag controllers.

The activity of using the cascade-PI, PID and lead-lag-controller to control the SynRM speed and torque could be descript by the next Figures. Therefore, the result of simulation could be determined as the description below:

A. Figure 3.13 shows the speed control of SynRM about 1500 rpm started with (0 to 1500) rpm from (0 to 0.1) seconds at 25 Hz of the frequency with no load condition. Then, the motor speed continues stable as the curve between 1504 and 1510 that started from 0.1 seconds and continue during each operating period of the SynRM.
B. Figure 3.14 represent the control of SynRM torque that started from 2000 at the first moment of operating time, then decreased to be stable at about 350 in the 0.1 second of operation time. Thereafter, it’s continue stable at this value during each operating period of the SynRM.
C. Figure 3.15 represent the running stapes of the SynRM speed at 25 Hz of the frequency with no load condition that started from (0 to 500) rpm in the first moment of the operating time. The second stage has started in the 0.7 second of time to change the motor speed in to 1000 rpm. Hence, the third step has started in the 1.5 second of the motor speed to change the motor speed in to 1500 rpm.
D. Figure 3.16 represent the torque of SynRM at the change steps of SynRM speed. The

first step show the torque has reach to 400 at the first moment of the operating time and after that it has decreased to reach and be stable on 30 in the 0.85 second. The second step has started from 0.85 second to 1.5 second of time to change the torque from 30 in to 500 after that the torque decease to 188 at the seam step. Finally, the third step has started from 1.5 second of time and continue during each operating period, the torque start with 810 and after that decease to 188 in the seam step to be stable during each operating period.

E. Figure 3.17 represents the motor speed with no control action and frequency of 25 Hz operation frequency start from zero second and continued increasing to reach 1500 rpm in the 0.8 seconds of the operating time. Then after applied 50 Nm load at 3.5 seconds, the motor speed has decreased from 1500 rpm to 1350 rpm at 3.5 seconds after that continue rising at 3.7 seconds of time to reach the 1475 rpm gain in the second 10 of operating time to be stable at the same speed during each operating period.

F. Figure 3.18 represents the motor torque with no control action and frequency of 25 Hz operation frequency start from zero second and continued increasing to reach 1500 in the zero seconds of the operating time after that decrease to be stable at 200 in the second 0.8. Then, when applied 50 Nm load at 3.5 seconds, the motor speed has increased from 200 to 350 at 3.5 seconds after that continue rising at 3.7 seconds of time to reach the 360in the second four of the operating time to be stable at the same speed during each operating period.

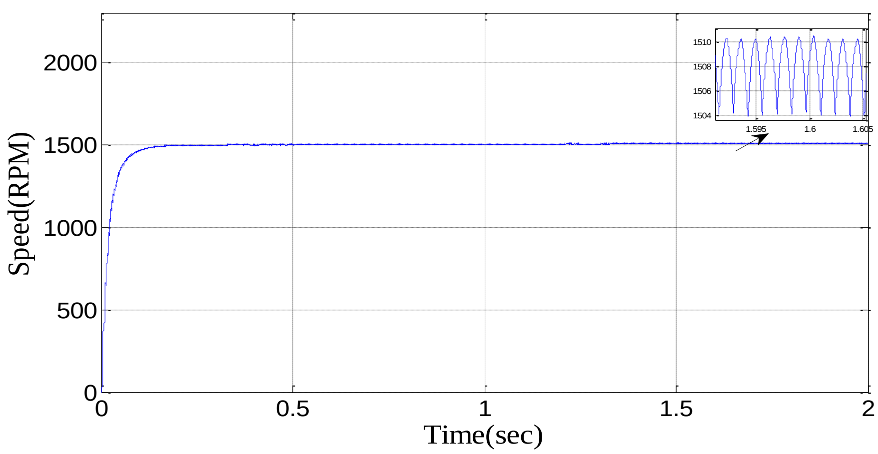

Figure 3.13. The SynRM speed control at 1500 rpm with no load condition.

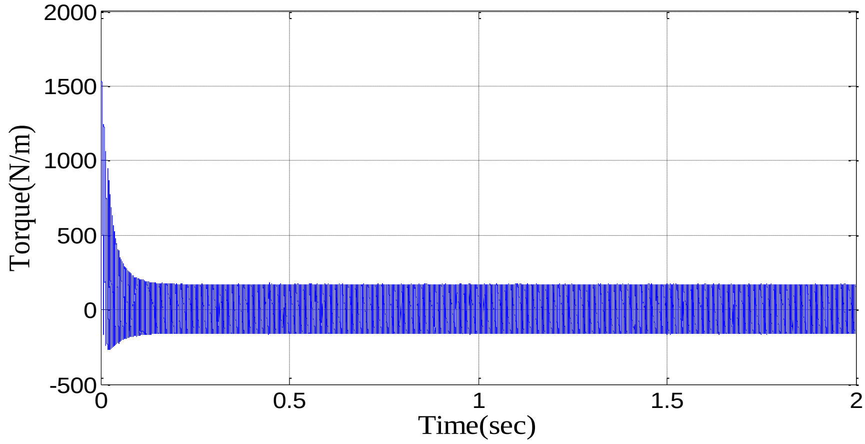

Figure 3.14. The SynRM torque control at 1500 rpm with no load condition.

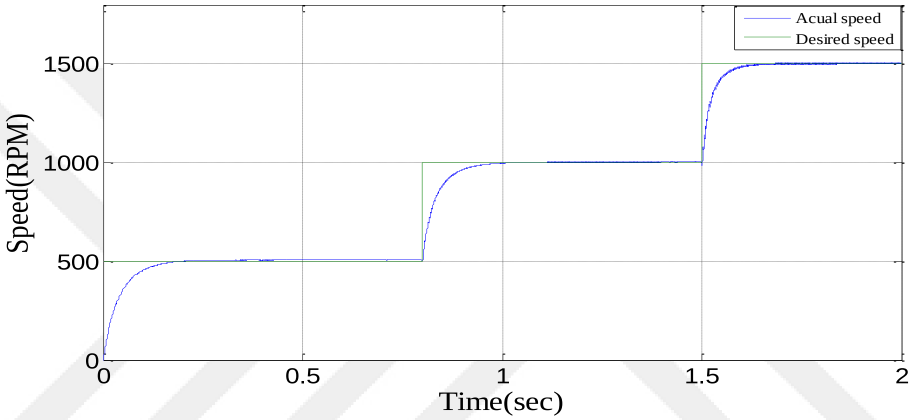

Figure 3.15. The SynRM speed control with steps of speed.

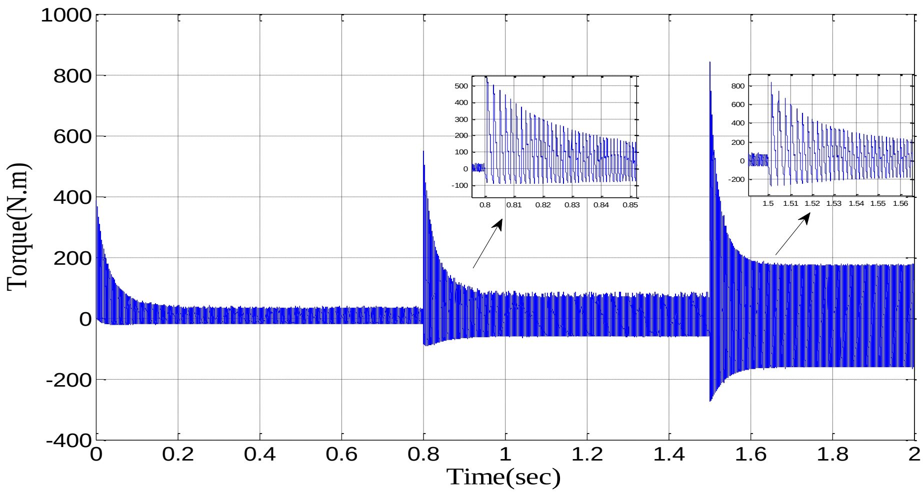

Figure 3.16. The SynRM torque control with steps of speed.

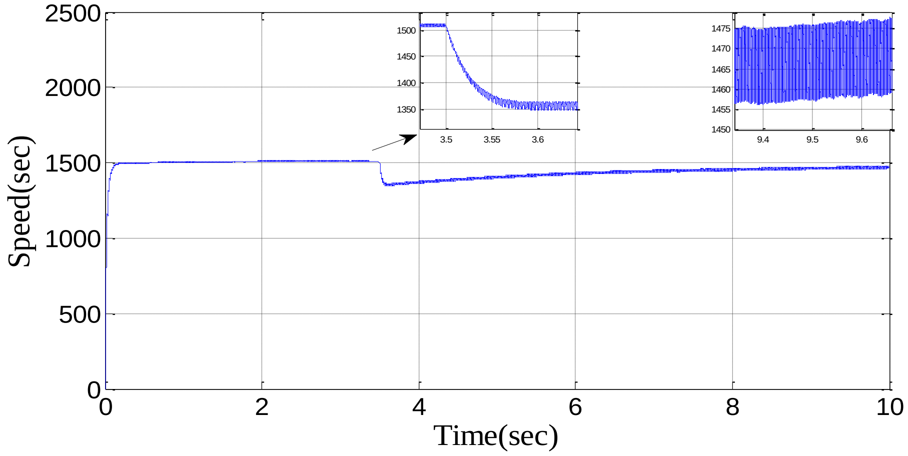

Figure 3.17. The SynRM speed control with 1500 rpm and 50 Nm step of load applied at 3.5 second.

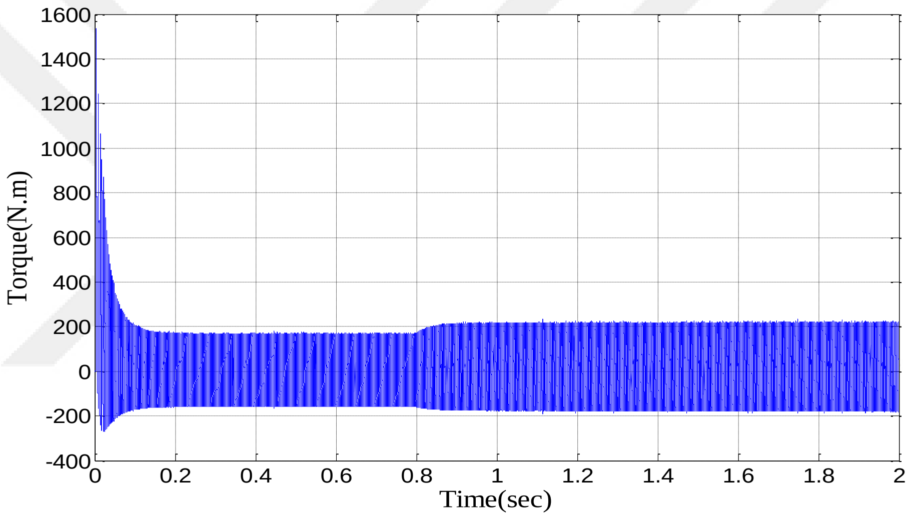

Figure 3.18. The SynRM torque control with 1500 rpm and 50 Nm step of load applied at 3.5 second.

3.2 The PSO Algorithm

Particle swarm optimization (PSO) commons rely on computational schemes their central concept came in the simulation of societal mindset as known as “social-psychological methods”. Besides, the simplest example of understanding this hypothesis could be offered at fish swarm and bird flocking. The PSO strategy was initially designed and developed by both Eberhart and Kennedy. After that, they have added inertia weights proposed in 1998 (Reddy et al., 2012; Effatnejad, et al., 2013).

Moreover, this concept has made to be effective in solving issues exhibiting or the non-linearity along with the non-differentiability. The PSO strategy has developed from the study on natural swarms like bird flocking swarm and fish swarm.

Rather than utilizing the evolutionary processes like variation and crossover which were utilized for calculations exploitation at the PSO algorithm, none of those processes are utilized the dynamics of the populace simulates as known as a "bird flocks" or "fish swarm" mind-sets. Whereas, the sociably sharing of data takes the significant portion of work and each could benefit from detecting and former expertise of all the other escorts through the exploration and searching of meals procedure. Each particle represents an ideal way to solve the optimization issue (Effatnejad et al., 2013). The perfect status seen by the particle has an impact on the particle position, which is the particle encounter.

Therefore, the very best particle status in the particle community as known as the “Neighboring Particles Encounter” (Ch and Obulesh, 2011). The local best place is known as (l_{best}) refers to some other particle that provides the best swarm position, which contains the minimal fitness value. In addition, the international best location is known as (g_{best}) refers to the very best particle index of particles in a populace. Based on the optimization issue each particle performance has quantified by upgrading its corresponding fitness function. The PSO algorithm structure is shown below on the flowchart in Figure 3.19 (Soni and Bhatt, 2013; Sharaf and El-Gammal, 2009).

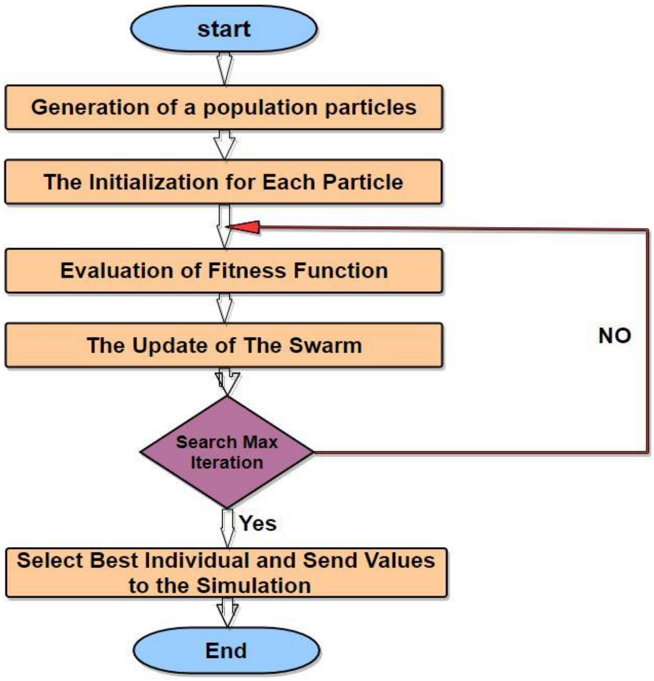

Figure 3.19. General flow chart for PSO algorithm.

Moreover, the steps of the PSO algorithm could be explained as flowing:

A. <u>Generation of population particles</u>

This part considers as the first of the PSO structure procedure could explain it by the below points:

1. A population is made of representatives known as particles distributed uniformly over x.
2. The number of particles has been chosen,
3. The amount of iterations has been chosen.
4. The hastening coefficients C_1 and C_2 have tuned.
5. The inertia weight (w) and arbitrary numbers R_1 R_2 and R_3 are corrected to begin the perfect solution searching.

B. <u>The initialization for each particle</u>

This part is the second of the PSO structure procedure could explain it by the below points:

1. The present posture $xi(t)$ and the velocity $vi(t)$ has initialized for every particle.
2. The particles have created randomly in the selection of the maximum and minimum limitations of parameters value.
3. Every particle is treated as a stage in a D-dimension space.

4. The ith particle is determined as xi $= (xi_1, xi_2, .., xi_D)$.
5. The velocity for the particle (i) is determined by vi $= (vi_1, vi_2, ..., vi_D)$.
6. Subsequently initialization of the local greatest place (l_{best}) along with the international best place (g_{best}).

C. Evaluation of fitness function

The general performance of the whole system effects with three section; the interchange of the speed rate, efficiency and PSO optimization precision. Besides, the system depends on the fitness function, which supervises the process search optimization. The fitness function is preferred the fitness center functions considered depending upon the standards that were essential to make the most of the domain limitations or to decrease the taste constraints. The most typical performance standards that upon the error grade are; Integrated Absolute Error (IAE), Integrated of Time weight Square Error (ITSE) and Integrated of Square Error (ISE), which calculate analytically from the frequency domain (Rahimian and Raahemifar, 2011; Tahi et al., 2011). In this chapter, there are several fitness functions have been used depending on the standard ISE and overshoot Mp. The functions are shown as below:

$$Fitness\ function = min\ (ISE) + min\ (M_p) \quad (3.4)$$

$$ISE = \int e^2(t)dt \quad (3.5)$$

$$M_p = max(n) - (n_{ref}) \quad (3.6)$$

$$e(i) = D(i) - y(i) \quad (3.7)$$

Where:

- $y(i)$: The model output.
- $D(i)$: The desired output.
- n : An actual speed.
- n_{ref} : The reference speed.

D. Update of the swarm

The velocity $v_i(t)$ and the current position $x_i(t)$ are update for each character in the swarm strategy has applied depending on equations 3.22 and 3.23. In addition, starting the fitness function along with the loop are calculated to upgrade the positions and the character of contaminants. When the new value is much better than the other is l_{best}, the new value will put to l_{best}.

In precisely the same way, the g_{best} value could be updated just like the ideal (*lbest*). The speed of each agent could be updated from the following:

$$v_i^{k+1} = w * v_i^k + c_1 * R_1 * (lbest_i - x_i^k) + c_2 * R_2 * (gbest_i - x_i^k) \tag{3.8}$$

Moreover, the current position has upgraded depending on the following Equations:

$$x_i^{k+1} = x_i^k + v_i^{k+1} \tag{3.9}$$

Where:

- x_i^k: The present position of particle I at iteration k.
- v_i^{k+1} : The speed of particle I in iteration k.
- w: The inertia weight that could be revealed in equation 3.10.
- C_1, C_2: represent positive stride constants.
- R_1, R_2: The random variables, which distributed uniformly from the range [0, 1].

$$w = w_{max} - \frac{(w_{max} - w_{min})}{iter_{max}} \tag{3.10}$$

Where:

- w_{min} : The initial weight.
- w_{max} : The final weight.
- $iter_{max}$: The maximum number of the iteration.

E. Step five: Stopping criteria

As well known in the structure of the algorithm that the designated shape represents the search phase of the probe condition. At this stage of the PSO algorithm that has referred in Figure 3.19 can be expressed as follows:

“When the current iteration value reaches the specified maximum iteration number, then exit. Else, do some other initialization for every particle and then repeat the procedure”.

3.2.1 Simulink and results for the cascaded-controller with PSO

The cascaded PID, PI and lead-lag compensator have used to simulate the SynRM model depending on the result of the PSO algorithm that has discovered by utilized the PSO algorithm with the Simulink system. The control system has performed as shown in the Figure 3.21. The Simulink results reveal characteristics and feature the PSO algorithm, which provides optimum parameters value of both PID, PI and lead-lag compensator to boost the system functionality. The strategy parameter PID and PSO shows in Table 3.4 and Table 3.5.

Besides, the Figures that have started with 3.20 and end with 3.26, represent the SynRM speed control and the torque control through PSO algorithm parameters of the cascaded control, which the number of integration is about 50. PID Simulink System By apply The PSO Algorithm is shown in Figure 3.21.

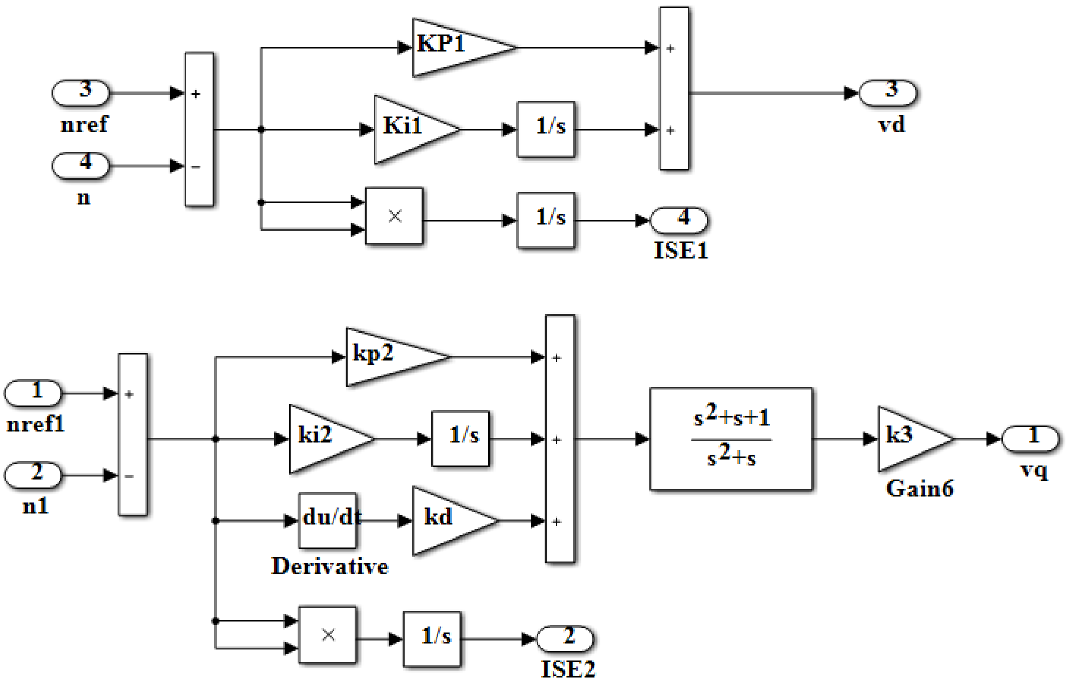

Figure 3.20. Simulink model for PSO fitness-function.

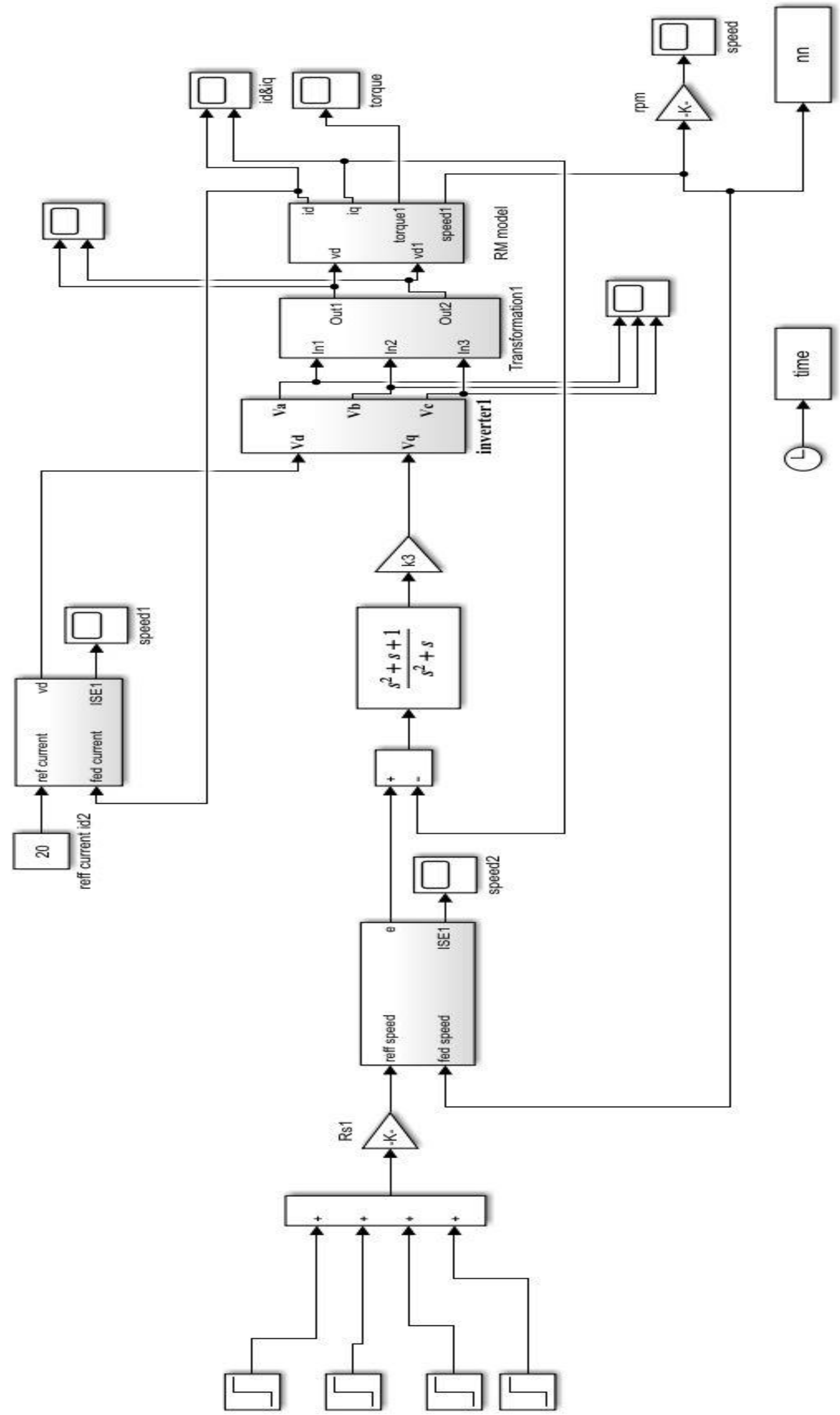

Figure 3.21. PID simulink system by apply the PSO alograthim.

Table 3.4. The characteristics of PSO algorithm.

The Parameters	The Value
The Size of the swarm	50
Maximum iteration number	50
The Swarm Dimension	16
C_1 parameter	1.3
C_2 parameter	1.3
W_{max}	0.8
W_{min}	0.3

Table 3.5. PSO strategy tuned in cascade controller parameters.

The type of Controller	Speed Controller Parameters			Quadratic axis Current Controller		
Parameter	K_P	K_I	K_d	K_3	K_P	K_I
value	200.64	8.8182	0.7914	20.879	2130	9.8

The activity of using the cascade-PI, PID and lead-lag-controller with PSO algorithm to control the SynRM speed and torque could be descript by the next Figures. Therefore, the result of simulation could be determine as the description below:

A. Figure 3.22 shows the speed control of SynRM about 1500 rpm started with (0 to 1500) rpm from (0 to 0.1) seconds at 25 Hz of the frequency with no load condition. Then, the motor speed continues stable as the curve between 1501 and 1504 that started from 0.1 seconds and continue during each operating period of the SynRM.
B. Figure 3.23 represent the control of SynRM torque that started from 2000 at the first moment of operating time, then it has decreased to be stable at about 350 in the 0.1 second of operation time. Then, continue stable at this value during each operating period of the SynRM.
C. Figure 3.24 represent the running stapes of the SynRM speed at 25 Hz of the frequency with no load condition that started from (0 to 500) rpm in the first moment of the operating time. The second stage has started in the 0.7 second of time to change the motor speed in to 1000 rpm. Hence, the third step has started in the 1.5 second of the motor speed to change the motor speed in to 1500 rpm.
D. Figure 3.25 represent the torque of SynRM at the change steps of SynRM speed. The first step show the torque has reach to 400 at the first moment of the operating time

and after that it has decreased to reach and be stable on 30 in the 0.8 second. The second step has started from 0.8 second to 1.5 second of time to change the torque from 30 in to 500 after that the torque decease to 188 at the seam step. Finally, the third step has started from 1.5 second of time and continue during each operating period, the torque start with 810 and after that decease to 188 in the seam step to be stable during each operating period.

E. Figure 3.26 represents the motor speed with no control action and frequency of 25 Hz operation frequency start from zero second and continued increasing to reach 1500 rpm in the 0.8 seconds of the operating time. Then after applied 50 Nm load at 3.5 seconds, the motor speed has decreased from 1500 rpm to 1480 rpm at 3.5 seconds after that continue rising at 3.7 be stable at the same speed during each operating period.

F. Figure 3.27 represents the motor torque with no control action and frequency of 25 Hz operation frequency start from zero second and continued increasing to reach 1500 in the zero seconds of the operating time after that decrease to be stable at 200 in the second 0.8. Then, when applied 50 Nm load at 3.5 seconds, the motor speed has increased from 200 to 400 at 3.5 seconds after that continue rising at 3.7 seconds of time to reach the 360in the second four of the operating time to be stable at the same speed during each operating period.

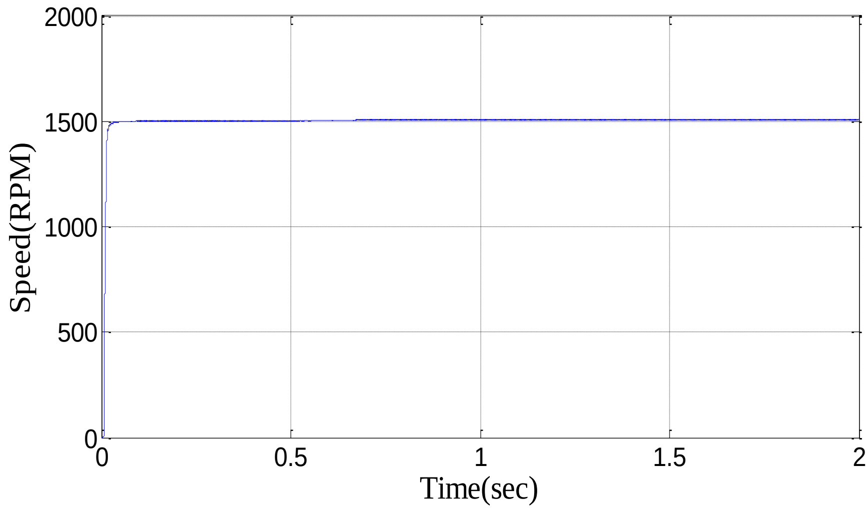

Figure 3.22. The SynRM speed control with 1500 rpm and no load condition.

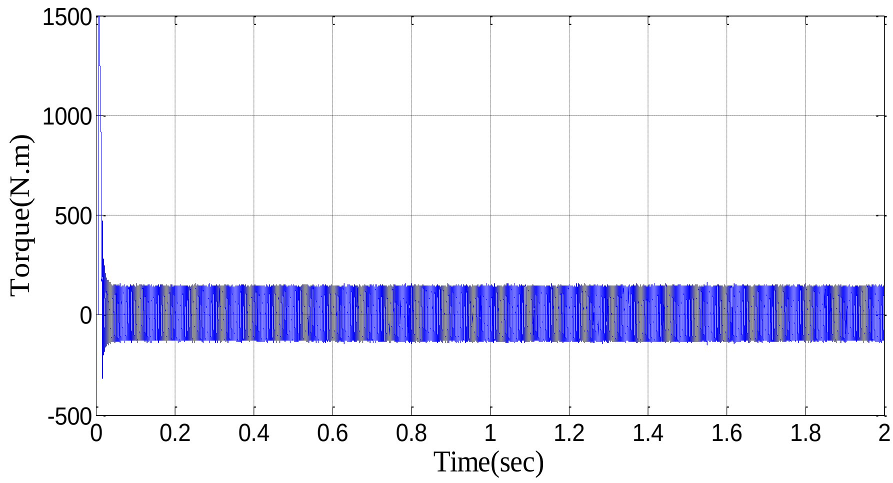

Figure 3.23. The SynRM torque control with 1500 rpm with no load condition.

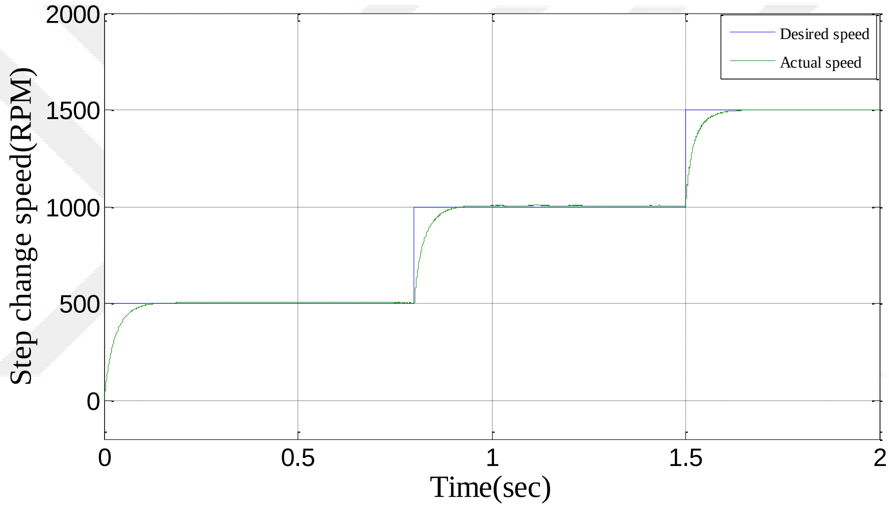

Figure 3.24. The SynRM speed control with steps of speed.

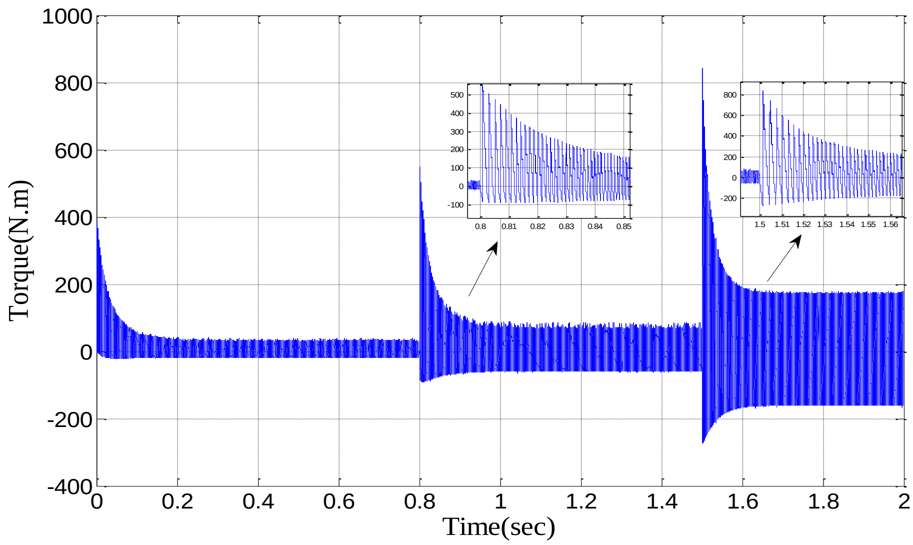

Figure 3.25. The SynRM torque control with steps of speed.

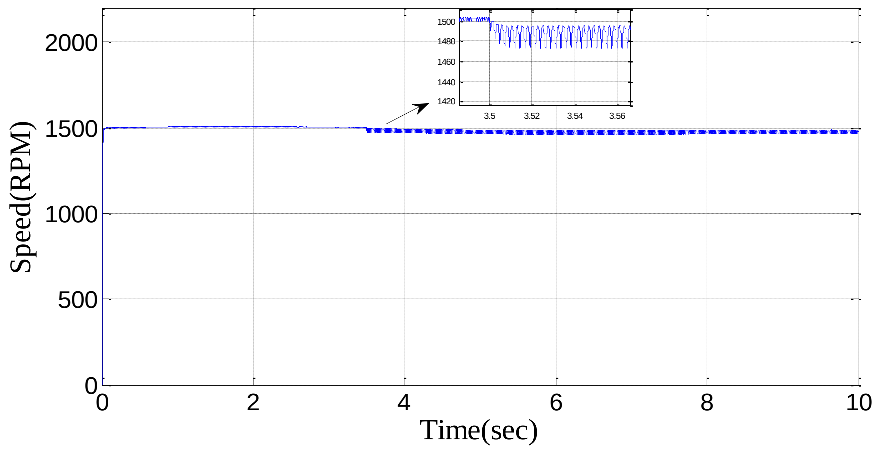

Figure 3.26. The SynRM speed control with 1500 rpm and 50 Nm steps of load at 3.5 second.

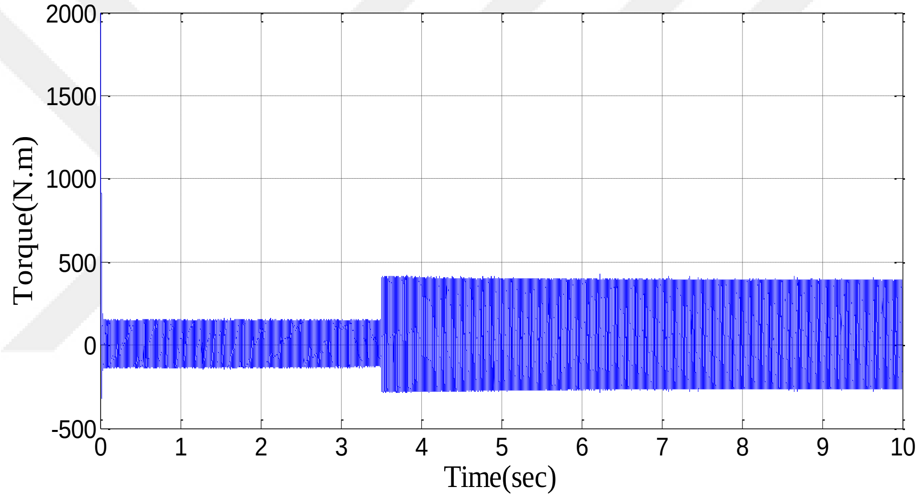

Figure 3.27. The SynRM torque control with 1500 rpm and 50 Nm steps of load applied at 3.5 second.

3.3 Conclusions

The cascaded-PI and PID controllers have utilized with a lead-lag compensator for controlling the motor speed. In addition, the Simulink controls have utilized to control the motor speed in a broad selection and can offer decent speed and torque reaction and reveal their validity at controlling the motor speed rate in different operating conditions. Moreover, the PSO algorithm has simulated controlling the parameters of their cascaded controls to reach a more significant performance than conventional controllers have mentioned in this chapter. Finally, the simulation shows the test and analysis of each one of the controller's systems in several conditions. Hence, could conclude that the proposed PSO strategy provides the best control parameters that improve system performance and particularly in the loading state.

4. THE PROPULSION ELECTRIC VEHICLE CONSTRUCTION

4.1 The Components of Propulsion Electric Vehicle System

The most current invention in the type of vehicles manufacturing are the electric vehicles (EV). EV is entirely different of traditional vehicles, an EV or as called Pure Electrical Vehicle (PEV) uses electric motors for propulsion. Instead of the gearbox, an electronic differential controller (EDC) has been used. EV is not a modern discovery, it was the first proposed in the mid of 19^{th} century. Despite its long being, it never became as famous as vehicles with internal combustion engine (ICE) in telling recent years (Roukas, 2013). Because of the significant obstacles to electric vehicles are component high cost exceptionally high voltage batteries are too expensive, limited range and sparsely of infrastructures of charging stations as well (Karamuk et al., 2013). The technological development of countries over the years, infrastructure. The EV of industries that led to the arising of environmental contaminate here then the need began to arise for the presence of vehicles that reduce the burden of pollution (Chan, 2002). The market demand on EV is expected to increase in the very near future are anticipated to increase.

As mention in chapter one, there are two types of electric vehicle, which are hydride electric vehicle (HEV) and pure electric vehicle (PEV). These two types considered as the major types of EVs and minor natures are divided from these two types depending on different aspects related to the driving system, configuration, costumers order and other concerns rely on the designing specification. The proposed EV system in this chapter called propulsion type EV that are consists of two motors that ensure the driver of the two rear driving wheels.

Besides, each SynRM drives separately from the other and the whole system is controlled by an EDC and the MCMMS, which guarantees the robustness of the vehicle. This type of EVs are the most recommended type by the mechanical experts because of slipping issues in the curvature and highroad in this type of vehicle. The rear wheel drive system of the EV is shown in Figure 4.1 (Chan, 2002; Van den Bossche, 2003).

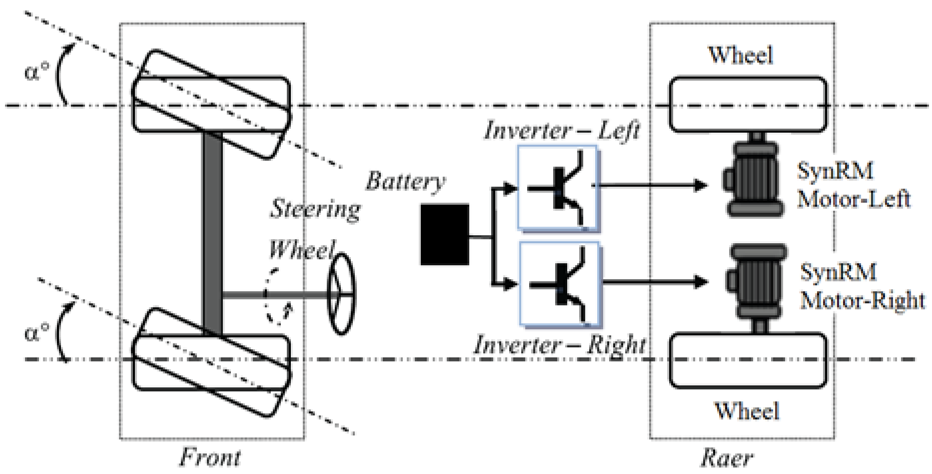

Figure 4.1. The main components of the propulsion EV system platform (Chan, 2002).

4.1.1 The electronic device (EDC)

The electronic differential controller (EDC) is an electronic device that guarantees deliver a maximum value of the torque and control the both of driving wheels, so each of wheel may turn at different speed rates in virtually any curve or precisely the exact same rate of speed in the right line road. According to the road condition and especially the steering angle control of the vehicle, the electric power is distributed by EDC to each electric motor (Boyd and Nelson, 2006). In addition, the most critical beholding in the plan of the EVs will be to make sure that car is secure when cornering and under slippery road conditions. Figure 4.2 reveals the model for your vehicle structure pushed in a curve, also Figure 4.3 explains the inputs and outputs of the EDC (Chan, 2002).

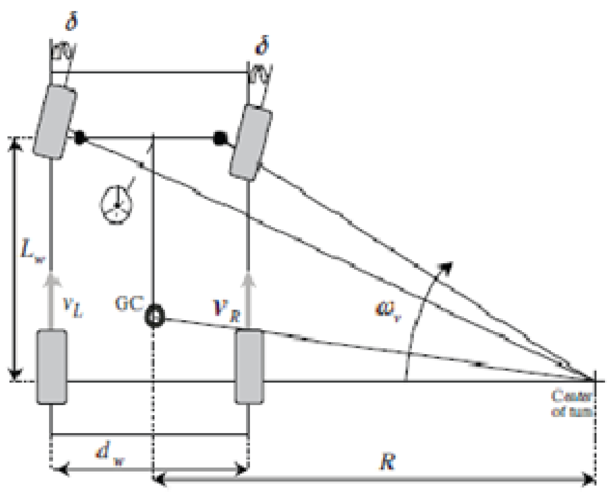

Figure 4.2. An EV platform driven in a curve road (Chan, 2002).

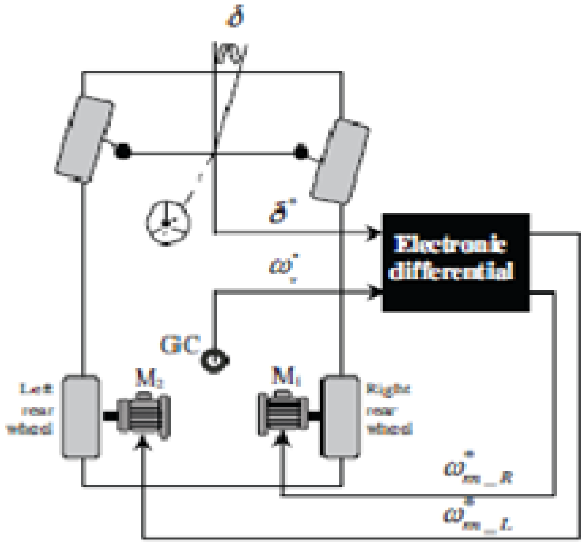

Figure 4.3. The input and output of the EDC on the curve road (Chan, 2002).

The calculation of the speed rate of the vehicle is a task of EDC work, also is based mostly on; the driver, vehicle dimension and street condition. The linear speed rate as well as the steering angle that has awarded by the driver, which imply that both of inputs regarded as the input reference to the EV system.

At the beginning of the vehicle's turn in the curve road, the driver utilizes the curve steering angle to the steering wheel to drive and control the vehicle. In this case, the EDC reacted quickly and calculate the benchmark speed of each wheel ought to be operating that appropriately and synchronous to ensure the equilibrium of the EV functionality within the curve street by increasing the speed rate of an outer motor and diminishing the speed rate of the Internal motor (Salem, 2013; Tabbache et al., 2011). The mathematical of the EDC represents as follows (Hartani et al., 2009; Van den Bossche, 2003; Hassan et al., 2005; Azzeh, 2007):

$$V_L = \omega_v \left(R + \frac{d_\omega}{2}\right) \tag{4.1}$$

$$V_R = \omega_v \left(R - \frac{d_\omega}{2}\right) \tag{4.2}$$

Where:

- V_L: The left wheel linear speed in (km/h).
- V_R: The right wheel linear speed in (km/h).

- ω_v: The vehicle linear speed in (km/h).
- d_ω: The width of EV in meter (m).
- R: The curve radius of the road.

In addition, R can be obtained as following below:

$$R = \frac{L_\omega}{\tan\delta} \tag{4.3}$$

Where:

- L_ω: The length of the EV.
- δ: The steering angle of the road.

Moreover, the angular speed rate in a curve road for both wheels can obtain by the following bellow:

$$\omega_L = \frac{L_\omega + \frac{d_\omega}{2}\tan\delta}{L_\omega}\omega_v \tag{4.4}$$

$$\omega_R = \frac{L_\omega - \frac{d_\omega}{2}\tan\delta}{L_\omega}\omega_v \tag{4.5}$$

The difference of speed between both of the right and left wheels can be write as follow:

$$\Delta\omega = \omega_L - \omega_R = \frac{d_\omega\ .\tan\delta}{L_\omega}\omega_v \tag{4.6}$$

Besides, the reference of the speed rate for both of wheel motor can be described as follows:

$$\omega_{Lr} = \omega_v + \frac{\Delta\omega}{2} \tag{4.7}$$

$$\omega_{Rr} = \omega_v - \frac{\Delta\omega}{2} \tag{4.8}$$

The conditions of the steering angle in both of curve or straight road are:

- First conditions: Turn right→ ($\delta>0$)
- Second conditions: straight ahead→ ($\delta=0$)
- Third conditions: Turn left→ ($\delta<0$)

4.1.2 The propulsion electric vehicle drive system

The electric vehicles have a drive system in its construction as stated earlier in chapter one. In addition, the propulsion drives are suggested in this chapter which is composed of two SynRMs that been put in the wheels of the pure electric vehicle "The Propulsion Electric Vehicle". The description and design of this SynRM version have previously introduced in chapter two. Besides, each SynRM in the electric vehicle has controlled from the MCMMS. Therefore, the MCMMS system has made up of a few drive systems. The control and the drive system of the SynRM are discussed in chapter three. Figure 4.4 reveals a propulsion series drive by one electric motor (Hartani et al., 2009).

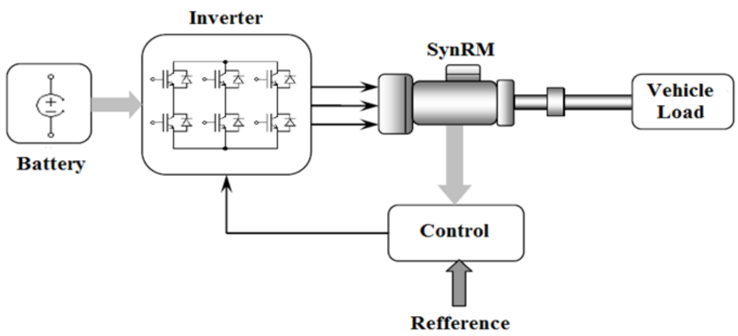

Figure 4.4. The propulsion EV chain-construction drive by one motor.

4.1.3 The source of energy in an electric vehicle

The principle working of the electrochemical device is to converts the chemical energy into equivalent electric power throughout the discharging state. As in the opposite, it converts the electrical energy to equal chemical energy through the charging state. Therefore, it is known as a rechargeable battery. There are several types of batteries that have been used in various industrial applications.

Moreover, the Lithium-Ion-rechargeable battery is the favored battery in the electric vehicles, because it has a high energy density, greater energy density and rapid of charging reaction (Yao et al., 2013) . The facts of the Lithium-Ion-battery are displayed in Appendix B.

4.2 The Simulation of EDC Model

The Matlab/Simulink program has utilized to simulate the EDC model. The essential equations to design the EDC are begin from equation 4.6 to 4.8. In addition, the simulation diagram of the EDC system model is shown in the Figure 4.5.

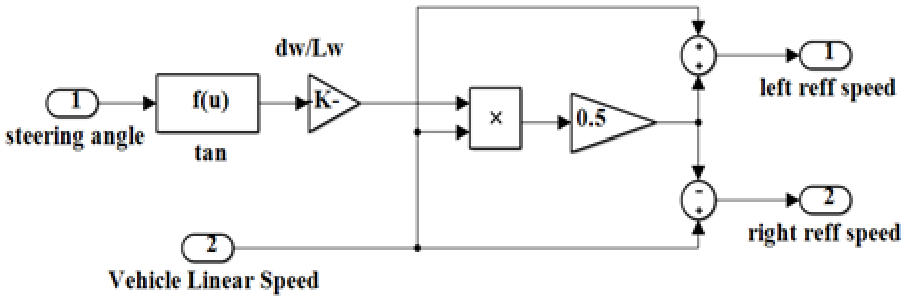

Figure 4.5. The simulation of EDC system.

4.2.1 The simulation and result of the EDC system

The simulation and result in this section has applied by using Matlab/Simulink program to described and test the validity of the EDC system in the EV. Besides, the simulation result of the system includes different cases, which are turn steering wheels right and left as represented in Figures 4.7 to 4.9. Besides, the Figure 4.7 signifies the straight road case, which the both of wheels in EV should be changed at the same speed rate. Therefore, when the EV turn right in the curve road, the left wheels move at a slow rate of speed as a compared with the right wheels of the EV as shown in Figure 4.8. As in the opposite, when the EV turn left in the curve road, the right wheels move at a high rate of speed as a compared with the left wheels of the EV as shown in Figure 4.9.

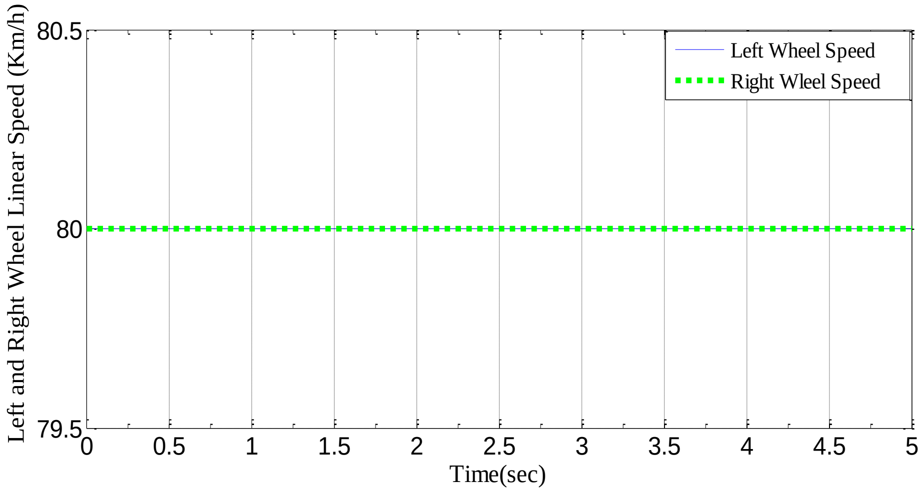

Figure 4.6. The EV moving with 80 km/h speed rate at the straight road.

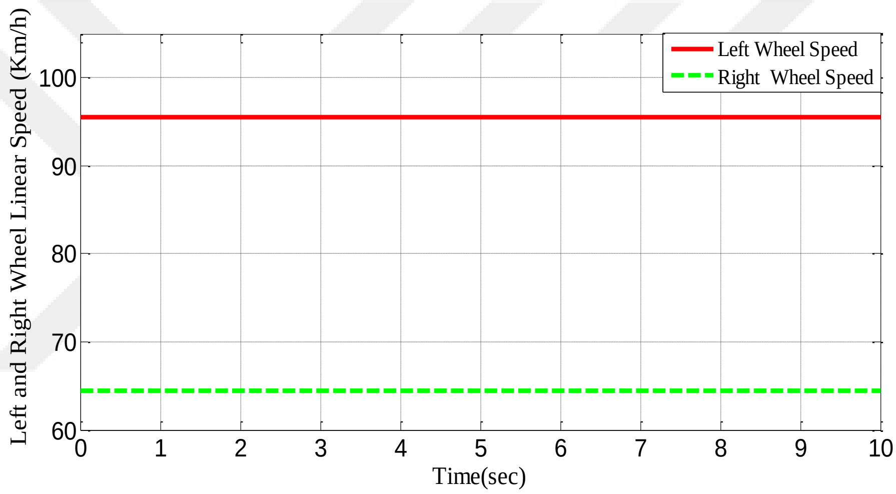

Figure 4.7. The EV turn right with 80 km/h speed rate at the curve-road with +11 degree steering angle.

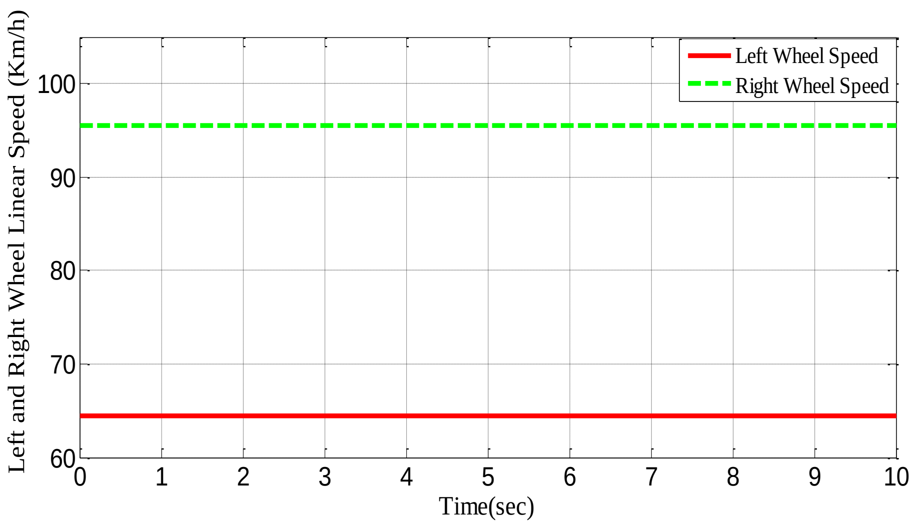

Figure 4.8. The EV turn left with 80 km/h speed-rate at the curve-road with +11 degree steering angle.

4.3 Simulation Result of The PEV System

The Matlab/Simulink program has utilized for modeling and analyzed the PEV system model in this chapter. As mentioned earlier, the propulsion drive system design in the EV includes two SynRMs that attached directly on the wheels of the vehicle “right and left wheels” without reduction equipment, energy origin signified by Lithium-Ion rechargeable battery power sours, EDC and VS-SVPWM inverter. The parameters of the Electric vehicle system are recorded in Appendix C. Hence, the simulated process of the electric vehicle is displayed in Figure 4.9.

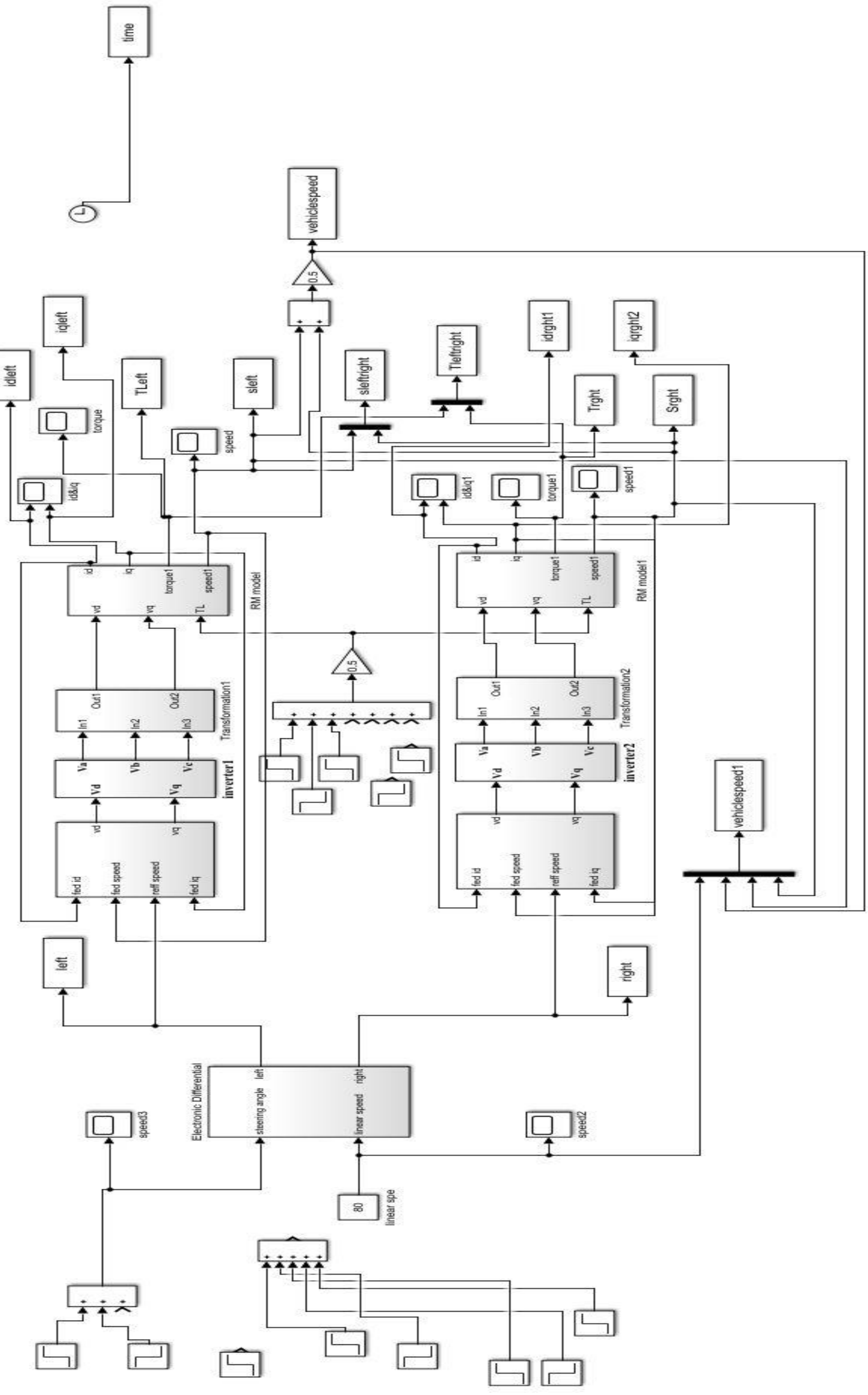

Figure 4.9. Modelling and simulation of PEV model.

4.4 The Resistive Forces of EV

Usually, The EV considered as a series of loads that described by several forces chiefly or resistive torque. Besides, the forces could include three parts, which are the rolling resistance, the aerodynamic resistance and the slope “incline” resistance. The forces acting on an Electric vehicle moving across an inclined road is shown in Figure 4.10.

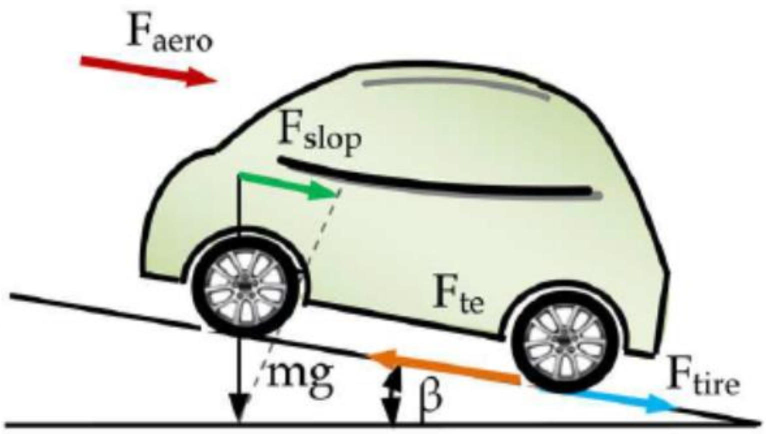

Figure 4.10. The effective forces of the EV in an inclined road (Gasbaoui, 2012).

The resistive forces that affected directly on the EV are described as the following below:

$$T_r = T_{aero} + T_{slope} + T_{tire} \quad (4.9)$$

The force of the rolling resistance can be described as the following equation:

$$T_{tire} = mgf_r \quad (4.10)$$

Where:

- m: The vehicle total mass in (kg).
- g : The gravity acceleration in (m/s).
- f_r: The rolling resistance force constant.

The force of the aerodynamic-resistance can be explained as the following below:

$$T_{aero} = 1/2 \rho_{air} A_f C_d V^2 \quad (4.11)$$

Where:

ρ_{air}: The density of air in(k_g/m^3).

A_f: The frontal surface area in (m^2).

C_d: The aerodynamic drag coefficient.

V: The linear speed of the vehicle in (km/h).

Moreover, the force of the slope "incline" resistance describes as the equation below:

$$T_{slope} = mg \sin \beta \tag{4.12}$$

Where:

β: The slope angle "inclined angle" of the road.

4.4.1 Simulink model of the resistive torque in EV

The important task for the EDC that is the distribution of the torque, where the resistive forces are dispersed evenly on both of the electric motors in the case of a straight road. Besides, the complete resistive of the torque is divided into two parts "two-halves", which is each half distributed on a single motor. The torques supply is the EDC-assignment. The parameters of these forces have recorded in Appendix C. The modulation and simulation of the resistive force is represented in Figure 4.11.

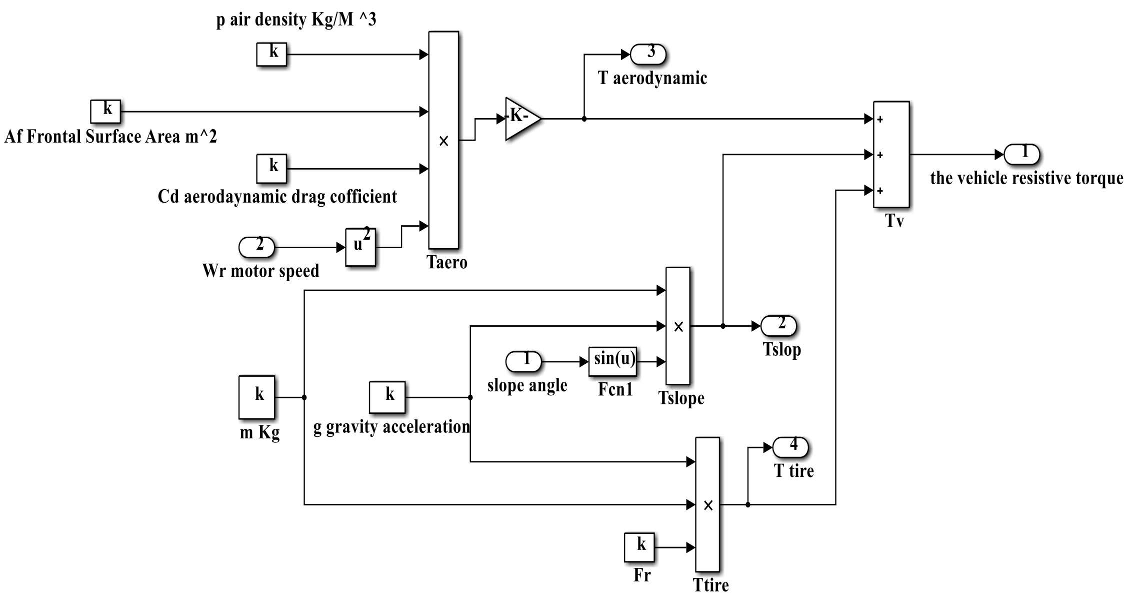

Figure 4.11. Modelling and simulation of the resistive force.

4.5 The Driving Cycle of the Electric Vehicle

The driving cycle topology has applied to the PEV in this thesis by using Matlab/Simulink program to check the system design and reveal the functionality beneath multi-speeds and difference of the resistive torque. In addition, the driving cycle topology has applied depending on the road conditions, which many stages are implemented in this system. Each stage has several different speed rate and resistive forces. The stages of the road conditions that applied in the driving cycle topology are shown below (Chan, 2002;Van den Bossche, 2003):

A. Fist case: straight road

As mentioned earlier, the two of wheels of the PEV that moving by the SynRM should have the same rate of speed on both of them in this case. Besides, there are several different conditions could be employed on the electric vehicle in accordance with the road condition this stage like; acceleration, deceleration and incline angle road. Moreover, the road condition is depended upon by the resistive forces of the vehicle and could be redistributed as the critical points below (Azzeh, 2007):

- In the case of acceleration, the aerodynamic power well increases.
- In the case of deceleration, the aerodynamic lift power will decrease.
- In the case of an inclined road, there are two sub-conditions can be found on the road, which is climbing uphill or downhill.
- In the case of faulty, the resistive force of an electric vehicle could be rise that is the reverse of downhill the vehicle slide due to the incline angle of the downward road.

B. Second case: steering angle

The steering angle is considered as a significant factor on the road, it affects directly on the itinerary of the electric vehicle. This property will be employed in this thesis to demonstrate the validity and stability of the PEV. Based upon the EDC task both of wheels that controlled by the SynRM will turn at the same change rate of speed depending on the steering wheel angle. The direction of wheel turn is represented by the inner wheels and ought to operate at a lower rate of speed than the outer wheel. The resistive forces that effect on the EV should not change " increase" when the EV change its direction such as turn left or right (Van den Bossche, 2003; Chan, 2002).

4.6 The Simulation Result of Driving Cycles System

The purpose of modeling and simulating of the driving cycle system in the EV construction model, it's to test the stability and response of the EV in various road and various condition. In addition, the simulation of the system has applied by using Matlab /Simulink program. The complete drive cycle simulink system is shown in Figure 4.29. The result of the system can be described at the flowing below to be more clear and understanding:

4.6.1 The first driving cycle

The EV moving at 80 km/h of speed rate as shown in Figure 4.12, which include three stages. Besides, the distribution of the resistive-force which effects on the EV at these stages of simulation are different from one stage to other. These stages are described as the points below:

1. The first stage: the EV moving in the straight road and the moving start with the second zero and end in the second two of the estimated time.
2. The second stage: the EV turns right in the curve road with 2.5 degrees of the steering wheel and the moving start from two second two and end with the second four of the estimated time.
3. The third stage: the EV descents in incline road with 10 degrees of incline angle and the moving start from the second four and end with the second six of the estimated time.

The result of the simulation the first drive cycle that have referred to the Figure 4.12 for each stage is explained in the points below:

A. Figure 4.13 represent the linear speed of the EV that has started from zero to reach the 77 km/h at stage1 in the second one and continued to reach the 78.5 km/h at the stage2 in the second two of the moving time also continue to reach the 80 km/h in the second four of the moving time at the last step of simulation in the slop road.
B. Figure 4.14 represent the linear speed of the left wheel of the EV that has started from zero to reach the 77 km/h at stage1 in the second one and rise up to reach the 83 km/h at the stage2 because the EV has turn right and this stage show the effect on the left wheel of the EV. The last stage after the decease to reach the 80 km/h at of simulation in the slop road.

C. Figure 4.15 represent the linear speed of the right wheel of the EV that has started from zero to reach the 77 km/h at stage1 in the second one and decease to 75 km/h at the stage2 because the EV has turn right and this stage show the effect on the right wheel of the EV. The last stage after the decease to reach the 80 km/h at of simulation in the slop road.

D. Figure 4.16 represent the torque of the left-wheel of the EV. The torque has reach the 600 at the first moment of the EV moving in the stage1 after that decease to be stable at 200 during this stage. In the second two of the moving represent the stage2 of the simulation, the torque decease to 50 because of the curve road after that increase to be stable at 200 during this stage. The second four represent the stage3 and the torque rise up to 600 at this second and after that decrease to be stable at 188 in the slop road.

E. Figure 4.17 the torque of the right-wheel of the EV. The torque has reach the 600 at the first moment of the EV moving in the stage1 after that decease to be stable at 145 during this stage. In the second two of the moving represent the stage2 of the simulation, the torque increase to 300 because of the curve road after that increase to be stable at 180 during this stage. The stage3 starts in second four of the moving time and the torque decease to 50 because of the curve road after that increase to reach and be stable 150.

F. The loaded that effect on the EV for each stage is represented in Table 4.1.

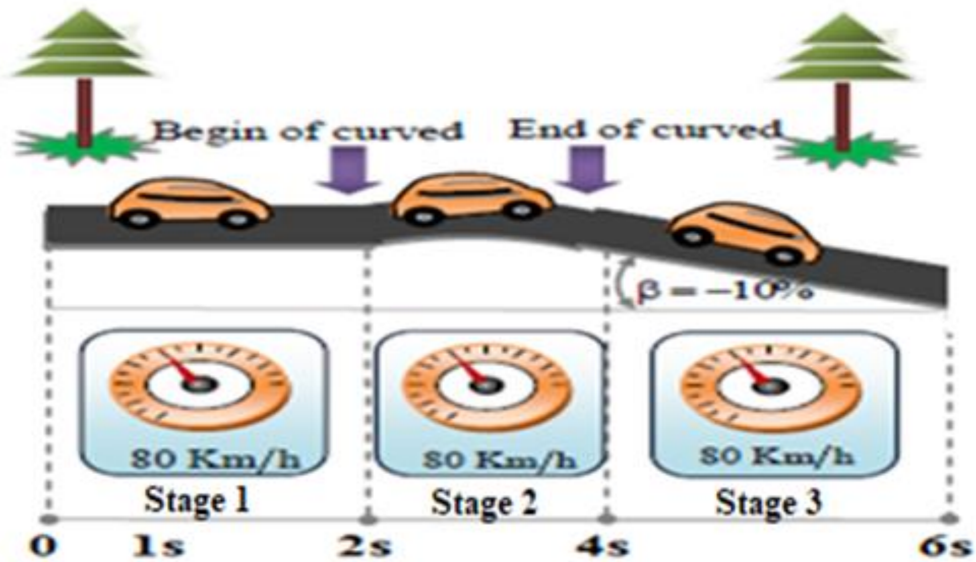

Figure 4.12. The first driving cycle of the EV includes three stages.

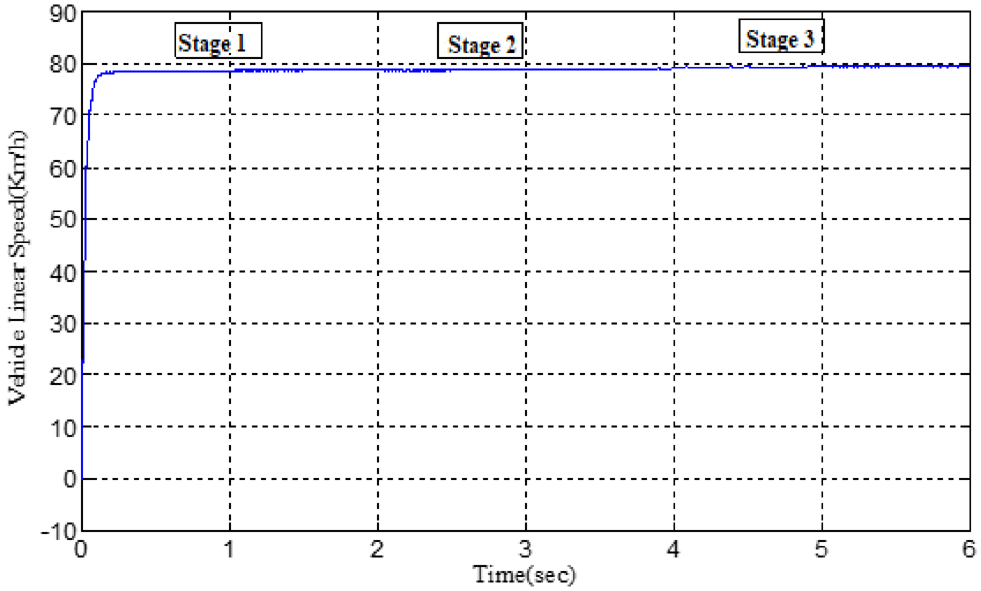

Figure 4.13. The linear speed of the EV.

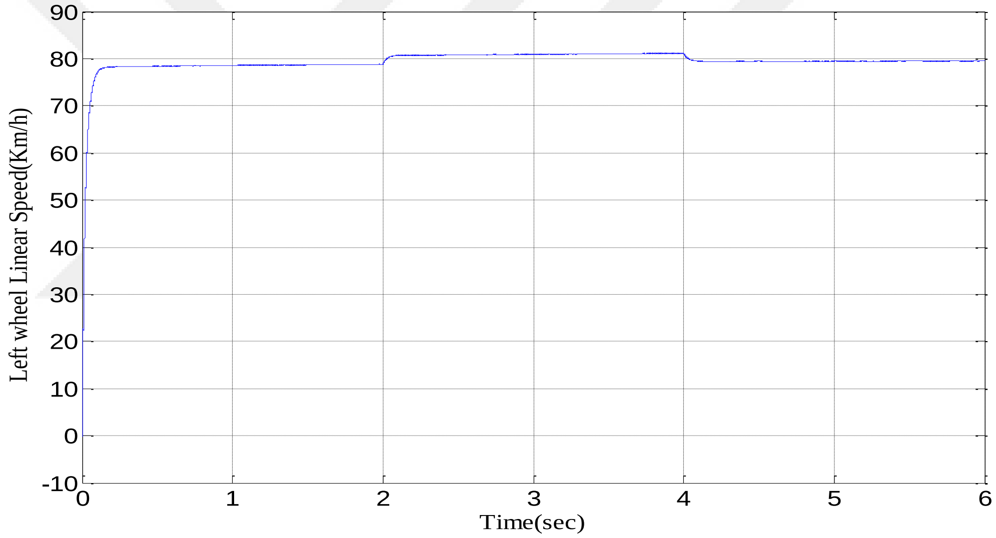

Figure 4.14. The linear speed at the left wheel of the EV.

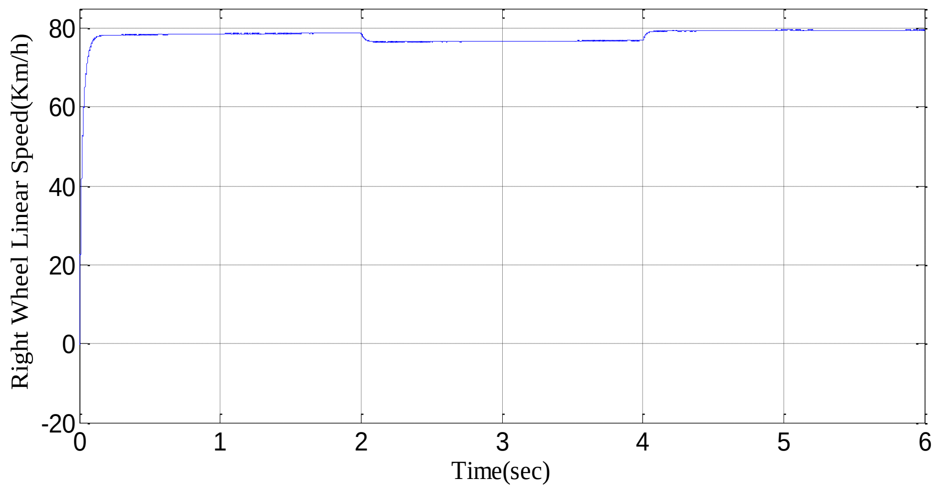

Figure 4.15. The linear speed at the right wheel of the EV.

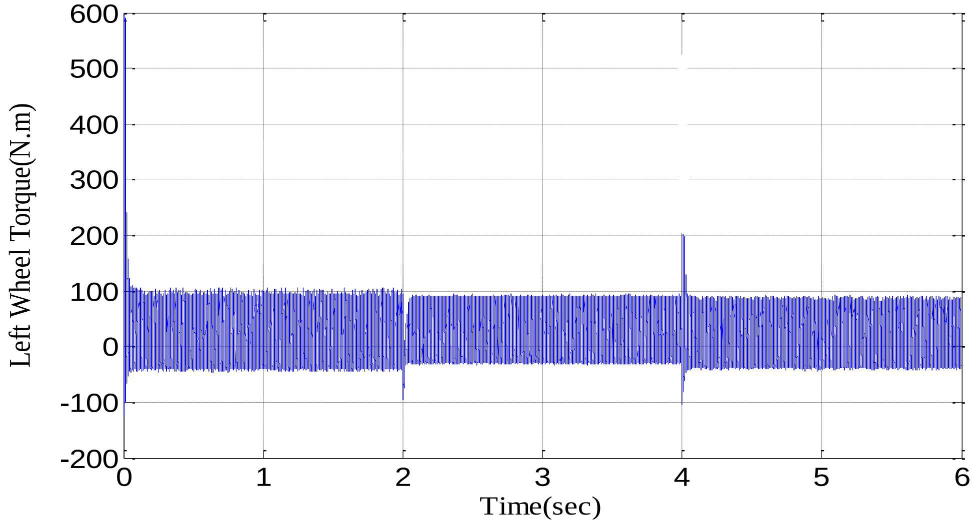

Figure 4.16. The torque at the left wheel of the EV.

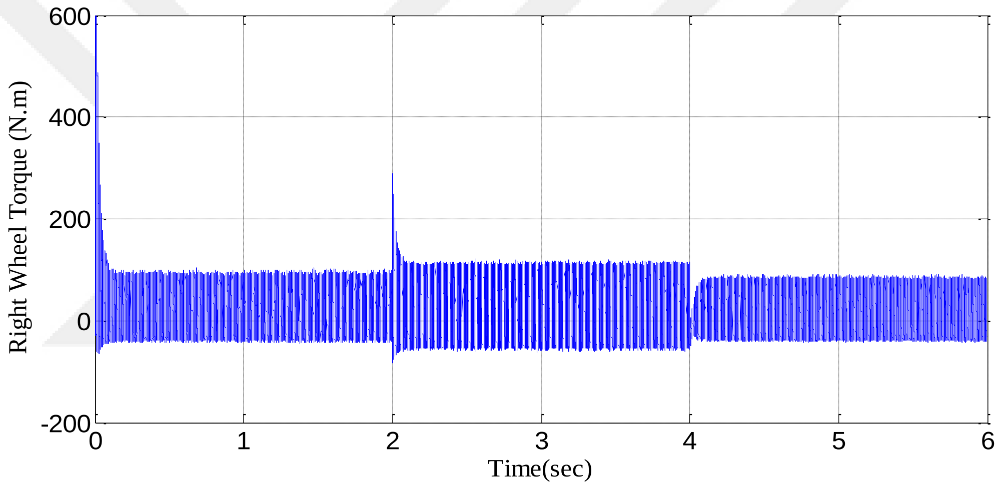

Figure 4.17. The torque at the right wheel of the EV.

Table 4.1. The load information for the first driving cycle.

The Time	From 0 to 4 second	From 4 to 6 second
The Load	32.52 Nm	25 Nm

4.6.2 The second driving cycle

This cycle includes three various stages as shown in Figure 4.18, in each stage the EV is moving with different speed rate at various slope-angle of the road, the distribution of the resistive force which effects on the EV at these stages of simulation if different from one stage to other and these stages are describe as the points below:

1. <u>The first stage:</u> the EV moving in the straight road with 60 km/h of speed rate and the moving start with the second zero and end in the second two of the estimated time.
2. <u>The second stage:</u> the EV is decelerating to 30 km/h of speed rate with 30 degrees of steering wheel angle and the moving start from two second two and end with the second four of the estimated time.
3. <u>The third stage:</u> the EV is accelerated to the maximum speed rate which is 80 km/h with 10 degrees of incline angle and the moving start from the second four and end with the second six of the estimated time.

The result of the simulation the second drive cycle that have referred to the Figure 4.18 for each stage is described as the points below:

A. Figure 4.19 represent the linear-speed of the EV that has started from zero to reach the 58 km/h at stage1 in the 0.1 second and continued to reach the 60 km/h at the last of stage1. The stage2 has started in the second two of the moving time and the speed decease to 30km/h because of the EV starting to move on slop road and continue at this rate of speed to the last of stage2 in the second four of the moving time. Stage3 has started from the second four of the moving time and the speed rise up to reach 80 km/h in this stage.
B. Figure 4.20 represent the linear-speed of the right wheel of the EV that has started from zero to reach the 58 km/h at stage1 in the 0.1 second and decease. Stage2 has started form the second two of the moving time and the speed rate decease to 30 km/h because the EV has turn right and this stage show the effect on the right wheel of the EV. Stage3 has started in the second four and the speed rate has raised up to 80 km/h when the EV finish the slop.
C. Figure 4.21 represent the torque of the right-wheel of the EV and Figure 4.22 is torque of the left-wheel of the EV. Both of these torques have started in the zero second at stage1 to reach the 500. Stage2 has started in the second two of the moving

time and the torques has decrease to -100 after that it raised in the 2.2 seconds to reach the 50 and stay stable at the end of this stage. Therefore, the stage3 in the second four of the moving time to reach the 200 after that decease in the 4.2 second to be stable at 85 to end of this stage.

D. The loaded that effect on the EV for each stage is represented in Table 4.2

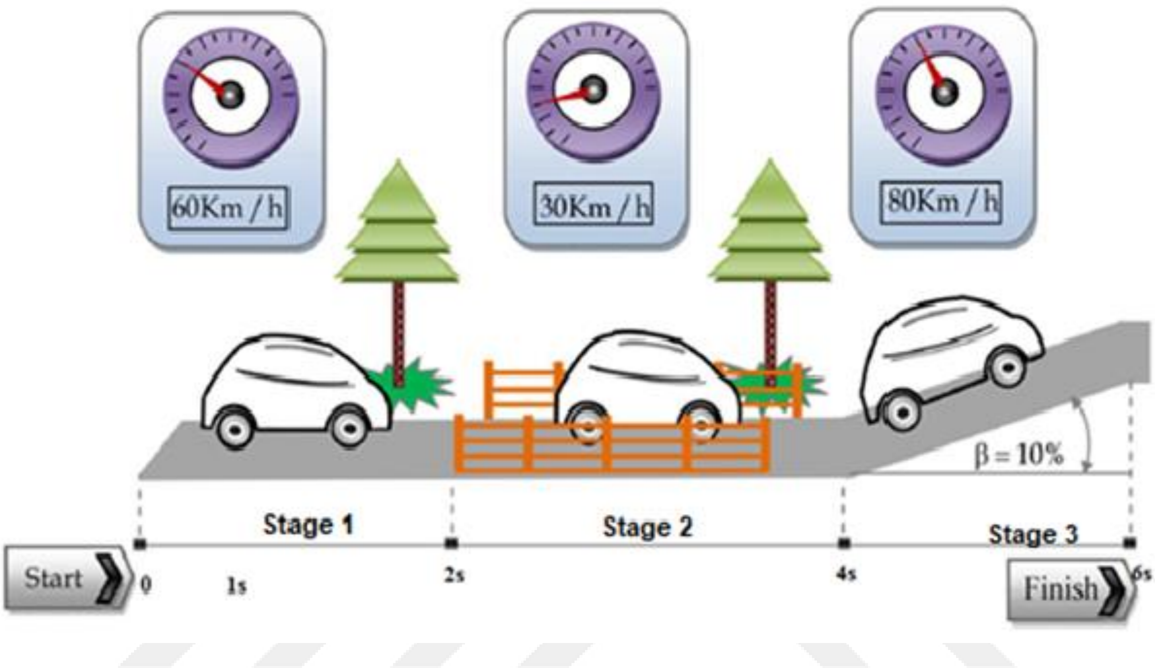

Figure 4.18. The second driving cycle of the EV include three different stages.

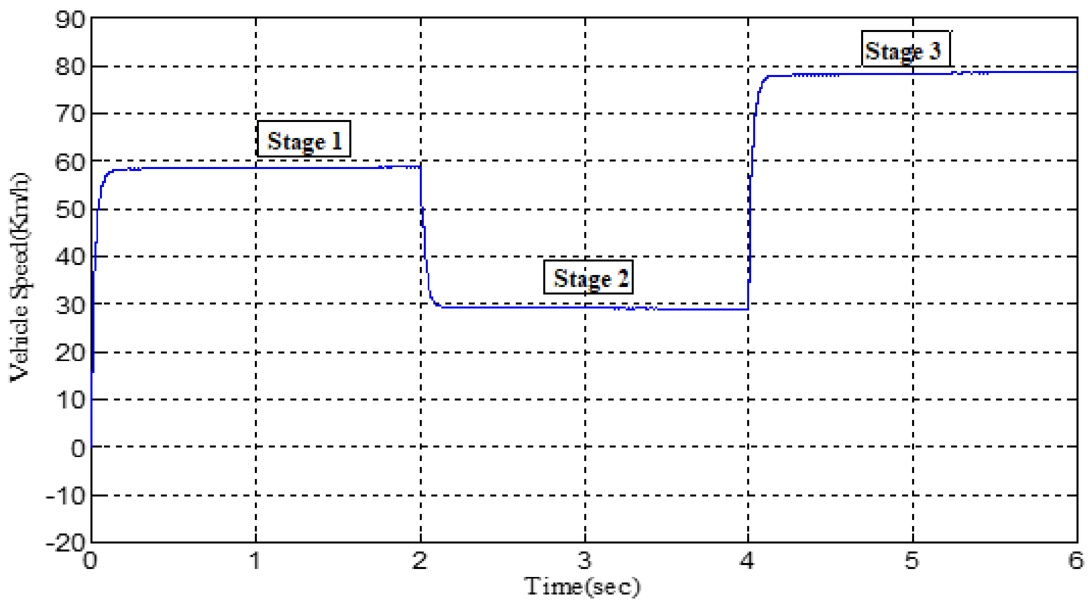

Figure 4.19. The linear speed of the EV at three stages.

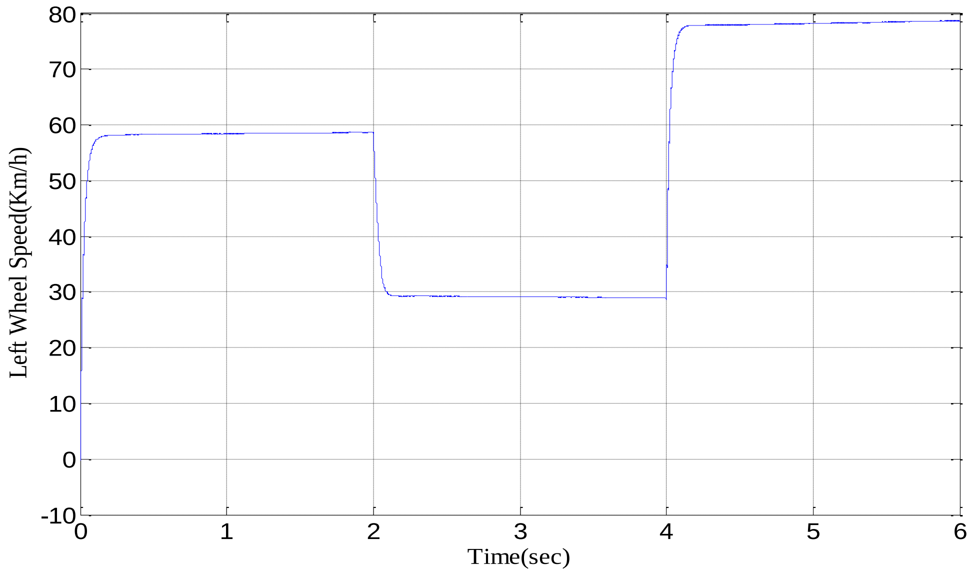

Figure 4.20. The linear speed at the right wheel the EV.

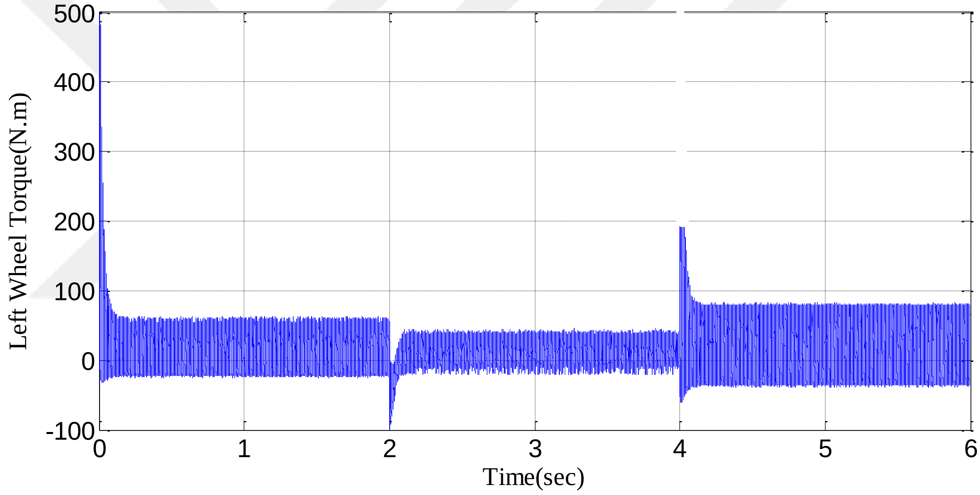

Figure 4.21. The torque at the right wheel of the EV.

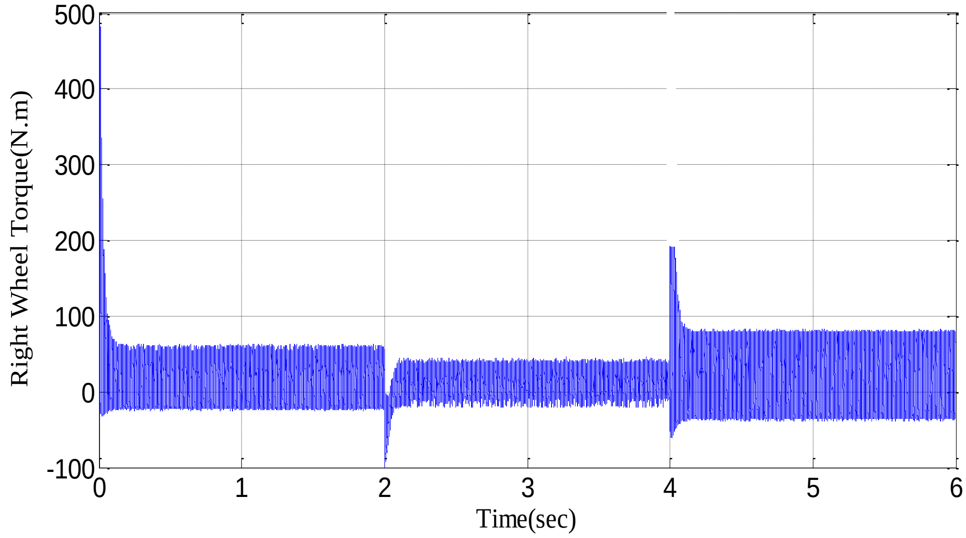

Figure 4.22. The torque of the left wheel of the EV.

Table 4.2. The load information for the second driving cycle.

The Time	From 0 to 5 second	From 5 to10 second	From10 to 15 second	From 15 to 20 second
The Load	32.53 Nm	32.53 Nm	32.53 Nm	29.17 Nm

4.6.3 The third driving cycle

This cycle includes four stages as shown Figure 4.23, in each stage the EV is moving with different speed rate at various slope-angle of the road. The distribution of the resistive force which effects on the EV at these stages of simulation which it's different from one stage to other. These stages are explained in the points below:

1. The first stage: the EV moving straight ahead with 80 km/h of speed rate and the moving start with the second zero and end in the second five of the estimated time.
2. The second stage: the EV steering in the curve road with 80 km/h of speed rate and 1.5 degrees of steering angle, also the EV moving start with the second five and end in the second ten of the estimated time.
3. The third stage: the EV rise up in the incline road with 80 km/h of speed rate and 10 degree of inclined angle, also the EV moving start with the second ten and end in the second fifteen of the estimated time.
4. The fourth stage: the EV is decelerating to 60 km/h of speed rate in the straight path after the climb from the inclined road and the moving start from second fifteen and end with the second twenty of the estimated time.

The result of the simulation the third drive cycle that have referred to the Figure 4.23 for each stage is described as the points below:

A. Figure 4.24 represent the linear speed of the EV. Stage1 has started in the zero second of the moving time start from zero to 80 km/h. Stage2 has start in the second five and the speed rate is stable on 80km/h. Therefore, stage3 stars in the second ten of the moving time and the speed rate is stable at 80 km/h. Stage4 represent that EV moving on the slop road and the speed rate deceased to 60km/h during this stage.

B. Figure 4.25 and Figure 4.26 are represent the linear speed of the left wheel and right wheel of the EV. Stage1 has started in the zero second of the moving time start from zero to 80 km/h. Stage2 has start in the second five and the speed rate is stable on 80km/h. Therefore, stage3 stars in the second ten of the moving time and the speed rate is stable at 80 km/h. Stage4 represent that EV moving on the slop road and the speed rate deceased to 60km/h during this stage.

C. Figure 4.27 and Figure 4.28 are represent the torque of the left and right wheel of the EV for the four stages. Firstly, in stage1 the torque has started in the second zero of the moving time to reach 145 of torque and then decrease to be stable at 95 during stage1 and stage2. Then, in the stage3 the torque rise up to 190 in the second ten of the moving time. Finally, the torque decrees to 35 in the second 15 at stage4 when the EV moving on the slop road, then, the torque rise up to reach 75 value of torque in the second 15.2 of the moving time at stage4.

D. The loaded that effect on the EV for each stage is represented in Table 4.3.

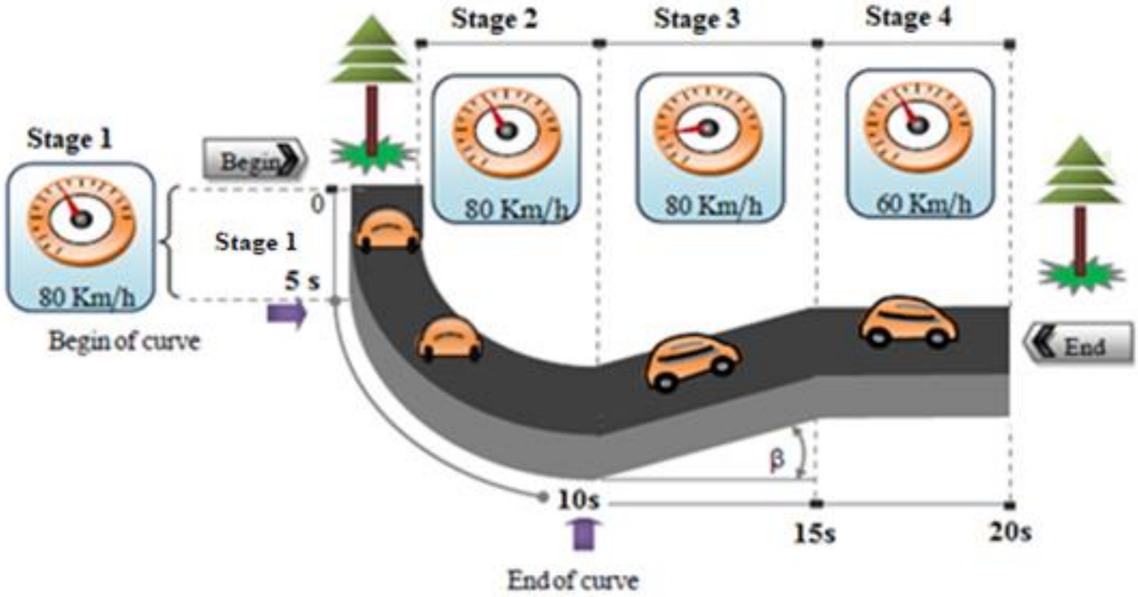

Figure 4.23. The third drive-cycle with four stages.

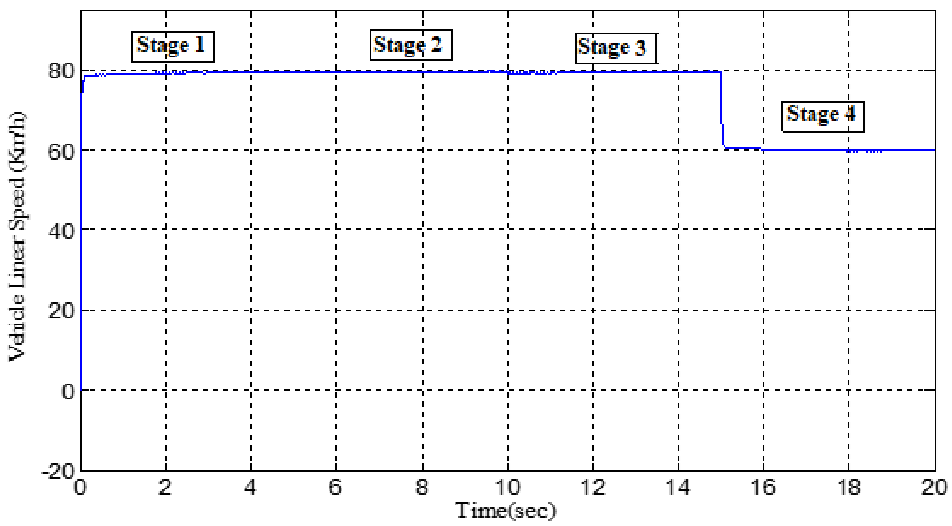

Figure 4.24. The linear-speed of the EV at 80 km/h of speed rate.

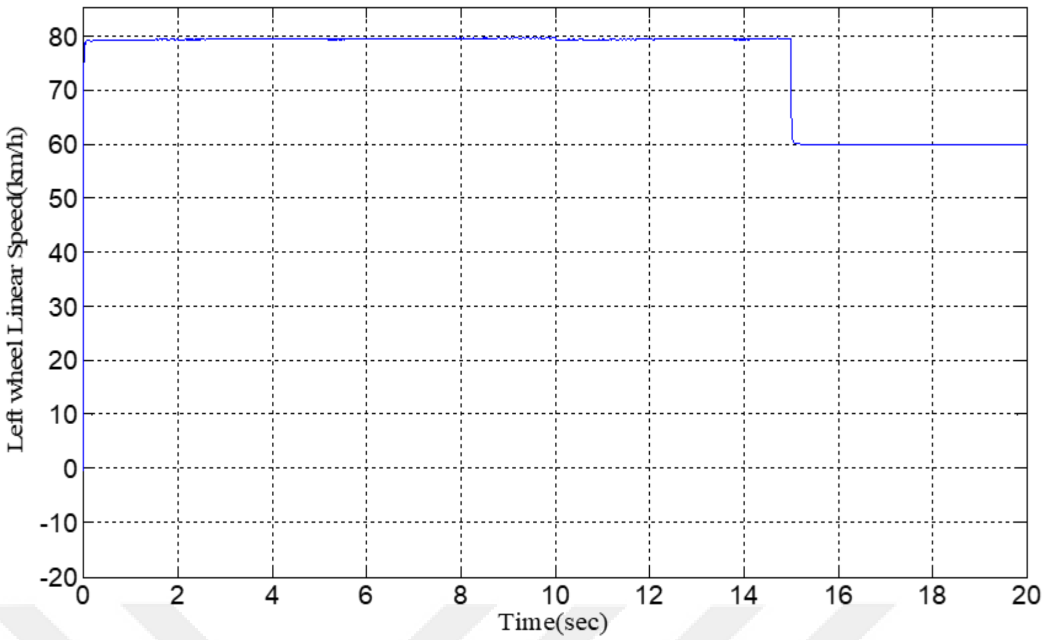

Figure 4.25. The linear speed of the left wheel.

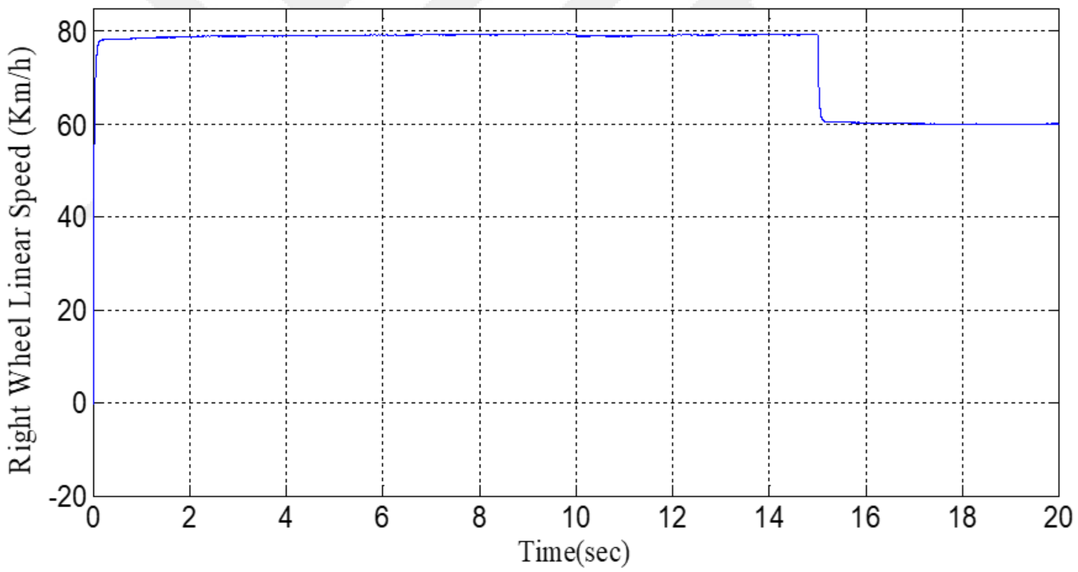

Figure 4.26. The linear speed of the right wheel.

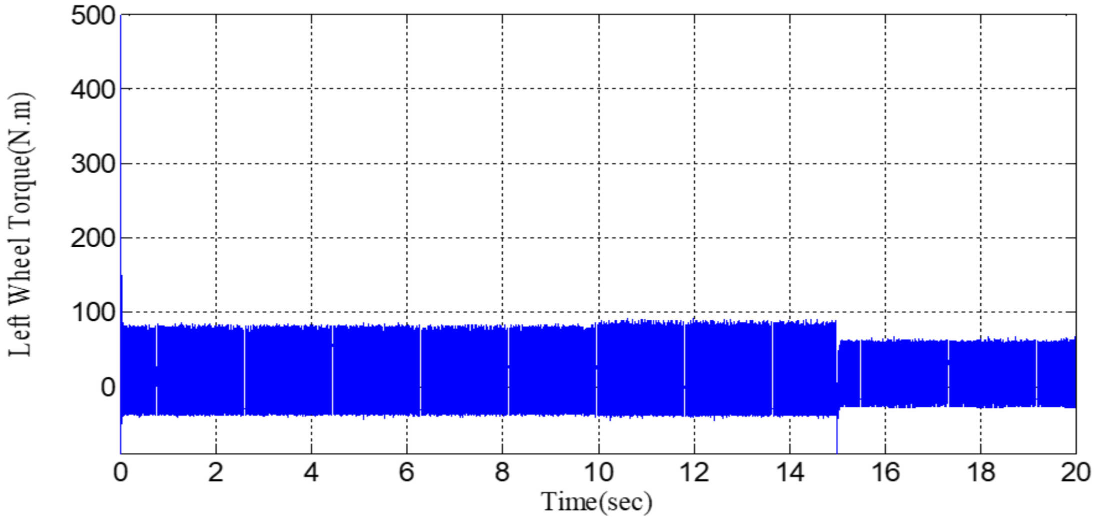

Figure 4.27. The torque of the left wheel.

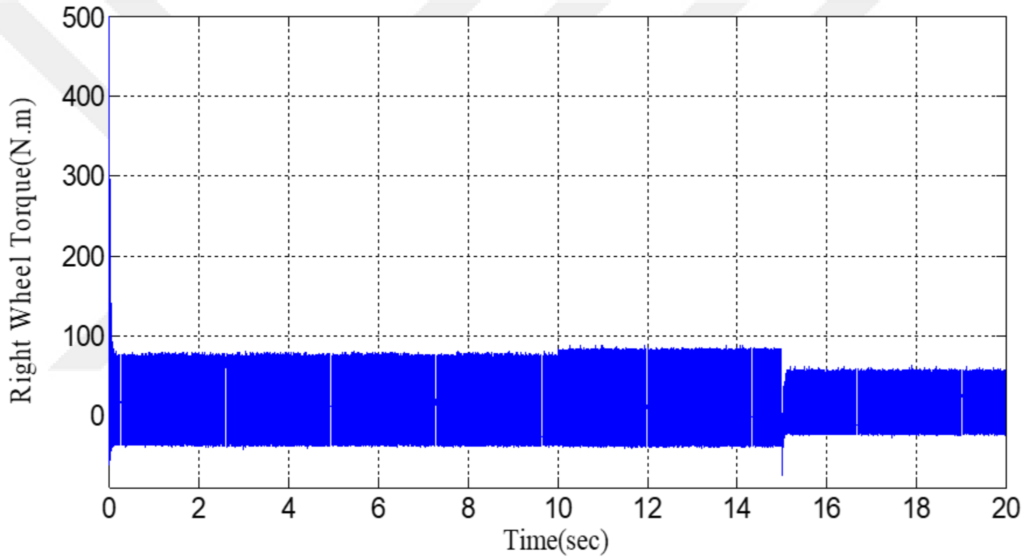

Figure 4.28. The torque of the right wheel.

Table 4.3. The loads information for the third cycle.

The Time	From 0 to 5 second	From 5 to10 second	From 10 to 15 second	From 15 to 20 second
The Load	32.52 Nm	32.52 Nm	32.52 Nm	29.15 Nm

4.7 Conclusion

The EDC topology has applied in this simulation to test the functionality and stability of the EV under several road conditions and road angles. In addition, the simulation includes three various drive-cycles, each drive cycle has many stages with several road-condition. The linear speed of the EV can be calculated by finding the consequent of the right and left wheels linear speeds. The driving cycle reveals the vehicle equilibrium along the whole cycle to reach the end of the cycle. According to the simulation result, the EV construction has stability and high response in many different conditions with 80 km/h maximum speed rate at the straight road. The complete drive cycle simulation system is shown in Figure 4.29. In addition, to ensure the safety of the work of the electrical device in the actual electric vehicle must be tested individually on the simulators control the wheel of the vehicle and the angle of deviation of the vehicle by applying different torque rates as shown in Figure 4.30.

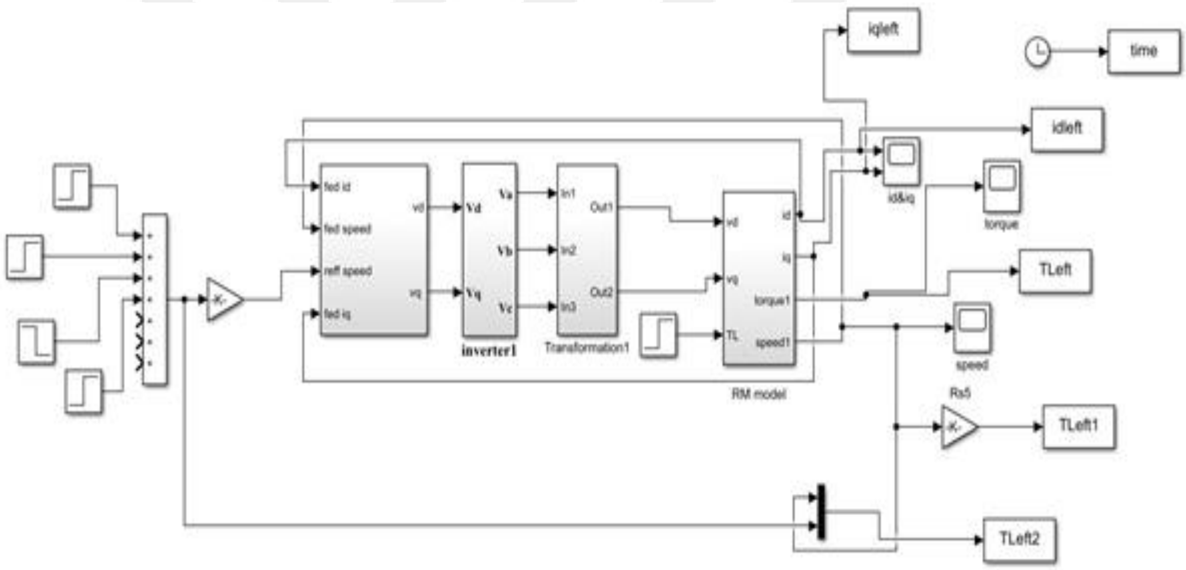

Figure 4.29. The complete drive-cycle simulink system.

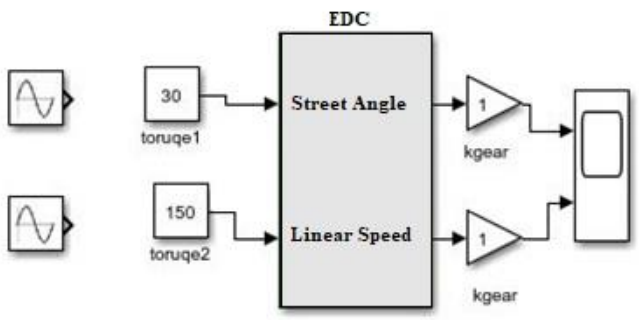

Figure 4.30. Single simulator system for testing the steering wheel.

5. CONCLUSIONS AND FUTURE WORKS

5.1 Conclusions

This thesis has fully studied about the propulsion electric vehicles design and analysis by applied the EDC technical instead of the gearbox to control the EV with driving cycles technology to test the functionality and stability of the EV under different road conditions angles. Besides, this thesis represents a full design of the synchronous reluctance motor model, which has used to drive the EV with applied many various condition in the minimum and maximum speed rate of the motor to test the stability of the motor. The main conclusions represents as the points below:

5.1.1 The aim of using the SynRM in the PEV

The three-phase Synchronous reluctance motor model has designed and analyzed. Besides, the result has shown the activity of the SynRM and seem to be much compatible to the EV design. Moreover, the SynRM has a rotor made of layers of magnetically soft material. These ferromagnetic layers orient along the stator magnetic field and follow it as it rotates.
SynRM has a cost advantage as they do not need expensive rare earth elements. They tolerate abuse well, as there are no magnets to overheat and demagnetize. Certain designs can also offer advantages at higher speeds (no field weakening). They generally have lower starting torque and poorer power to weight ratio than IM, BLDC, PMSM and SRM. Some sources claim SynRM are more nonlinear and harder to control.

Besides, the SynRM also successfully compete with induction motors for variable speed fan and pump drives (lower size, lower losses especially at partial load and cooler rotor resulting in longer bearing life). Therefore, the feature of SynRM depending on the current and torque result of the simulation that has showed the section two with the different conditions for load and frequencies to get the maximum stable rate of speed witch it 3000 rpm show that the SynRM is good chose of modelling the PEV.

As a compare the result of the SyRM with the switch reluctance motor (SRM) that have designed for the pure electric vehicle also , the result below show that the SynRM is more powerful, stable and has a high features than SRM (Takau and Round, 2003). Table 5.1 represents a compression with result between SynRM and SRM features that has applied at the EV system.

Table 5.1. A compression with result between SynRM and SRM features that has applied at the EV system.

Characteristics output	SynRM	SRM	Units
The output power	46	22	kw
The maximum rate of speed	3000	1500	rpm
Operation frequency	100	150	Hz
Efficiency at full load	94.8%	92%	--
Current	103	200	A
Torque	144	150	Nm
Torque ratio	1.6	2.3	--
The maximum speed of the EV that drive by the motor	80	60	km
Number of motor sectors	6	6	--
Number of pols	2	2	--

5.1.2 The SVPWM technology

The SVPWM technology has used to modelling and simulation the SynRM model without rotors cage or magmatic material. The six sectors of mechanical SynRM have converted to six MosFET transistors and electrical power supply to represent the fundamental of three-phase voltage source. The SVPWM inverter is one of the complicated scheme that produce a high voltage fed to the motor so that results a low total harmonic distortion. The aim of the several modulation schemes are having a variable output with a maximum fundamental component which may be produce as possible minimum harmonics. According to the location of the output voltage vector in each sector of the space vector sectors, the switching instants calculation is done by using SVM scheme relying on the representation of the switching vectors in the rotating or stationary frame plane. Hence, the SVPWM technology has consider as the optimal choose to modelling and simulate the SynRM without rotor cage or any magnetic material in the Matlab/ Simulink program or any others simulation programs and the full description of this schema has represented in the section three of this thesis.

5.1.3 The PSO strategy

This algorithm has applied to simulate social behaviour. Thing is next; a set of independent variables given, then by some set of rules it is iterative manner moved each by each on a new position, according to some optimum criteria. This happens until some appropriate solution appears, each time improving candidate solution on some measure of quality. Each point has its own position, velocity and moving in some space called search area. Thus movement according to some math formulae happens. Also on simulating a set of live organisms and its behaviour, e.g. fish swarm etc. human crowd etc. Also, apply the quasi-newton method and descent gradient can optimize irregular noise problems. The swarm of points moves on the search area, permutation in a new candidate solution until criteria of the search. Also used for so-called swarm intelligence projects. Hence, the PSO strategy has utilized to discover the best parameters of the controllers.

5.1.4 The purpose of using EDC

The EDC is represent the gearbox as located in electric vehicles. Whose role is to move the speed and change the direction from the wheels to the central engines responsible for providing the wheels of the vehicle with sufficient torque for rotation and driving the EV. Besides this device controls the angle of the vehicle and makes it stable in the direct roads and other ways that have been simulated by hypotheses in this research. Hence, the EDC technology has used to control the linear speed of the EV and ensure the vehicle stability under several road conditions as shown in the section four.

5.1.5 The cascaded-PI and PID controllers

The cascaded-PI and PID controllers have utilized with a lead-lag compensator for controlling the motor speed. The simulation controls have utilized to control the motor speed in a broad selection and can offer decent speed and torque reaction and reveal their validity at controlling the motor speed rate in different operating conditions. Hence, the simulation shows the test and analysis of each one of the controller's systems in several conditions.

5.1.6 The driving cycle

The driving cycle topology has applied to the PEV in this thesis by using Matlab/Simulink program to check the system design and reveal the functionality beneath multi-speeds and difference of the resistive torque. Besides, the driving cycle topology has applied depending on the road conditions, which many stages are implemented in this system. Besides, each stage has several different speed rate and resistive forces.

Moreover, the testing system is consist of three driving cycle:

A. First driving cycle: include three different stages condition.
B. Second driving cycle: include three different stages conditions.
C. Third driving cycle: include four different stages conditions.

The result of simulation shown that the EV is stable under many different conditions and roads at the maximum speed which is 80 km as shown in the section four of this thesis.

5.2 Future Works

From the experiences and the result that has gained duo to the work on this thesis, the topics below can be suggested to the future works:

A. The modeling and simulation of the propulsion electric vehicles, SynRM and EDC have been designed in the Matlab/Simulink program. Otherwise, this work can be applied to reality through a simplified model or a complete model if the equipment is available to build these engineering parts.

B. The EV and working hours depend entirely on the size and efficiency of the batteries instead of the fuel as usual. In this case, the battery capacity can be developed to get high working efficiency and extra hours for long distance parts.

C. The other types of the EV that has mentioned in chapter one of this thesis, can be constructed depending on the same equipment that has been used to design the of propulsion electric vehicles with some change according to the EV needs.

D. The propulsion electric vehicles and the other types of EV can be constructed by using other types of the reluctance motor like; variable reluctance motor, switched reluctance motor, variable reluctance stepping motor and BLDC motor.

E. The parameters and emulator equations that have applied to design the SynRM can be used to redesign the SynRM with more features on another simulation program or design prototype in reality.

REFERNCES

Alkhafaji, M. A., and Uzun, Y., 2018. Design simulation and analysis of synchronous reluctance motor, The International conference on innovative research in Science Engineering and Technology (IRSET), Belgrade, Serbia.

Ansari, U., Alam, S., and Jafri, S. M. un N., 2011. Modeling and control of three phase bldc motor using pid with genetic algorithm, UkSim 13th International Conferenceon Computer Modelling and Simulation, 5,3,189-194.

Azzeh, A., 2007. CAN Control system for an electric vehicle, Master Thesis, Electrical and Electronic Department, University of Canterbury, Christchurch, New Zealand Ahgtey.

Boyd, S. J., and Nelson, D., 2006. Hybrid electric vehicle control strategy based on power loss calculations hybrid electric vehicle control strategy based on power loss calculations, master thesis, Mechanical Engineering, Virginia Polytechnic Institute and State University, Blacksburg, VA 24061, USA.

Ch, R., and Obulesh, Y. P., 2011. Multi-objective optimization using evolutionary computation techniques, International Journal of Computer Applications, Tadepalligudem, India, *27*,11,19-25.

Chan, C. C., 2002. The state of the art of electric and hybrid vehicles, Proceedings of the IEEE, 90, 2, 247-275.

Consoli, A., Member, S., Russo, F., Scarcella, G., and Testa, A., 1999. Low- and zero-speed sensorless control of synchronous reluctance motors, IEEE Transactions On Industry Applications, 35, 5, 1050-1057.

Daud, A.-K., and Alsayid, B., 2013. DSP based simulator for speed control of the synchronous reluctance motor using hysteresis current controller, Scintific Reach of Energy and Power Engineering, 9, 5, 363-371.

Effatnejad, R., Bagheri, S., Farsijani, M., and Talebi, R., 2013. Economic dispatch with particle swarm optimization and optimal power flow, Technical and Physical Problems of Engineering, 5, 14, 9-16.

Emadi, A., 2005. Handbook of automotive power electronics and motor drives, Illinois Institute of Technology, Chicago, Illinois, U.S.A.

Fellani, M. a, and Abaid, E., 2013. Modeling and simulation of reluctance motor using digital computer, International Journal of Computer Science and Electronics Engineering,1, 2 ,148-152.

Fratta, A., and Vagati, A., 1992. A Reluctance motor drive for high dynamic performance applications, ieee transactions on industry applications, 28, 4, 1-2.

Garpinger, O., 2015. Analysis and design of software-based optimal pid controllers, PhD Thesis, LUND University, Department of Automatic Control, SE-221 00 LUND, Sweden.

Gasbaoui, B., 2012. A novel 4WD electric vehicle control strategy based on direct torque control space vector modulation technique, Intelligent Control and Automation, 03, 3, 236-242.

Haddoun, A., Benbouzid, M. E. H., Diallo, D., Abdessemed, R., Ghouili, J., and Srairi, K., 2008. Modeling analysis and neural network control of an EV electrical differential, IEEE Transactions on Industrial Electronics, 55, 6,2286-2294.

Hartani, K., Bourahla, M., Miloud, Y., and Sekour, M., 2009. Electronic differential with direct torque fuzzy control for vehicle propulsion system, Turkish Journal of Electrical Engineering and Computer Sciences, 17, 1, 21-38.

Hassan, R., Cohanim, B., and Weck, O., 2005. A comparison of particle swarm optimization and the genetic algorithm, 1st AIAA Multidisciplinary Design Optimization Specialist Conference, 1-13.

He, H., Peng, J., Xiong, R., and Fan, H., 2014. An acceleration slip regulation strategy for four-wheel drive electric vehicles based on sliding mode control, Energies, 7, 6 , 3748-3763.

Huang, H. P., Jeng, J. C., Chiang, C. H., and Pan, W., 2003. A direct method for multi-loop PI/PID controller design, Journal of Process Control, 13, 8, 769-786.

Karamuk, M., Emin Çepni, M., and Gür OTAM AŞ, S., 2013. Electric vehicle powertrain development, automotive technologies R and D center, Istanbul-Turkey.

Khubalkar, S., Junghare, A., Aware, M., and Das, S., 2017. Modeling and control of a permanent-magnet brushless DC motor drive using a fractional order proportional-integral-derivative controller, Turkish Journal of Electrical Engineering and Computer Sciences, 4223-4241.

Malan, J., and Kamper, M. J., 2001. Reluctance synchronous machine technology, IEEE Transactions On Industry Applications, 37, 5, 37, 1319-1324.

Nasri, A., Hazzab, A., Bousserhane, I. ., Hadjeri, S., and Sicard, P., 2010. Fuzzy logic speed control stability improvement of lightweight electric vehicle drive, Journal of Electrical Engineering and Technology, 5, 1, 129-139.

Nasri, A., Hazzab, A., Bousserhane, I. K., Hadjeri, S., and Sicard, P., 2009. Fuzzy-sliding mode speed control for two wheels electric vehicle drive, Journal of Electrical Engineering and Technology, 4, 4, 499-509.

Rahimian, M. S., and Raahemifar, K., 2011. Optimal pid controller design for avr system using particle swarm optimization algorithm. IEEE Ccece , Toronto, Ontario, Canada, 337-340.

Ravi, A., and Palani, S., 2013. Robust electronic differential controller for an electric vehicle, American Journal of, Applied Sciences 10, 11, 1356-1362.

Reddy, M. B., Obulesh, Y. P., and Raju, S. S., 2012. Particle swarm optimization based optimal power flow for volt-var control, ARPN Journal of Engineering and Applied Sciences, 7, 1, 1819-6608.

Roukas, M., 2013. Development of the control system for an electric vehicle, Master of Science Thesis, Department of Signals and Systems, Chalmers University of Technology, Göteborg, Sweden.

Salem, F. a., 2013. Modeling and control solutions for electric vehicles, European Scientific Journal 9,15, 1857-7881.

Sathyan, S., 2013. Synchronous reluctance motor for household applications, Master Thesis, Department of Electrical Engineering, AALTO University School of Electrical Engineering, Espoo, Finland.

Sharaf, A. M., and El-Gammal, A., 2009. A novel particle swarm optimization PSO tuning scheme for pmdc motor drives controllers, 2nd International Conference on Power Engineering, Energy and Electrical Drives Proceedings, 134 -139.

Sivanandam, S. N., 2007. Multiprocessor scheduling using hybrid particle swarm optimization with dynamically varying inertia, International Journal of Computer Science and Applications, 4 , 3, 95-106.

Soltani, J., and Zarchi, H. A., 2004. Robust optimal speed tracking control of a current sensorless synchronous reluctance motor drive using a new sliding mode controller, Department of Electrical and Computer Engineering, Isfahan University of Technology, 17, 2, 170-185.

Soni, Y. K., and Bhatt, R., 2013. Simulated annealing optimized pid controller design using ISE, IAE, IATE and MSE error criteria, International Journal of Advanced Research in Computer Engineering and Technology, 2, 7, 2333-2336.

Tabbache, B., Kheloui, A., and Benbouzid, M. , 2011. An adaptive electric differential for electric vehicles motion stabilization, IEEE Transactions on Vehicular Technology, 60, 1, 104 -110.

Tahi, S., Ibtiouen, R., and Bounekhla, M., 2011. desing optimization of two synchronous reluctance machine structures with maximized torque and power factor, Progress In Electromagnetics Research, 35, 369-387.

Tran, P. H., 2012. Matlab/Simulink implementation and analysis of three pulse-width-modulation, Master of Science in Electrical Engineering, Boise State University.

Tuncay, R. N., Ustun, O., Yilmaz, M., Gokce, C., and Karakaya, U., 2011. Design and implementation of an electric drive system for in-wheel motor electric vehicle applications, IEEE Vehicle Power and Propulsion Conference, 1-6.

Yao, L. W., Kong, P. Y., and Idris, N. R. N., 2013. Modeling of lithium-ion battery using matlab/simulink, Power Electronics and Drives Research Group, Department of Electrical Power Engineering, Universiti Teknologi Malaysia, 81300 Skudai, Johor, Malaysia 1729-1734.

Takau, L., and Round, S., 2003. Design of a switched reluctance motor for an electric vehicle, Australasian Universities, Power Engineering Conference, AUPEC.

Donaghy-Spargo, C. M. 2016. Synchronous reluctance motor technology opportunities challenges and future direction, Durham University, Engineering and Technology Reference, 1-15.

URL-1 <https://www.new.abb.com/motors-generators/iec-low-voltage-motors/process-performance-motors/synchronous-reluctance-motors>, Data of access: 26/11/2018.

URL-2 <https://new.abb.com/abb-ability/transport/electric-vehicles/ev-chargin>, Data of access: 26/11/2018.

THESIS APPENDIX

Appendix A. Switching condition and vectors of the output.

The Vectors of The Voltage	The Vectors of Switching			Line to Standard Voltages			Line to line Voltages		
	A	B	C	V_{an}	V_{bn}	V_{cn}	V_{ab}	V_{bc}	V_o
$\boldsymbol{V_0}$	0	0	0	0	0	0	0	0	0
$\boldsymbol{V_1}$	1	0	0	2/3	-1/3	-1/3	1	0	-1
$\boldsymbol{V_2}$	1	1	0	1/3	1/3	-2/3	0	1	-1
$\boldsymbol{V_3}$	0	1	0	-1/3	2/3	-1/3	-1	1	0
$\boldsymbol{V_4}$	0	1	1	-2/3	1/3	1/3	-1	0	1
$\boldsymbol{V_5}$	0	0	1	-1/3	1/3	2/3	0	-1	1
$\boldsymbol{V_6}$	1	0	1	1/3	-2/3	1/3	1	-1	0
$\boldsymbol{V_7}$	1	1	1	0	0	0	0	0	0

Appendix B. Characteristics of the EV's battery.

The Type of Battery	Lithium-Ion	-
The Voltage of single Cell	1.2	volt
The Total Capacity of cells	240 [6 cells*40 modules]	-
Voltage	288	volt
Published Capacity	6.5	Ah

Appendix C. Electric vehicle parameters.

d_ω	Width of EV	1.8 m
R_w	The Radius of single Wheel	0.23 m
f_r	Rolling Resistance Force Constant	0.02
m	The Total Mass of EV	$710K_g$
ρ_{air}	The Density of Air	$1.3K_g/m^3$
A_f	Frontal Surface	$2.8m^2$
C_d	The coefficient of aerodynamic-drag	0.34

Appenix D. Tuning of PID controller using Particle Swarm Optimization

```
%% Initialization
clear all
clc
%--------------------------------------------------------%
n =50;          % Size of the swarm " no of birds "
bird_setp  =50;   % Maximum number of "birds steps"
dim = 4;
%-----------------------------------------------%
wwww=0
local_best_position=0;
globl_best_position=0;
K=0;
F=0;
F2=0;
HHH=inf;
fitness=0;
current_fitness=0;
R1=0;
R2=0;
current_position=0;
velocity=0;
dif1=0;
dif2=0;
GG=0;
g1=1;         % Dimension of the problem
KKK=ones(bird_setp, dim);
%------------------------------------------------------------------%
xmax=[20  5   0.7  6 ] ;
xmin=[15 3.5  0.4  3  ];
%----------------------------------------------------------------%

c2 =1.2;         % PSO parameter C1
c1 = 1.2;        % PSO parameter C2
w =0.9;          % pso momentum or inertia
fitness=0*ones(n,bird_setp);
R1 = rand(n,dim);
R2 = rand(n,dim);
current_fitness =0*ones(n,1);
globl_best_position=ones(n,dim);
local_best_position=ones(n,dim);
K=ones(n,dim);
dp=ones(1,dim);
                                        %----------------------------%
                                        %    initialize the parameter %
                                        %----------------------------%

R1 = rand(n,dim);
R2 = rand(n,dim);
current_fitness =0*ones(n,1);
```

```
%-----------------------------------------------%
% Initializing swarm and velocities and position %
%-----------------------------------------------%


for i= 1:n
    for j= 1:dim
     current_position (i,j)=rand*(xmax(j)-xmin(j))+xmin(j);
    end
end
  %------------------------------------------------------------------------------------------------%



%current_position = abs(10*(rand(dim, n)-.5));
velocity = .3*randn(n,dim) ;
local_best_position  = current_position ;


 K=current_position;

%-------------------------------------------%
%     Evaluate initial population          %
%-------------------------------------------%

for zzz=1:n

        kp=K(zzz,1);
        ki=K(zzz,2);
        kd=K(zzz,3);
        k3=K(zzz,4);

             simopt = simset('solver','ode5','SrcWorkspace','Current','DstWorkspace','Current');  %
Initialize sim options
         [tout,xout,yout] = sim('pidrpso11',[0 10],simopt);
              sys_overshoot=max(nn)-150;
         e=abs(e2);
         e3=sum(e);
         F1(zzz)=e3+sys_overshoot;

end

local_best_fitness  = F1 ;

[global_best_fitness,g] = min(local_best_fitness) ;

for i=1:n
    globl_best_position(i,:) = local_best_position(g,:) ;
end
globl_best_position;
```

```
dif1=local_best_position-current_position;
dif2=globl_best_position-current_position;

                                        %-------------------%
                                     %  VELOCITY UPDATE  %
                                        %-------------------%

velocity = w *velocity + c1*(R1.*(local_best_position-current_position)) +
c2*(R2.*(globl_best_position-current_position));

                                        %------------------%
                                     %   SWARMUPDATE    %
                                        %------------------%


current_position = current_position + velocity ;

                                      %------------------------%
                                     %  evaluate anew swarm   %
                                      %------------------------%


%% Main Loop
iter = 0 ;        % Iterations’counter
while  ( iter < bird_setp )
iter = iter + 1

for zzz=1:n
         kp=K(zzz,1);
        ki=K(zzz,2);
        kd=K(zzz,3);
        k3=K(zzz,4);


             simopt = simset('solver','ode5','SrcWorkspace','Current','DstWorkspace','Current');  %
Initialize sim options
         [tout,xout,yout] = sim('pidrpso11',[0 10],simopt);
            sys_overshoot=max(nn)-150;
         e=abs(e2);
         e3=sum(e);
         F1(zzz)=e3+sys_overshoot;




end
current_fitness=F1;

for i = 1 : n
        if current_fitness(i) < local_best_fitness(i)
           local_best_fitness(i)  = current_fitness(i);
           local_best_position(i,:) = current_position(i,:) ;
```

```
        end
 end


 [current_global_best_fitness,g] = min(local_best_fitness);


if current_global_best_fitness < global_best_fitness
   global_best_fitness = current_global_best_fitness;

    for i=1:n
        globl_best_position(i,:) = local_best_position(g,:);
    end

end


 velocity = 0.5 *velocity + c1*(R1.*(local_best_position-current_position)) +
c2*(R2.*(globl_best_position-current_position));
 current_position = current_position + velocity;

 sprintf('The value of interation iter %3.0f ', iter );

K=current_position;
for i=1:n
    for j=1:dim
        if K(i,j)<xmin(j)
            K(i,j)=xmin(j);
        elseif K(i,j)>xmax(j)
            K(i,j)=xmax(j);
        else
            K(i,j)=K(i,j);
        end
    end
end
current_position=K;

for i=1:n
    for j=1:dim
        if globl_best_position(i,j)<xmin(j)
            globl_best_position(i,j)=xmin(j);
        elseif globl_best_position(i,j)>xmax(j)
            globl_best_position(i,j)=xmax(j);
        else
            globl_best_position(i,j)=K(i,j);
        end
    end
end
if global_best_fitness<HHH
HHH=global_best_fitness;
else
```

```
HHH=HHH;
end
KKKK(iter)=HHH

KKK(iter,:)=globl_best_position(1,:);
it(iter)=iter;

end
Figure(1)
plot(it,KKKK)
Figure(2)
    plot(it,KKK)
       K(1,:)=globl_best_position(1,:);
 zzz=1;
         kp=K(zzz,1);
        ki=K(zzz,2);
        kd=K(zzz,3);
        k3=K(zzz,4);



             simopt = simset('solver','ode5','SrcWorkspace','Current','DstWorkspace','Current');  %
Initialize sim options
         [tout,xout,yout] = sim('pidrpso11',[0 50],simopt);
```

CURRICULUM VITAE

Name and surname : Mohammed Ayad Radhi Alkhafaji

Address : Iraq / DhiQar/ Al Nassiriyah

E-mail address : eng.mark30@gmail.com

EDUCATION INFORMATION (Institution and Year):

Bachelor's Degree : Alrafidain University College 2010-2011

Master degree : Aksaray Üniversitesi, 2018-2019

PROFESSIONAL EXPERIENCE AND AWARDS:

1. Network team leader at Scopesky Telecommunication Company (2012-2013).
2. Communication engineering at Asiacell Telecommunication Company (2013-2015).
3. Engineering at Imam Jaafar Al-Sadiq University laboratories (2013-2015).
4. Maintenance engineer at korek Telecommunication Company (2013-2015).
5. Engineering at electrical department of Mazaya University College (2015-2018).
6. Sales Manager at El-Misk company for IT solutions (2016- yet).
7. Acknowledgments in the management from Al-Sadiq University's laboratories.
8. Acknowledgments from Asiacell and Iraq for Reconstruction.
9. Acknowledgments from General Union of Cooperative Societies.
10. Appreciated appreciation from El-Misk Company for Technical Solutions.

PUBLICATIONS, PRESENTATIONS AND PATENTS

Alkhafaji, M. A., and Uzun, Y., 2018. Design, simulation and analysis of synchronous reluctance motor, The International conference on innovative research in Science Engineering and Technology (IRSET), Belgrade, Serbia.